Cape Peninsula University of Technology

DESIGN OF A CONICAL TERMINATED TEM CELL FOR EMC TESTING

by

INGE CHLEO PEARCE

Thesis submitted in fulfilment of the requirements for the degree

Master of Engineering: Electrical Engineering

in the Faculty of Engineering and the Built Environment

at the Cape Peninsula University of Technology

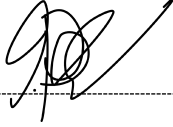**Supervisor: Dr Gideon Wiid**
Co-Supervisor: Dr Kessie Govender

Bellville

August 2023

DECLARATION

I, Inge Chleo Pearce, declare that the contents of this thesis represent my own unaided work, and that the thesis/dissertation has not previously been submitted for academic examination towards any qualification. Furthermore, it represents my own opinions and not necessarily those of the Cape Peninsula University of Technology.

---   25 October 2023
Signed   **Date**

ABSTRACT

This research focuses on the design, manufacture, and testing of a conical terminated Transverse Electromagnetic (TEM) cell. The conical terminated TEM cell will be used for pre-compliance electromagnetic testing at the Cape Peninsula University of Technology. The requirement is focused on designing such a cell that is suitable for desktop use and capable of operating across a frequency range of DC to 1.0 GHz with a working volume of 10 × 10 × 10 cm.

This thesis presents a comprehensive overview of the principles as laid out by Giri and Baum, 1996. Design considerations are discussed after which calculations, determining the cell geometry, are performed. The conical terminated TEM cell is simulated in AltairFeko and various adjustments are made to determine which model results in an S_{11} lower than -10 dB across the prescribed frequency range. The S_{11} study includes the determination that the model is negligibly affected with the insertion of, and in the absence of a device under test. S_{11} measurements are conducted up to 2.5 GHz, to test the S_{11} response at a frequency higher than what the cell is designed. Electromagnetic studies are conducted in AltairFeko to determine the largest achievable working volume by investigating electric field uniformity. These studies also include the worst-case effect that a device under test of ≈ 10 × 10 × 10 cm has on the working volume. The model that meets the criteria is manufactured. Manufacturing components are dictated by guidelines based on the literature study.

S_{11} measurements are conducted using a nanoVNA vector network analyzer and then using a RF analyzer with a vector network analyzer capability, in an unshielded laboratory environment. Measured results are then analyzed in AltairFeko and Matlab. From 0.4 GHz to 2.5 GHz the S_{11} remains below -10 dB. Considering the measured results with and without a DUT we observe similar results with the insertion of a DUT having a negligible effect on the S_{11}.

As verification, the working volume is simulated and analyzed using 3 electromagnetic slices closest to the ground plane, intersecting the middle of the volume parallel to the top-plate and another slice closest running parallel to the top-plate. These studies are observed at 0.5 GHz and 1.0 GHz, with and without a device under test. Field uniformity was validated by the IEC 61000-4-3 standard; with 75 % of the measured points within the working volume measured to be within 0 dB to + 6 dB.

This confirms that the manufactured conical terminated TEM cell complies to the relevant standards for use as an EMC pre-compliance test setup.

ACKNOWLEDGEMENTS

DEDICATION

Thank you, God.

To my parents, Elizabeth and Beresford, thank you for instilling in me the value of education and the importance of using the gifts I have been blessed with. For your constant encouragement and 'keep going' whispers, thank you Melissa. Taryn, you have walked this journey and every other with me, you are the sun.

To my brother, Ulrich, you continue to inspire me. This would not be possible without you.

My world is beautiful with all of you in it.

"Many of life's failures are people who did not realize how close they were to success when they gave up." ~ Thomas A. Edison

TABLE OF CONTENTS

LIST OF FIGURES

LIST OF ACRONYMS/ABBREVIATIONS

5G	5th Generation
Altair Feko	Computational EM software
CGE	Comb generator emitter
CISPR	International Special Committee on Radio Interference
CPUT	Cape Peninsula University of Technology
DUT	Device under test
EM	Electromagnetic
EMC	Electromagnetic compatibility
EMI	Electromagnetic interference
EMP	Electromagnetic pulse
FAR	Fully anechoic rooms
GTEM	Gigahertz transverse electromagnetic cell
IEC	International Electrotechnical Commission
IoT	Internet of things
MATLAB	Matrix Laboratory (Software)
OATS	Open area test site
RAM	Radio absorbing material
RF	Radio frequency
RQ	Research question
SARAO	South African Radio Astronomy Observatory
SANSA	South African National Space Agency
SMA connector	subMiniature Version A connector
TDR	Time domain reflector
TE	Transverse electric
TM	Transverse magnetic
TEM	Transverse electromagnetic
VNA	Vector network analyzer
VSWR	Voltage standing wave ratio

CHAPTER 1: INTRODUCTION

1.1 Introduction

Conferences that dealt with electromagnetic compatibility (EMC) related areas began in the 1950s (Testing for EMC Compliance: Approaches and Techniques, 2004). The introduction of more consumer electronics in the 1970s necessitated EMC/EMI regulatory requirements. Today electronics exists all around us in telecommunications, entertainment, space, transport, health and engineering sectors and with the introduction of the Internet of things (IoT) and 5th generation networks (5G) continues to grow. The plethora of devices radiating radio frequency (RF) energy on the market increases the risk of inadvertent frequency interference.

Equipment is required to undergo electromagnetic (EM) qualification to ensure accuracy; and that quality and safety standards are met. These standards are included in the International Electrotechnical Commission (IEC) 61000 series of international standards and International Special Committee on Radio Interference (CISPR) 16 series of international standards for EM testing.

Radiated emissions (RE) and radiated immunity (RI) tests are conventionally conducted using anechoic chambers, open area test sites (OATS) and reverberation chambers. These test facilities all require large areas of space. OATS are weather dependent and there exists the challenge of ambient frequencies. Anechoic chambers are costly, in the order of millions of Rands, depending on application, frequency range and materials used.

In the following section we explore RE and RI concepts in more detail.

1.2 EMC concepts

It is imperative that we can control and predict the EM behavior of electronic devices as the introduction of EMI in a system may cause a device to malfunction or may result in performance degradation (Omollo, 2019). EMC testing thus ensures that a device can function in its environment without interfering with itself or other devices.

Electromagnetic interference (EMI) can be described as the temporary or permanent perturbation of an electrical circuit caused by man-made or natural EMI sources. This phenomenon occurs when EM energy is transmitted between devices (or intrinsically) through radiated or conducted paths, pictured in Figure 1.1 below.
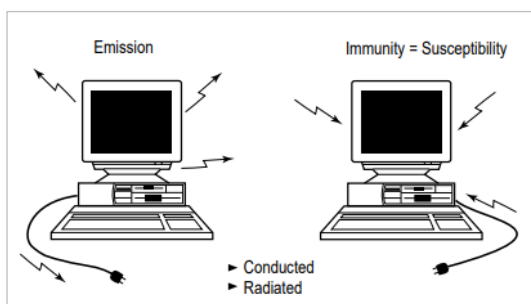
Figure 1.1: Radiated emissions and radiated immunity (Hewlett-Packard Company, 1998).

The focus of this research will be on radiated immunity and radiated emissions testing, these concepts are defined below:

- Radiated Immunity (RI) testing: The evaluation of a device under test (DUT) RF and/or EM response when exposed to a radiated RF and/or EM field (International Electronical Commission, 2006).
- Radiated Emissions (RE) testing: The measurement of the unintentional EM field emissions generated by a DUT.

For electronic equipment to meet EMC design requirements it is necessary to suppress unwanted EM energy. EMI suppression occurs at three design levels: circuit board level, equipment interfaces and enclosures (Clark *et al.*, 1995).

Circuit board level suppression considers the grounding and layout of the circuit board, limiting the speed and bandwidth of a signal, and selection of electronic components.

EMI suppression at the equipment interface level is achieved by filtering, isolation and shielding. Filtering and isolation concern the prevention of EMI via conducted paths, whereas shielding of equipment interfaces involves the prevention of EMI via radiated paths.

Suppression by enclosures and the term EMI shielding may be used interchangeably. An EMI shield is a barrier used to control the propagation of electric and magnetic fields between two regions by either reflecting or absorbing the electromagnetic field.

Having discussed methods of RI and RE testing we consider the EMC standards that govern testing conducted to ensure that electronic devices do not generate or are affected by EM interference.

1.3   EMC standards

The IEC 61000 and CISPR series of standards provides several international EMC standards concerning radiated emissions and radiated immunity. Provided below is a list of CISPR standards regarding EMC testing setups/methods and general radiated emissions and radiated immunity standards:

- CISPR 16-1, Specification for radio disturbance and immunity measurement apparatus and methods - Part 1: Radio disturbance and immunity measuring apparatus (IEC CISPR, 16-1-1 ed5.0, 2019).
- CISPR 16-2, Specification for radio disturbance and immunity measurement apparatus and methods - Part 2: Methods of measurement of disturbances and immunity (IEC CISPR, 16-2 ed2.0, 2003).
- CISPR 16-3, Specification for radio disturbance and immunity measurement apparatus and methods - Part 3: Reports and recommendations of CISPR (IEC CISPR 16-3 ed4.0, 2020).
- CISPR 16-4, Specification for radio disturbance and immunity measurement apparatus and methods - Part 2: Uncertainties, statistics, and limit modelling — Uncertainties in standardized EMC tests (IEC CISPR 16-4 ed2.2, 2018).

IEC 61000-4 series of standards that discuss EMC testing setups/methods and general radiated emissions and radiated immunity are:

- IEC EN 61000-4-3, EMC Part 4-3: Testing and measurement techniques - Radiated, radio-frequency, electromagnetic field immunity test (IEC 61000-4-3 ed4.0, 2020).
- IEC 61000-4-20, EMC – Part 4-20: Testing and measurement techniques – Emission and immunity testing in TEM waveguides (IEC 61000-4-20 ed2.0, 2010).
- IEC 61000-4-21, EMC – Part 4-21: Testing and measurement techniques – Reverberation chamber test methods (IEC 61000-4-21 ed2.0, 2011).

An additional military standard, MIL-STD 461 (Mazzola, 2009), for electromagnetic compatibility methods is also considered in the discussion of reverberation chambers. The IEC 61000 and CISPR series of standards above for RE and RI testing can be applied at various stages: pre-compliance, post-modification tests and final compliance, these project phases are discussed in the following section.

1.4 Requirements and use cases for EMC testing

EMC testing is required to ensure that devices have been designed to meet safety and regulatory standards. Due to global trade, countries and organizations stipulate those products need to adhere to various EMC regulatory requirements such as the IEC 61000 and CISPR 16 international standards.

It is necessary to consider EMC requirements in all project phases, from design to implementation, refer to Figure 1.2. The list below covers the various EMC testing phases. For this research we focus on the design of a testing setup purposed for the pre-compliance stage.

- Pre-compliance: A cost-effective manner to determine whether the DUT will pass or fail final compliance testing at a laboratory.
- Post-modification: On-going compliance checks to evaluate EM changes before and after modification of a product.
- Component Evaluation: Comparing EMI performance of components from different/the same manufacturer.
- Final compliance: Final stage of testing to ensure product meets regulatory standards.
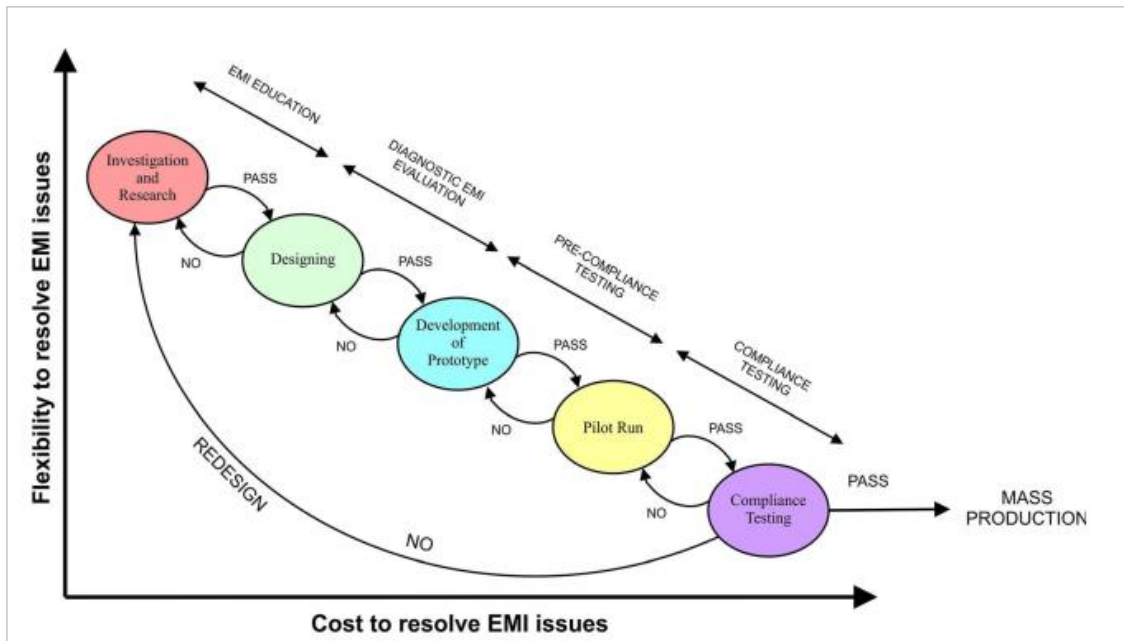
Figure 1.2: Product development flowchart indicating EMC tests at various stages (Mathur & Raman, 2020)

Although the focus is on the pre-compliance of EM equipment at The Cape Peninsula University of Technology (CPUT), the conical terminated TEM cell will also be capable to perform post-modification EMC testing within the lab environment at CPUT. This is described in the following section where we introduce the research problem.

1.5 Statement of research problem

With the financial and time limitations imposed on users required to perform in-house EMC testing a need has arisen to design and manufacture an EMC testing setup suitable for a lab environment. A small, versatile bench-top testing setup is required that is cost-efficient and space-efficient and will allow for testing of smaller components at lower frequencies (DC to 1 GHz). The length of the cell is limited to less than 1.2 m to ensure suitability for benchtop use.

One such solution proposed in this research, is a conical terminated transverse electromagnetic (TEM) cell with operational frequency DC to 1 GHz. The focus of the research

will be on E-field immunity. The cell will be used for pre-compliance EMC testing at CPUT and will be designed, manufactured, and assessed.

The research questions and objectives below guide us in the design, manufacturing and assessment of the conical terminated TEM cell.

1.6 Research questions and objectives

Looking at the requirement of the conical terminated TEM cell used for pre-compliance testing at CPUT we define the research questions and objectives.

- **Research Question (RQ) 1**: What is the maximum achievable working volume inside the conical terminated TEM cell with dimensions practical enough for benchtop use?
- **Objective to RQ 1:** To design a conical terminated TEM cell with a useful working volume large enough to accommodate a 1U CubeSat (10 cm × 10 cm × 10 cm).

- **RQ 2:** What is the range of operating frequencies of the conical TEM cell?
- **Objective to RQ 2:** To determine the cut-off frequency and range of frequencies at which measurements are stable across the test volume, preferably up to 1 GHz or above.

- **RQ 3:** How does the performance of the conical terminated TEM cell compare to a conventional TEM cell of similar size?
- **Objective to RQ 3:** To assess the performance characteristics of a conical terminated TEM cell versus a conventional TEM cell.

- **RQ 4:** How does the performance of the conical terminated TEM cell compare to other test facilities such as a reverberation chamber?
- **Objective to RQ 4**: To assess the accuracy of the terminated TEM cell compared to a reverberation chamber.

The research questions and objectives defined above will ensure fulfilment of a versatile bench-top test setup that is cost-effective and space-efficient, operating between DC and 1 GHz.

We provide a list of expected research outcomes that will be derived from the research questions.

1.7 Expected outcomes

The following outcomes are expected to derive from this research:

- A manufactured conical terminated TEM cell, with operating frequency range of DC to 1 GHz, able to house a DUT with minimum dimensions of 10 cm × 10 cm × 10 cm.
- Thesis
- Research publication

This body of research will document the literature review, manufacture of the artefact, findings, conclusion, and recommendations of a versatile benchtop conical terminated TEM cell operating between DC to 1 GHz after which a research article will conclude the research.

1.8 Significance of the research

CPUT will be able to conduct in-house radiated immunity and radiated emissions testing on-site in their lab facilities. This will aid in pre-compliance, diagnostic, post-modification EMC tests and provide a fair indication whether devices developed at CPUT will pass final compliance EMC tests. The desktop conical terminated TEM cell that is manufactured will accelerate time-to-market of products and save money where hiring of other EMC testing facilities will only be required for final compliance testing.

Below we describe the research methods that will be employed to answer the research questions and achieve the related objectives.

1.9 Research methodology

We use Saunders Research Onion (Saunders *et al.* 2019) to define the research methodology and design that is employed in this research.

The research techniques and procedures define the type of data being used, how this data is collected, and which data analysis methods and data analysis tools are used.
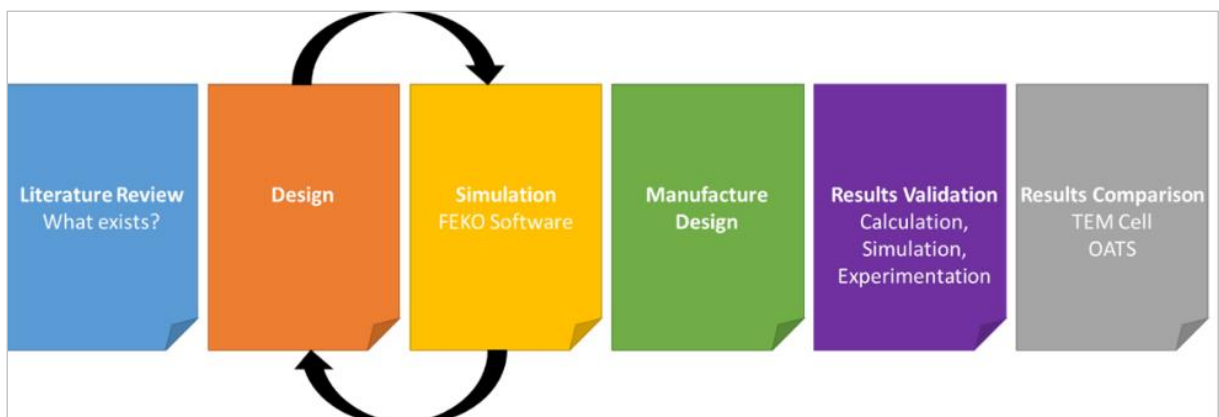
Figure 1.3: Flow diagram illustrating the research methodology approach.

Figure 1.3 illustrates the research methodology approach employed in this research and is further explained below.

- Literature review: Identify what EMC testing setups currently exist. What are their advantages, disadvantages and how they compare, in theory, to the conical terminated TEM cell?

- Design: Design the terminated TEM cell with design considerations (mentioned in Chapter 3).

- Simulation: Model and simulate results in FEKO (computational EM software), to determine if the model meets the criteria as stated in the design.

- Manufacture design: Model will be built according to design parameters.

- Validate results:

  - Simulation: Compare observed results from model and DUT to expected results as per FEKO simulations.

  - Experimentation: Compare observed results from model and DUT to TEM cell.

- Compare results: Compare observed results from model to:
  - TEM cell.
  - OATS.
  - Anechoic chamber.

We conclude the discussion of the research methodology employed in this body of research and explore various EMC testing facilities and their uses cases in Chapter 3.

1.10 Thesis layout

To design and manufacture the conical terminated TEM cell a literature survey is done (Chapter 2) wherein various EMC testing facilities and use cases are presented. The cell is then designed according to the guidelines as presented by Giri and Baum, 1996 (Chapter 3 and Chapter 4) after which it is modelled in Altair Feko (Altair Feko, n.d) to determine the S_{11} reflection coefficient, working volume and the near-field output.

After manufacturing and testing the cell, simulated and measured results are presented and analysed (Chapter 5 and Chapter 6). Chapter 7 covers recommendations for future work after which this research is concluded.

CHAPTER 2: LITERATURE REVIEW

2.1 Introduction

The TEM cell was first introduced by Myron L. Crawford in 1974, used to generate a standard, uniform electromagnetic field in a shielded environment. The cell was proven to be useful in testing the radiated emissions and immunity of small to medium sized equipment at frequencies ranging between DC and 0.5 GHz. At the time established techniques for performing radiated emissions and immunity testing included gain horns and parallel plate lines (Crawford, 1974). However, both these testing methods presented a drawback in that they radiate EM energy into the ambient environment, introducing EMI in the measurements.

The ideal environment in which to conduct EMI measurements is therefore in a shielded environment. In the past radiated emission and radiation immunity testing has typically been conducted using reverberation chambers, anechoic chambers and OATS, this remains largely true today. The TEM cell has its advantages over these EMC testing setups as it (depending on design specification) does not require a fixed area of installation, is easier and cheaper to manufacture and is scalable over a wide range of frequencies. We now look at various types of EMC test facilities and methods.

2.2 Types of EMC test facilities and methods

There exists an array of testing facilities/methods. These setups include reverberation chambers, semi-anechoic chambers, fully-anechoic chambers, OATS, probes and gigahertz transverse electromagnetic (GTEM) cells and TEM cells.

The choice of EMC testing facility/method is dependent on several variables, these are presented in tabular format below. In Table 1 we summarize the EMC testing methods/facilities and their characteristics as related to variables such as: application, budget, size of DUT, desired frequency range, space available, stage of design.

Table 1: EMC testing facility comparison

Testing facility	Application	Budget	DUT size	Frequency Range	Space available	Design stage
Reverberation Chamber	RE/RI	Hundreds of thousands to Millions (R)	Small to very large, dependent on chamber size	0.5 GHz – 18 GHz	Large, dedicated area	Pre, final and post-modification
Anechoic Chamber	RE/RI	Hundreds of thousands to Millions (R)	Small to very large, dependent on chamber size	0.3 GHz – 18 GHz	Large, dedicated area	Pre, final and post-modification
OATS	RE	Thousands to tens of thousands (R)	Small to very large, dependent on chamber size	30 MHz – 1 GHz	Large, dedicated area	Pre, final and post-modification
GTEM Cell	RE/RI	Thousands to tens of thousands (R)	Small, dependent on window size	RI < 2.3 GHz, RE < 2.4 GHz	Compact, can be transported	Pre, final and post-modification
TEM Cell	RE/RI	Thousands to tens of thousands (R)	Small, dependent on window size	DC – 4 GHz	Compact, can be transported	Pre-compliance

Consideration of these variables is important in determining which EMC test facility/method is best fit for purpose and are included in the discussion of each EMC test facility/method.

2.3   Reverberation chambers

When conducting EMC testing it is preferable to isolate a DUT from the ambient EM environment. It is also illegal to intentionally radiate high EM waves across a range of frequencies from a device whilst it is unshielded. The use of screened chambers for EMC testing gained popularity around the late 1960s in the military industry where equipment performance is mission-critical and thus required to meet strict specifications (Morgan, 1994).

The reverberation chamber was first introduced in 1968 by H. A. Mendes, designed for an array of RF applications which include but is not limited to: material, antenna and sensor characterization, EM radiated emissions and EM radiated immunity tests (Yousaf *et al.*, 2020).

A reverberation chamber is a screened chamber enclosed by conductive surfaces containing a transmitting antenna and receiving antenna wherein various frequency modes are randomly excited by mechanical stirrers. Repeated reflections of the conducting surfaces results in the EM environment within the chamber. The EM environment is the superposition of the generated plane waves, with random phase (Rajamani *et al.*, 2008).

Figure 2.1: Picture illustrating reflective surfaces and stirrers inside a reverberation chamber (Sim et al., 2019)

The reverberation chamber, as illustrated in Figure 2.1, offers advantages such as the generation of a high field strength without requiring high input power, rendering results in a relatively short duration (Yousaf *et al.*, 2020). Also, the structure and size of the chamber allows for a large DUT to be placed inside the testing volume. As The DUT is subjected to an EM field in all three axes simultaneously, compared to an anechoic chamber and OATS, it does not need to be rotated in different orientations to take measurements (Mathur & Raman, 2020). Depending on the size, reverberation chambers are capable of testing larger DUT in the order of 0.5 GHz – 18 GHz. The complexity of design and materials required does however necessitate a large budget. The use of reverberation chambers also requires a large, dedicated area in which to house this test setup.

2.4 Anechoic chambers

A fully anechoic chamber, refer to Figure 2.2, is an EMC testing setup completely covered in radio absorbing material (RAM), a highly absorptive material, and 'completely' free of reflective surfaces. With the floor also covered in RAM, reflections do not occur from the floor and as such the environment inside a fully anechoic chamber is free of reflections, thereby simulating a free-space environment.

RAM is intended to absorb RF energy, the type of RAM used in an anechoic chamber is unique to the use case for which the chamber is intended. There are three main shapes of RAM used, these are: pyramidal, wedge and convoluted. Depending on the material type of the RAM; urethane foam with carbon black, metallized plastic with foam supports or a hybrid material, each absorber operates at different frequency ranges and reflectivity. Depending on the shape, material and height of the RAM anechoic chambers can absorb frequencies in the order of 30 MHz to the higher GHz frequency range (Pywell & Midgley-Davies, 2017).
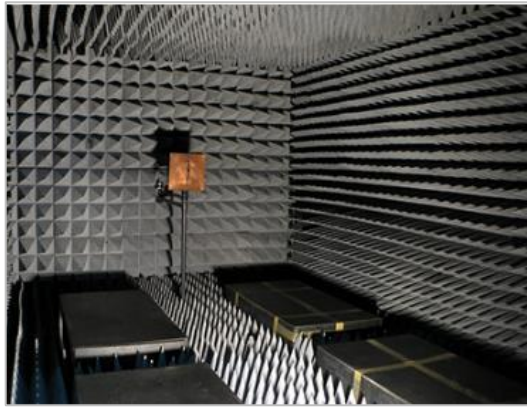
Figure 2.2: Fully anechoic chamber with pyramidal RAM (RF Design, 2019)

A semi-anechoic chamber is also a shielded room; however, the walls and ceiling are covered in absorbent material and the floor is not. The floor of a semi-anechoic chamber is covered in a metallic, conductive ground plane, meaning this facility is not entirely free of reflections as compared to its counterpart, the fully anechoic chamber. Semi-anechoic chambers, as seen in Figure 2.3, are usually selected over fully anechoic chambers where the DUT is considerably large and requires a load-bearing ground plane.

Figure 2.3: Semi-anechoic chamber at an Electronic Warfare Test Facility (Pywell & Midgley-Davies, 2017)

Typically used in the air force, automotive and military environments the anechoic chamber allows EMC testing on information-sensitive equipment and systems in a shielded environment.

Disadvantages of this testing facility include added cost and in-house area requirements. The addition of RAM is expensive and can vastly increase the cost. Besides the addition of absorbers, anechoic chambers need to be shielded to attenuate undesirable RF signals from the surrounding environment. These added design requirements make an anechoic chamber a very expensive testing facility to manufacture and build.

2.5   Open area test sites

An OATS is an open test area with a conductive ground plane. Radiated emissions from the DUT is measured using an adjustable (height) antenna above the ground plane, refer to Figure 2.4. For OATS measurements to be deemed accurate the antenna must be calibrated and the antenna factor (AF) determined. The AF provides the mathematical relationship between the DUT incident EM field and the antenna's output voltage.

Measurements are taken at 3 m and 10 m separation between the antenna and DUT. The allowable size of the DUT and antenna separation is specified in the CISPR 16 standard (Mathur & Raman, 2020).

Figure 2.4: A low level swept field OATS setup (Intel Platform Design).

OATS provides a major advantage over other EMC test setups where large-scale DUT such as aircraft can be tested. As it is an open test environment it does however present several pitfalls such as immunity to environmental EMI and adverse weather. The immunity to environmental EMI is a major pitfall where the radiated emissions of a DUT is considerably lower. At frequencies lower than 30 MHz ambient noise levels would render the test ineffectual (Dawson and Marvin, 1999).

OATS are thus ideally situated in remote locations, clear of reflections, to negate environmental noise pollution. This produces a logistical and costly issue where travel time and cost to site would be deemed unfeasible for a smaller organization.

2.6   GTEM cell

The GTEM cell, as included in the IEC 61000-4-20 "Emission and Immunity Testing in TEM Waveguides" standard, is a hybrid configuration of the anechoic-chamber and TEM cell.

The GTEM cell, as illustrated in Figure 2.5 and Figure 2.6 below, is a single-port shielded rectangular coaxial stripline which supports TEM mode (Ghosh *et al.*, 1999). In a conventional TEM cell, the inner and outer conductors have different lengths, limiting the usable frequency range as signals travel at different rates along the conductors. The GTEM cell is however

designed as a rectangular transmission line. The inner and outer conductors are of the same length, resulting in wide frequency bands as signals arrive at the load at the same time (Icheln, 1995). As GTEM cells are terminated cells with a resistive load and absorbers, they are suitable for radiated immunity tests up to 2.3 GHz and for radiated emissions tests up to 2.4 GHz far higher than the conventional TEM cell (Nothofer *et al.*, 2003).
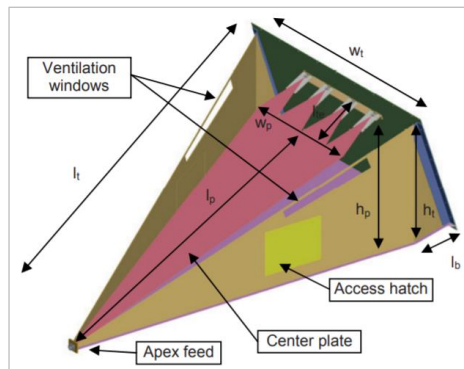
Figure 2.5: Computer Aided Design (CAD) model of a GTEM cell (Stander & Sinha, 2013).
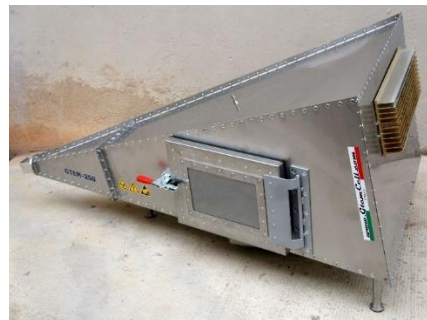
Figure 2.6: GTEM cell with access hatch (GTEM 250 F – GTEM250 F SAE – GTEM FV, Absolute EMC)

The application of hybrid termination within the GTEM cell is to minimize the reflections which affects field uniformity. Higher-order modes cannot be terminated by the sole use of resistors and so to reduce these wave-guide modes (EM waves reflected from the conductor walls) RAM is incorporated against the inside wall of the GTEM cell (Icheln, 1995).

Due to the shielding of the GTEM cell measurements are not adversely affected by the ambient EMI environment. As the GTEM is highly scalable, EMC measurements can be performed on small PCBs to vehicles and (dependent on design) can be compact. It is affordable compared to reverberation chambers and anechoic chambers it is a preferred method of EMC testing.

2.7   TEM cells

The TEM cell designed by Crawford in 1974 is a dual-port transmission line, rectangular in shape with tapered ends, which generates planar waves in TEM mode. The TEM cell was

originally used for radiated emissions and immunity testing, and the calibration of EM radiation hazard meters and field-strength meters. At the time, EMC testing of the applications were conducted using gain horns and parallel plate lines. These methods however radiate EM energy in the ambient environment and were therefore unfavourable, whereas the TEM cell produces a uniform EM field distribution in a shielded environment. These cells are used for wide-band EMC testing but are limited to small-to-medium size DUT as the cut-off frequency is a function of the geometry of the cell. Above the cut-off frequency higher-order modes are generated and measurements become less accurate. The upper usable frequency range of the TEM cell decreases as the size of the cell is increased, making the cell better suited for EMC testing of small-to-medium DUT (Crawford, 1974).

As illustrated in Figure 2.7, two variations of the conventional TEM cell exist; open and closed. The closed TEM cell has a window through which the DUT can be inserted, in this scenario the DUT is completely shielded from ambient EMI. In an open TEM cell there are no side walls, exposing the DUT to surrounding EMI.
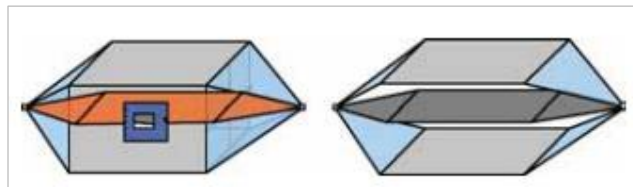
Figure 2.7: A closed (left) and open (right) TEM cell (Satav & Agarwal, 2008)

TEM cells can be designed to operate at lower frequencies in the order of DC to several MHz, allowing RE and radiated immunity tests in lower frequency bands. The closed TEM cell presents an advantage in the fact that it produces measurement results closely matched to those of an OATS. As a result, only closed TEM cells are qualified for performing final compliance EMC testing (Satav & Agarwal, 2008).

The use of a TEM cell as an in-house laboratory setup requires little space and measurement is automated. Compared to an OATS the TEM cell eliminates the requirement of an antenna to generate EM fields. TEM Cells are thus an affordable, reproducible, and accurate laboratory setup for conducting in-house EMC testing.

Figure 2.8: Photograph of a conventional TEM cell (emcsupplies.com, n.d)

TEM cells are typically terminated using a 50 Ω termination and designed with a 50 Ω characteristic impedance across the entire length of the cell ensuring that the current applied to the centre conductor is met by a matched load and thereby preventing reflections.

The height of the DUT inside the TEM cell is typically $\frac{1}{3}$ of the height between the inner and outer conductor. The physical dimensions as well as the angle of incidence at the tapered ends of the cell are of significance as it limits the usable frequency range of the cell, above which higher order modes are generated (Icheln, 1995).

TEM cells typically have a lower limit of 1 kHz as it is inversely related to the cross-section of the cell. This is a notable disadvantage compared to the GTEM cell that is not limited in frequency, operating in the GHz range, due its shape. Both these cells are, however, restrictive in the size of DUT that can be accommodated in the working volume of the cell (Bentz, 1996).

From the IEC 61000-4-3 standard for testing and measurement techniques concerning radiated, radio-frequency, electromagnetic field immunity tests a field is considered uniform if at least 12 of 16 points across a defined area are measured within - 0 dB to + 6 dB. This specification applies to a field uniformity across an area of 1.5m × 1.5m. It is thus translated to consider the smaller geometry of a TEM cell, meaning that to determine the useful working volume within a TEM cell 75% of the measured points needs to be within – 0 dB to +6 dB of each other. The useful maximum working volume of a TEM cell is traditionally accepted as "$\frac{1}{3}$ of the distance between septum and outer conductor $\times$ $\frac{1}{3}$ of the cell width" (Bentz, 1996).

Single-conductor waveguides support transverse electric (TE) and transverse magnetic (TM) wave propagation, evident in the presence of longitudinal magnetic and electric components. The TEM cell is however a dual transmission line and thus supports the propagation of waves in TEM mode, meaning that there are no longitudinal magnetic or electric components.

The TEM cell forms the basis of this research, in the following section we discuss TE, TM, and TEM wave propagation modes to better understand the conical terminated TEM cell design.

2.8   TEM mode

To interpret the conical terminated TEM cell design we observe the propagation modes for a waveguide with uniform cross-section along the length of the cell, adapted from Adams (2014):

Transverse Electric (TE) mode: Electric field (E) has only transverse components, magnetic field (H) has longitudinal and transverse components.

$$E_z = 0, H_z \neq 0 \hspace{4cm} \text{Equation (2.1)}$$

Transverse Magnetic (TM) mode: Magnetic field (H) has only transverse components, electric field has longitudinal and transverse components.

$$H_z = 0, E_z \neq 0 \qquad\qquad \text{Equation (2.2)}$$

Transverse electromagnetic (TEM) mode:

$$E_z = H_z = 0 \qquad\qquad \text{Equation (2.3)}$$

The TEM wave is characterised by the fact that the Electrical (E) and Magnetic (H) vectors are always perpendicular to one another in free space (377Ω) and transverse to the direction of propagation. TEM mode does not exist in a 1-conductor waveguide.

From Microwave Engineering by David Pozar, the electric and magnetic fields for wave propagation along the z-axis where $\bar{e}(x, y)$ describes the transverse electric field component and $\bar{h}(x, y)$ the transverse magnetic field component:

$$\bar{E}(x, y, z) = [\bar{e}(x, y) + \hat{z} e_z(x, y)]e^{-j\beta z} \qquad\qquad \text{Equation (2.4)}$$
$$\bar{H}(x, y, z) = [\bar{h}(x, y) + \hat{z} h_z(x, y)]e^{-j\beta z} \qquad\qquad \text{Equation (2.5)}$$

Assuming the transmission line region is source-free, Maxwell's equations can be written as:

$$\nabla \times \bar{E} = -j\omega\mu\bar{H} \qquad\qquad \text{Equation (2.6)}$$
$$\nabla \times \bar{H} = -j\omega\mu E \qquad\qquad \text{Equation (2.7)}$$

Electric and magnetic field components for each vector equation:

$$\frac{\partial E_z}{\partial y} + j\beta E_y = -j\omega\mu H_x \qquad\qquad \text{Equation (2.8)}$$

$$-j\beta E_x - \frac{\partial E_z}{\partial x} = -j\omega\mu H_y \qquad\qquad \text{Equation (2.9)}$$

$$\frac{\partial E_y}{\partial x} - \frac{\partial E_x}{\partial y} = -j\omega\mu H_z \qquad\qquad \text{Equation (2.10)}$$

$$\frac{\partial H_z}{\partial y} + j\beta H_y = -j\omega\epsilon E_x \qquad\qquad \text{Equation (2.11)}$$

$$-j\beta H_x - \frac{\partial H_z}{\partial x} = -j\omega\epsilon E_y \qquad\qquad \text{Equation (2.12)}$$

$$\frac{\partial H_y}{\partial x} - \frac{\partial H_x}{\partial y} = +j\omega\epsilon E_z \qquad\qquad \text{Equation (2.13)}$$

The four transverse field components (E_x, E_y, H_x, H_y) can be solved for in terms of E_z and H_z:

$$E_x = \frac{-j}{k_c{}^2}\left(\beta \frac{\partial E_z}{\partial x} + \omega\mu \frac{\partial H_z}{\partial y}\right) \qquad\qquad \text{Equation (2.14)}$$

$$H_x = \frac{j}{k_c{}^2}\left(\omega\epsilon \frac{\partial E_z}{\partial y} - \beta \frac{\partial H_z}{\partial x}\right) \qquad\qquad \text{Equation (2.15)}$$

$$E_y = \frac{j}{k_c{}^2}\left(-\beta\frac{\partial E_z}{\partial y} + \omega\mu\frac{\partial H_z}{\partial x}\right) \qquad \text{Equation (2.16)}$$

$$H_y = \frac{-j}{k_c{}^2}\left(\omega\epsilon\frac{\partial E_z}{\partial x} + \beta\frac{\partial H_z}{\partial y}\right) \qquad \text{Equation (2.17)}$$

and the cut-off wave number:

$$k_c{}^2 = k^2 - \beta^2 \qquad \text{Equation (2.18)}$$

Where k is defined as the wave number of the material filling the transmission line

$$k = \omega\sqrt{\mu\epsilon} = {}^{2\pi}/_2 \qquad \text{Equation (2.19)}$$

Equation (2.19) can be applied to various waveguides and are not specific to distinct wave types.

As mentioned, TEM mode wave propagation is characterized by the absence of longitudinal components in the electric and magnetic fields, Equation (2.3). Applying the condition $E_z = H_z = 0$, to Equations (2.13 to 2.16) and by eliminating H_x, we obtain:

$$\beta^2 E_y = \omega^2\mu\epsilon E_y \qquad \text{Equation (2.20)}$$

Or

$$\beta = \omega\sqrt{\mu\epsilon} = k \qquad \text{Equation (2.21)}$$

The cut-off wave number, k_c is thus zero for TEM waves.

The Helmholtz equation for E_x is given as:

$$\left(\frac{\partial^2}{\partial x^2} + \frac{\partial^2}{\partial y^2} + \frac{\partial^2}{\partial z^2} + k^2\right)E_x = 0 \qquad \text{Equation (2.22)}$$

but, for $e^{-j\beta z}$ dependence $\left(\frac{\partial^2}{\partial z^2}\right)E_x = -k^2 E_x$, therefore Equation 2.22 is reduced to

$$\left(\frac{\partial^2}{\partial x^2} + \frac{\partial^2}{\partial y^2}\right)E_x = 0 \qquad \text{Equation (2.23)}$$

A similar result applies to E_y. $\Delta_t^2 = {}^{\partial^2}/_{\partial x^2} + {}^{\partial^2}/_{\partial y^2}$ is the Laplacian operator in the x, y dimensions, the equation can thus be written as:

$$\Delta_t^2\bar{e}(x,y) = 0 \qquad \text{Equation (2.24)}$$

Indicating that $\bar{e}(x,y)$ of a TEM wave satisfies Laplace's equation. It is shown that $\bar{h}(x,y)$ also satisfies Laplace's equation:

$$\Delta_t^2\bar{h}(x,y) = 0 \qquad \text{Equation (2.25)}$$

TEM waves only exist in the presence of two or more conductors. However, they do not exist in closed conductors as the static potential would be zero, resulting in $\bar{e} = 0$.

Z_{TEM}, wave impedance describes the transverse field components and only depends on the material constants. The wave impedance of a TEM wave is given as the ratio of E_x, H_y:

$$Z_{TEM} = \frac{E_x}{H_y} = \frac{\omega\mu}{\beta} = \sqrt{\frac{\mu}{\epsilon}} = \eta \qquad \text{Equation (2.26)}$$

and

$$Z_{TEM} = \frac{-E_y}{H_x} = \sqrt{\frac{\mu}{\epsilon}} = \eta \qquad \text{Equation (2.27)}$$

Combining the two equations for the impedance of a TEM mode wave yield:

$$\bar{h}(x,y) = \frac{1}{Z_{TEM}} \hat{z} \times \bar{e}(x,y) \qquad \text{Equation (2.28)}$$

Z_{TEM}, wave impedance, should not be confused with Z_0, characteristic impedance, that associates voltage and current as a function of geometry. The equation for characteristic impedance is given as:

$$Z_0 = V/I \qquad \text{Equation (2.29)}$$

This concludes the discussion regarding wave propagation in TEM mode and wave impedance in a dual transmission line in understanding the design of the conical terminated TEM cell.

2.9   Conclusion

In this section we covered various EMC testing methods and facilities including OATS setups, shielded chambers, GTEM and conventional TEM cells. Having discussed TE, TM and TEM mode wave propagation in a multi-conductor waveguide and the wave impedance of a TEM wave pertinent to TEM cells. In the next chapter we discuss the focus of this research, being the conical terminated TEM cell.

CHAPTER 3: CONICAL TERMINATED TEM CELL DESIGN CONSIDERATIONS

3.1   Introduction

The focus of this research is the design, simulation and manufacturing of a conical terminated TEM cell as investigated in Giri and Baum, 1996. The foundation of their research was the generation of a TEM wave propagating in a waveguide, similar to that generated at a distance by an electromagnetic pulse (EMP).

EMP simulators can be vertically or horizontally polarized and include a wave receptor, wave launcher, pulser, terminator and parallel-plate region, see Figure 3.1.

Impedance, electric field and magnetic field discontinuities are introduced as the wave launcher and receptor interfaces have conical lines. Additionally, TE or TM mode wave excitation is expected where the bends on either side and these conical lines join the cylindrical line in the central region.
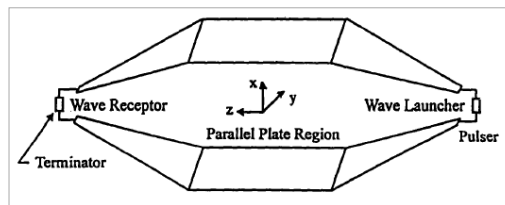
Figure 3.1: Example of a parallel-plate transmission line simulator (Giri & Baum, 1996)

To mitigate these concerns Giri and Baum propose an extended conical transmission line terminated using a distributed terminator, i.e. a conical terminated TEM cell. The benefit of this design includes: a decreased simulator length for a certain working volume, removed input/output bend at the central region and higher frequencies that do not necessitate termination.

However, the trade-off of these benefits is that; planar TEM waves are not generated, instead spherical TEM waves with a large radius resemble planar TEM waves and a large, distributed termination is required.

Giri and Baum present a conceptual sketch of a conical transmission line with distributed termination, consisting of a ground plane, top plate, pulser and termination; see Figure 3.2. This is a large-scale sketch and is contextual to the testing of vehicles, much larger to that which is being designed.

The top plate and ground plane each form one-half of a symmetrical conical waveguide which terminates spherical TEM waves with characteristic impedance, Z_0, between 80 Ω to 100 Ω.

The model and design covered in Chapter 4 will follow the principles and guidelines as explored by Giri and Baum, 1996.
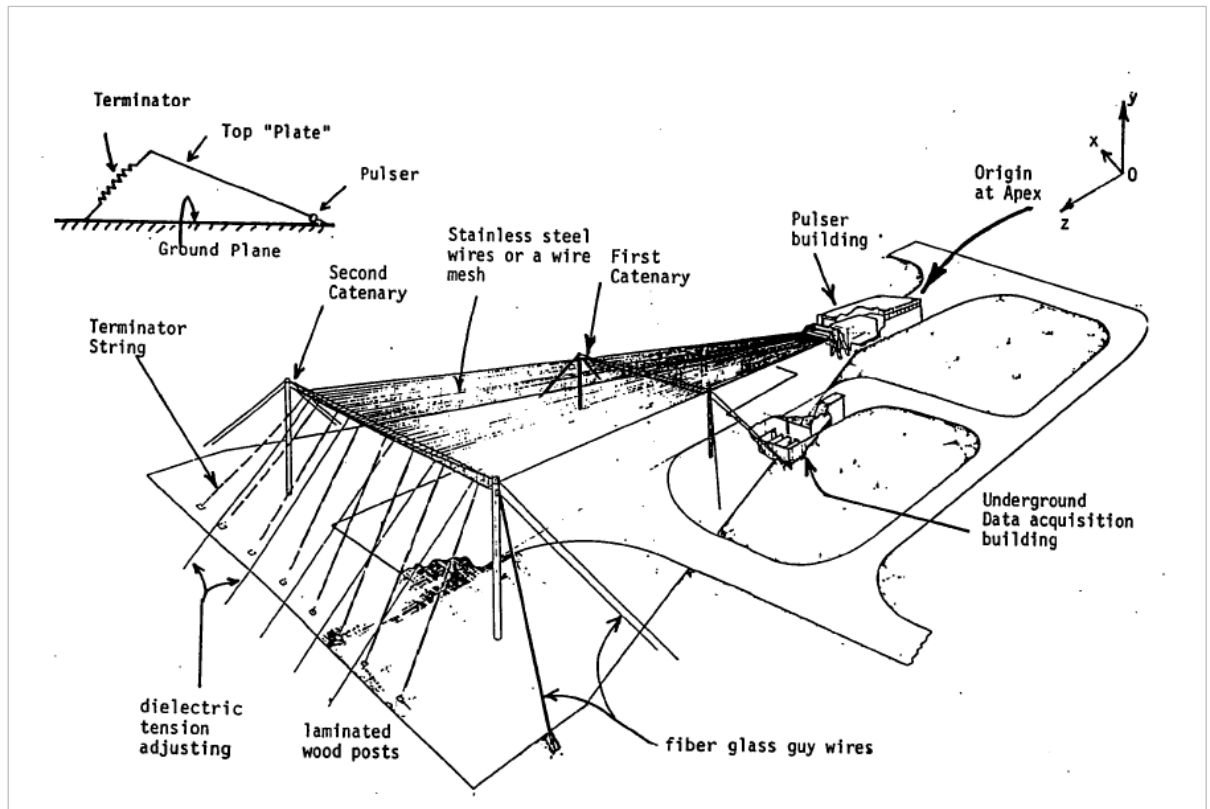
Figure 3.2: Conceptual drawing of a conical terminated TEM cell as envisioned by Giri & Baum, 1996.

We will discuss the following design aspects:

- The design of the top plate and ground plane with the objective of circumventing the generation of higher-order TEM waves.
- Regarding the termination as a transmission line and not solely as termination.
- To equally match the distributed termination to current distribution from the top plate.
- The investigation of how to minimize scattering TEM waves back towards the launcher and DUT.
- How to optimise the performance of the distributed termination.
- Special consideration is given to the distributed termination as it is arguably the most critical feature of this design.

The design aspects of the conical terminated TEM cell will be discussed in more detail in the following sections.

3.2 Top-plate and ground plane design considerations

The top-plate of the cell represents one conductor above the ground plane. In the context of a multi-conductor transmission line this forms one-line. We will use a solid top-plate as we only require DUT size of 10 × 10 × 10 cm within the working volume. Figure 3.3 illustrates the top-plate with respect to the ground-plane and DUT.
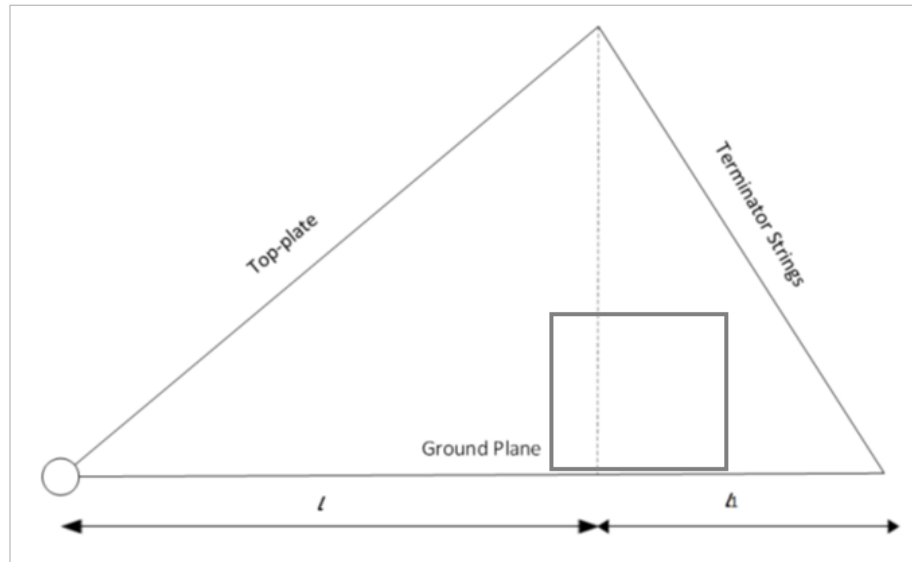
Figure 3.3: Side view of DUT directly placed on ground plane of the conical terminated TEM cell. Adapted from Giri & Baum, 1996.

In launching a spherical TEM wave the top-plate is crucial as an N-line conductor will support N-TEM modes, where there exists one principal TEM mode and N-1 unwanted TEM modes. It is desirable to evade unwanted TEM modes as the objective is the launching of a single TEM mode wave.

We explore the interaction between the simulator and DUT and their role in the excitation of non-TEM waves. When the TEM wave is encountered by the DUT it is possible for the incident scattered field from the DUT to bounce off conductive materials. This interaction results in spurious emissions and the launching of higher-order non-TEM waves. Furthermore, such spurious emissions can generate higher-order TEM waves propagating in the directions of the terminator strings and the source.

Interactions such as wave scattering and spurious emissions between the DUT and cell generate unwanted higher-order TEM waves or non-TEM waves. Giri and Baum thus define that in each cross-section of the cell the maximum height of the test object must be less than 60% of the height of the top-plate. The objective is to only launch a single TEM wave, so the size of working volume is limited.
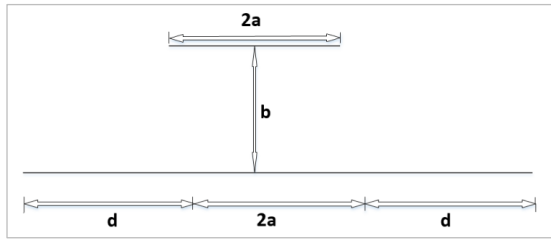
Figure 3.4: Two parallel plates of unequal breadths. Adapted from Giri & Baum, 1996.

Sufficient impedance matching in TEM cell design is another factor to consider. Good impedance matching ensures that the cell is well-matched to the coaxial connectors in testing. The TEM characteristic impedance, Z_0, is affected by the width of the ground plane where it exceeds the width of the top-plate, 2a, by 2d. Figure 3.4 illustrates the ground plane and top-plate width in respect to separating distance between the two.

Figure 3.5 shows the TEM impedance as a function of ground plane width and top-plate height. For field uniformity it is recommended that $d \geq b$ (Carlisle, 1969).
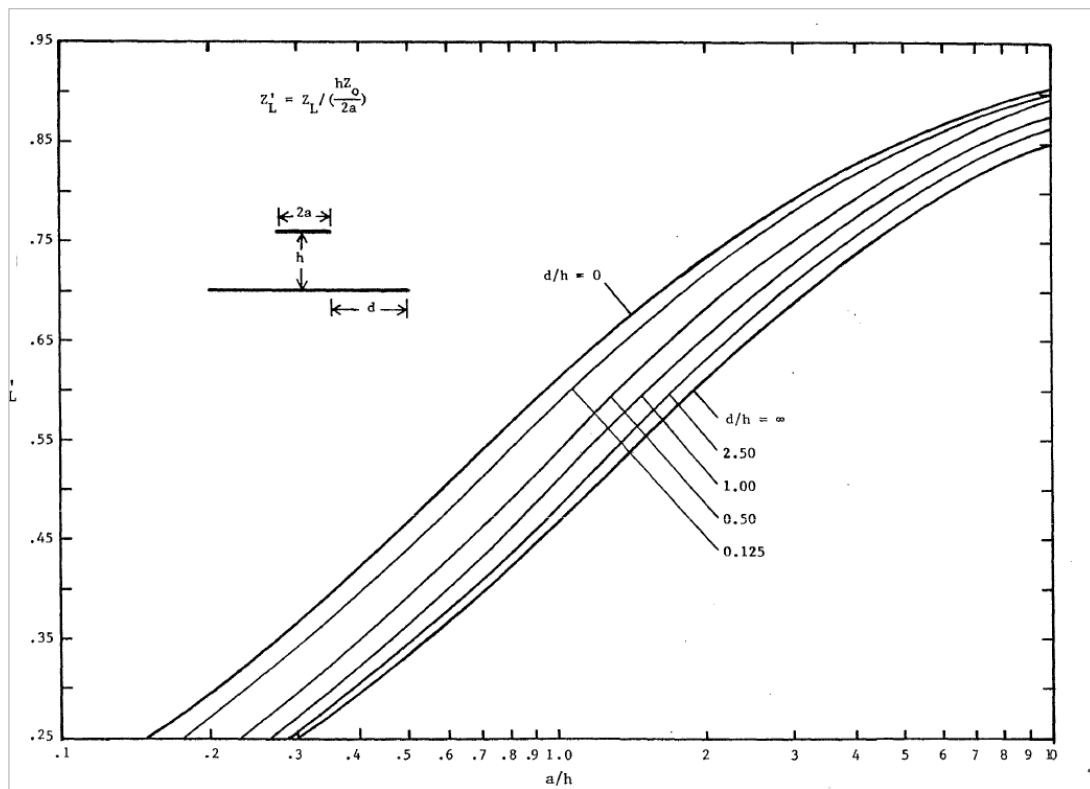
Figure 3.54: TEM impedance, as a function of (a/h), with (d/h) as a parameter (Carlisle, 1969)

A solid top-plate will be used for the purpose of this research. For larger structures a mesh top-plate with grounding rods are utilised around the perimeter of the ground-plane. Mesh is used for loading conditions and to minimise potential reflections emanating around the ground-plane.
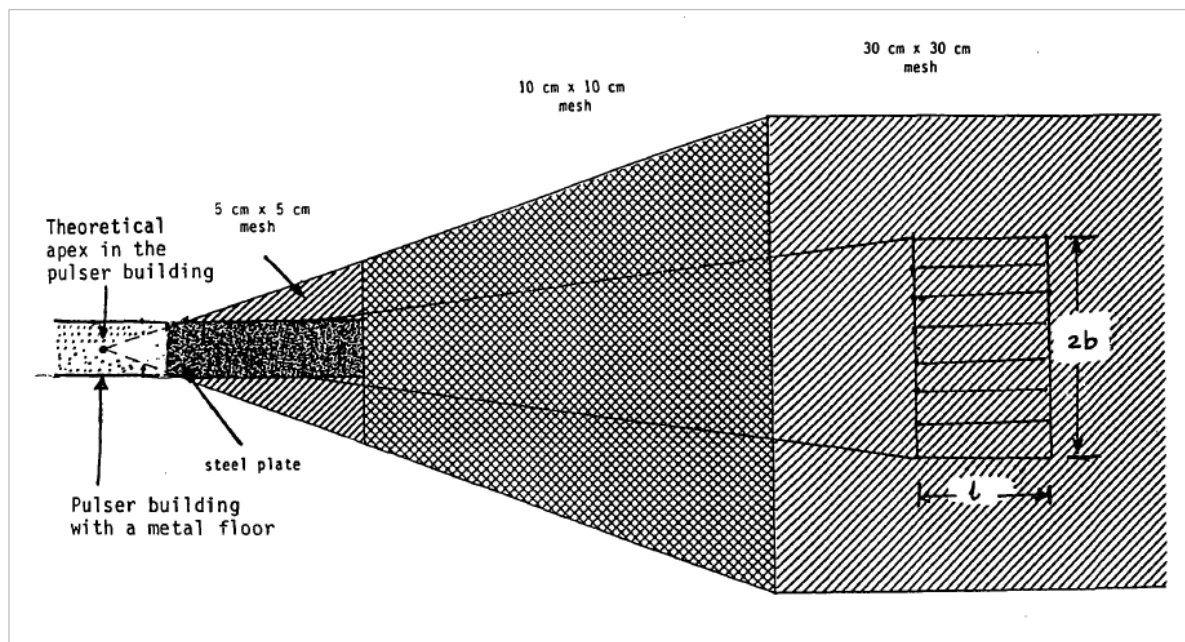
Figure 3.65: Ground plane layout of a terminated TEM cell (Giri & Baum, 1996)

Figure 3.6 illustrates a large-scale ground plane layout and approximate dimensions of top plate as compared to ground plane. For scale, the figure above is a conceptual sketch of a conical terminated TEM cell used for EMC testing on a DUT such as a vehicle. This research focuses on the design, manufacture and testing of a conical terminated TEM cell able to accommodate a DUT with a maximum size of 10 × 10 × 10 cm.

3.3   Terminator strings as a transmission-line

At lower frequencies where the cross section of a transmission line is small compared to its wavelength, a terminator with impedance equal to the transmission lines characteristic impedance results in perfect termination as the reflection coefficient $\rho = 0$.

$$\rho = \frac{Z_L - Z_C}{Z_L + Z_C}$$ Equation (3.1)

Where Z_L is the terminating impedance and Z_C is the transmission line impedance.

So at low frequencies where the terminating impedance is considered to be uniformly distributed along the plane of termination the assumption that $Z_L = Z_C$ is fairly accurate. Therefore, using the above equation we derive $\rho = 0$ (Giri *et al.*, 1980).

These assumptions can not be made at higher frequencies as you must observe the terminator as a distributed terminator as opposed to a lumped terminating element. Also to consider is the effect of free-space (outside the terminator) on the termination as the impedance of the incident wave is comprised of the parallel combination of the terminating impedance, Z_L, and the free-space impedance, Z_0.

Z_L is thus frequency-dependant for an efficiently matched system i.e., wave impedance inside the waveguide is equal to the combined impedance at the wave receptor ($Z_L \parallel Z_0$).

Terminating impedance can be described as the sum of resistance (*R*) and inductance (*L*) in a series configuration:

$$\widetilde{Z_L}\,(s) = R + sL, \text{ where } s \text{ indicates complex frequency.}$$

At low frequencies the wave only sees the real part of the terminating impedance, therefore $Z_L \cong R$. For terminator impedance to match characteristic impedance $R = Z_C$.

At high frequencies, electric and magnetic waves are related by free-space impedance, Z_0.

$$\text{As } s \rightarrow \infty \text{ and } Z_L \rightarrow \infty$$

$$\text{The combined impedance at high frequencies: } Z_L \parallel Z_0 = Z_0$$

Giri and Baum conceptualized the use of an admittance sheet with resistive and inductive qualities. They further investigated the concept of using of a sloped admittance sheet with coplanar conducting tapers, illustrated in Figure 3.7.
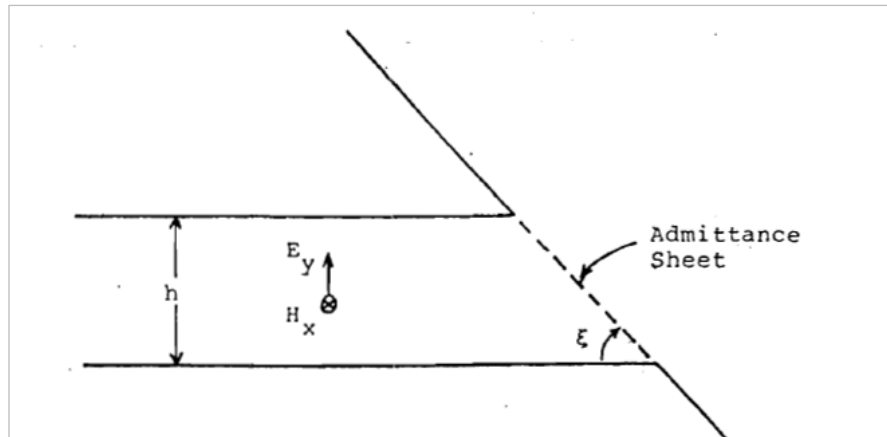
Figure 3.7: Sloped termination with tapers (Giri et al., 1980)

Assuming that there is no difference in the dimensions of the parallel plate in the transverse direction and the electric field is constant at the admittance sheet:

- The admittance sheet possesses a positive real-part if:

$$h < \frac{1}{3}\lambda \qquad\qquad \text{Equation (3.2)}$$

- For satisfactory impedance matching:

$$R = Z_0 \qquad\qquad \text{Equation (3.3)}$$

Practically it is more suitable and cost-effective to utilize a series of resistor strings in a parallel configuration to approximate an admittance sheet as each resistor possesses internal

inductance and inductive coupling between the strings. Such a configuration, as seen in Figure 21, using wire-wound resistors would not require added inductors for acceptable termination.

Consider a string termination with height, h, width, w, making an angle ε from the ground plane, M resistors, N resistor strings, R resistors, inductance L_R, radius r_R and resistor length l_R (see Figure 3.8).

Internal inductance is given by:

$$L_i = \frac{M}{N} L_R$$

Equation (3.4)
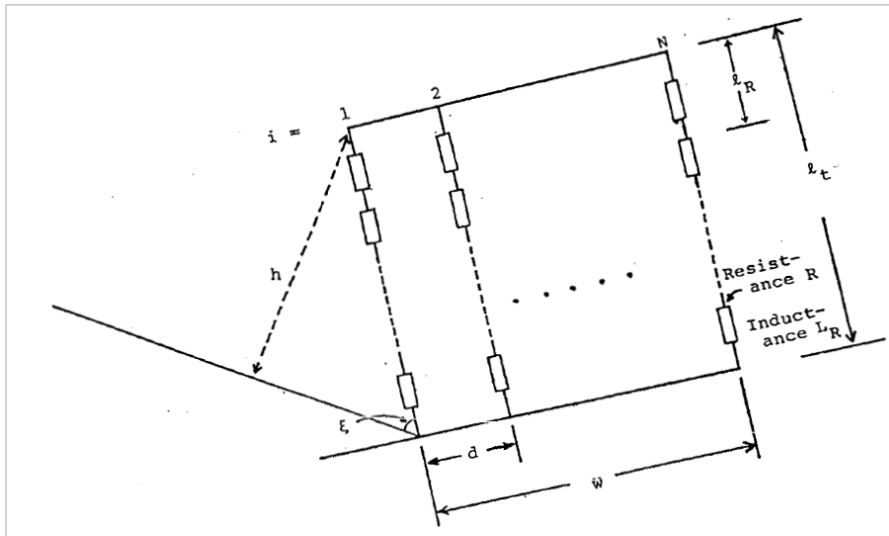
Figure 3.8: Figure illustrating distributed termination variables (Giri et al., 1980)

External inductance is however also present because of the inductive coupling between the resistor strings, this is given as:

$$L_e = \frac{M\, l_R}{N-1} \frac{\mu_0}{2\pi} \sin^2(\varepsilon) l_n(d/2\pi r_R)$$

Equation (3.5)

where $d = w/(N-1)$ is the separation between each resistor string.

Total inductance of the termination is thus the sum of Internal and external inductance:

$$L_t = L_i + L_e$$

Equation (3.6)

Total resistance is given as:

$$R_t = (M/N)\, R \sin \varepsilon$$

Equation (3.7)

The following impedance values are observed to be ideal so that R_t and L_t match the transmission line adequately.

$$R_{opt} = Z_c$$

Equation (3.8)

$$L_{opt} = \left(\frac{l_t}{w}\right) h\, \mu_0 \sin \varepsilon\, \beta_h^{opt} f_a$$

Equation (3.9)

Where $\qquad\qquad\qquad\beta_h^{opt} \simeq \sin \varepsilon$ $\qquad\qquad\qquad$ Equation (3.10)

And f_a is the factor taking fringe fields into account ($0 \le f_a \le 1$).

$f_a \lesssim f_{TEM}$; f_{TEM} is the TEM mode fraction.

Using the above expressions, it is possible to estimate the distributed termination's total inductance and account for it in design.

In short, the resistor termination must be capable of handling the voltage and energy being delivered by the transmission line.

Recommendations are as follows:

1. To ensure there is no air breakdown: maximum voltage/h < 10^6 V/m
2. To ensure no breakdown of resistors: maximum voltage rating > maximum available voltage
3. Available energy must not exceed the energy deposition of the resistors;

$$(\text{M} \times \text{N} \times \text{allowable energy deposition}) > \frac{1}{Z_C} \int_0^\infty v^2(t)\ dt \qquad \text{Equation (3.11)}$$

Where $v\ (t)$ is the terminator voltage (Giri *et al.*, 1980).

With reference to Figure 3.9, Z_C remains constant through the ground plane up to the point where the tapers meet the top-plate $z < z_1$. From this terminating section onwards to where the termination meets the ground plane Z_C becomes a function of z from $z = z_1$ through to $z = (z_1 + l)$ until the end of the termination where it becomes $z = 0$.
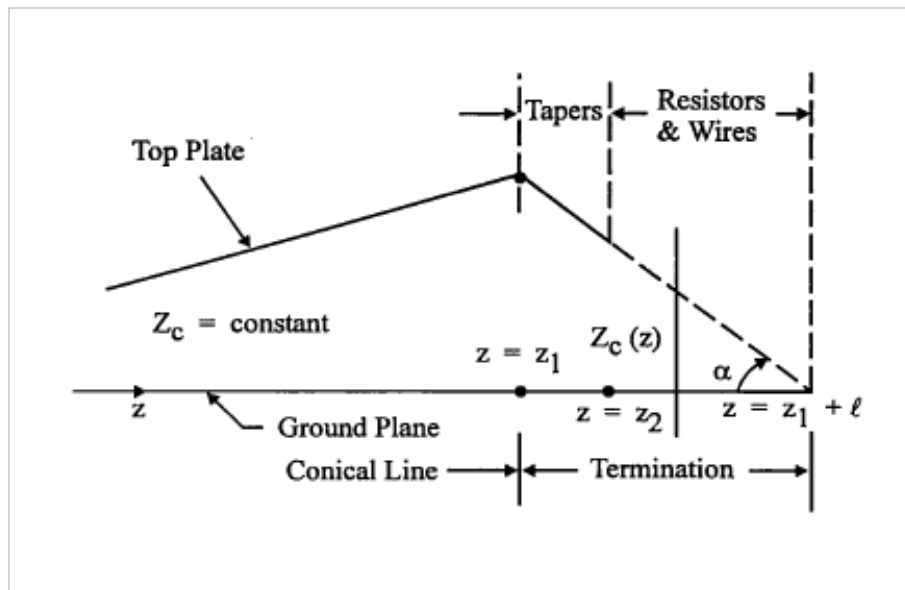
Figure 3.9: Side view of the conical TEM cell with distributed termination (Giri & Baum, 1996)

At the point where the tapering ends meet the top-plate ($z = z_1$) and where they meet the resistive strings ($z = z_2$) impedance as a function of z remains constant at Z_c. This is possible as the tapers decrease in height as well as width, keeping Z_c unchanged.

We calculate Z_c at the point where the tapered ends meet a uniform grid of parallel wires, where each wire is parallel to the direction of wave propagation on a transmission line.

From Baum, 1996 for a wire grid terminating a uniform field inside of the grid:

$$y_0 = \frac{1}{\pi}\mu_0 = \frac{1}{\pi}\ln(e^{\pi\frac{c}{d}} - 1);$$

Equation (3.12)

Where y_0 describes the position of the top-plate in relation to the termination strings. Where the top-plate is very wide (a>>b), Δy represents the shift in height (Giri & Baum, 1996):

$$\Delta y = \frac{(wire\ spacing)}{2\pi}\ln\frac{(wire\ spacing)}{\pi(wire\ diameter)}$$

Equation (3.13)

Where the top-plate is narrow in geometry we estimate the increase in impedance by using Z_0 multiplied by a factor ranging between $\Delta y/(2a)$ to $\Delta y/a$.

Tapers are required because an abrupt connection between the top-plate and the terminator strings would result in scattered fields reflected back towards the DUT.

Using the angle of the sloping terminator, α, (see Figure 3.9) the coordinate for z_2 is determined. The tapers connecting the conductive plane and the resistive strings are triangular and the base of the triangles are connected to the top plate.

This section explored the geometry, various configurations and methods of connecting the terminator strings as a transmission line. We also discussed the addition of tapers in avoiding a sudden connection between the top-plate and terminator strings. We now examine matching the current flow from the top-plate into the terminator strings thereby ensuring minimised reflections.

3.4 Matching distributed termination to current distribution from the top plate

As the conical terminated TEM cell is designed to propagate a spherical TEM wave it is advantageous to know the current distribution in matching it to the distributed termination. That is, knowing an equal amount of current is flowing from N tapers into each resistive string. Figure 3.10 illustrates a top plate with an equal number of terminator strings connected to the ground plane.
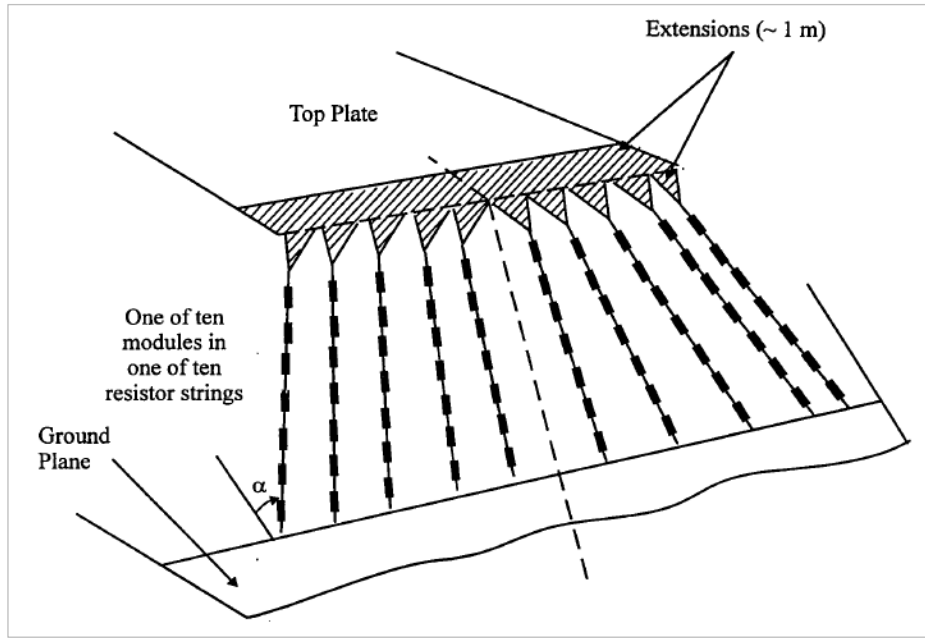
Figure 3.10: Conceptual diagram of distributed termination with even number of terminator strings (Giri & Baum, 1996)

With a total current, I_t flowing from the top-plate: $I_t/N = I$; equal current flowing out of each taper.

If $N = 2M$, and N is chosen to be an even number we can calculate, x_m, the width of the taper's base using the extension width, a:

$$\frac{x_m}{a} = \sin\frac{\pi m}{2M}$$

Equation (3.14)

Practically, we may need to regard the use of supportive dowels or some other structure to support the resistive termination and top plate. This section will conclude the discussion regarding physical geometry of the conical terminated TEM cell, we now expand on the propagation of a TEM wave within the conical terminated TEM cell and how we may prevent wave scattering towards the launcher.

3.5 Minimising scattering towards the DUT and launcher

We introduced the idea of mitigating the generation of non-TEM waves and high-order TEM waves. Basically, the cell's frequency range extends from 0 Hz to f_u, where f_u is the upper usable frequency. Above f_u unwanted higher-mode TEM waves are generated.

With a large test object it is evident that the transmission line's cross-sectional dimensions may exceed the source's wavelength (λ_s). So, at low frequencies the distributed termination satisfactorily terminates the launched TEM wave. However, it is ineffective at higher frequencies where the transmission lines cross-sectional dimensions exceed λ_s it is ineffective.

We aim to minimise scattering waves back towards the DUT and source i.e., the propagating TEM wave launched from the source should propagate forward and out through the distributed string termination. Scattering waves can, however, not be removed. The alternative is to re-direct the scattered waves in a direction other than toward the source and DUT, illustrated in Figure 3.11.
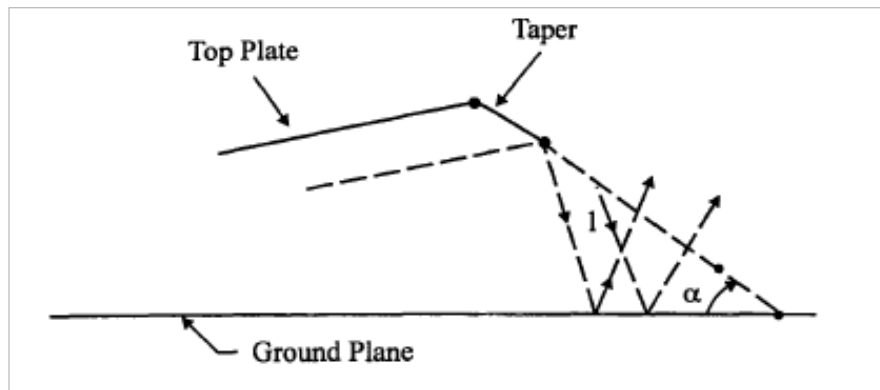
Figure 3.61: Scattering waves directed away from the source and terminator (Giri & Baum, 1996)

Another technique employed to minimise scattering waves towards the source or DUT is to stagger the resistive terminator strings in the direction of propagation. By staggering the resistive terminator strings, as in Figure 3.12, we ensure that scattering waves arrive at the source or DUT at different times and phases. This can be done by connecting the terminator strings in a fashion where they are not parallel to each other or are parallel to each other in a different plane.
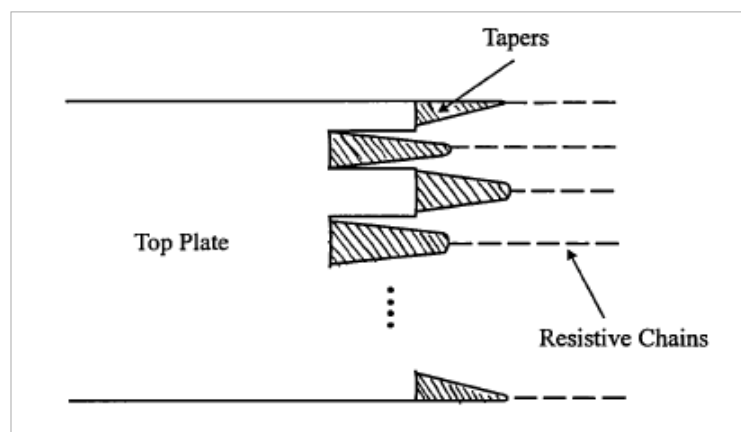
Figure 3.72: Staggered resistive terminator strings, shown from the top (Giri & Baum, 1996)

Giri, Baum and Schilling, 1978 further explores the attenuation of reflections in the transverse z-directions by connecting resistive sheets at TEM-equipotential surfaces, examples of such a configuration can be seen below in Figure 3.13.
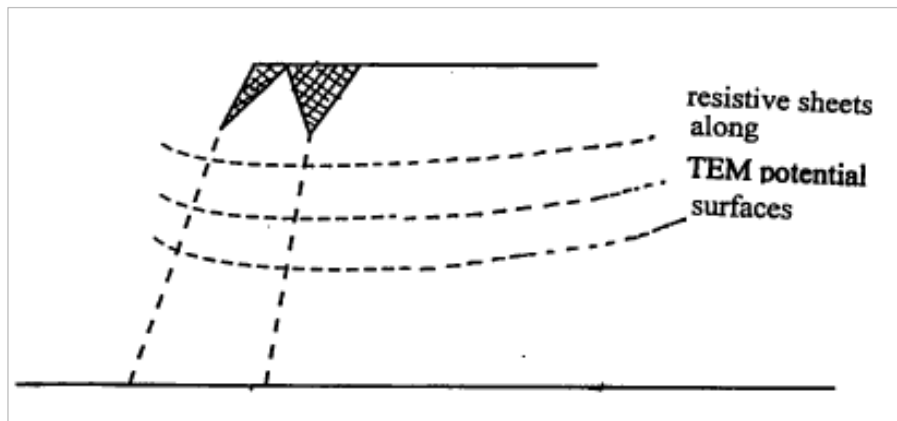
Figure 3.13: View of distributed termination with resistive sheets positioned at TEM-equipotential points to attenuate reflecting waves (Giri & Baum, 1996)

The idea conceived by Giri, Baum and Schilling, 1978, was with the objective of extracting energy from TE and TM mode waves.

Giri and Baum, 1996 further look at how the distributed termination may be optimised by observation of E and H fields. These two optimization techniques are discussed in the following section.

3.6   Optimising performance of the distributed termination

Initial design parameters are calculated using the equations in Section 3.2. These are, however, only estimates and as such we need to optimise the performance of the distributed termination. Two methods for optimising a time-domain EMP testing setup are given by Giri and Baum, 1996:

1. By measuring E and H within the working volume of the cell and observing the reflected waveform as it is decaying. The time at which this must be observed is at double the time it takes the wave to propagate between the observation point and termination.
2. By simultaneously measuring E and H; rendering a measurement solely of the reflected field as the combination of these two fields cancels out the incident field.

Two constraints Giri and Baum, 1996 further mention in the optimization process are:

1. TEM mode reflections should be minimised, this can be measured by voltage standing wave ratio (VSWR) and time domain reflector (TDR) at the source.
2. Without minimising TEM mode waves within the working volume, to minimise TE and TM waves within the working volume. TE and TM modes can be identified by measurement of the electric and magnetic fields' radial components, said components do not exist in a TEM wave.

This concludes the final design considerations and the optimization of the conical terminated TEM cell. These design concepts will define the design, manufacture and testing of a desktop conical terminated TEM cell with a working volume of 10 × 10 × 10 cm.

3.7   Conclusion

In this chapter we have considered the theory which dictates the design of the top-plate, ground-plane and distributed termination. In the following chapter we aim to design a conical terminated TEM cell with an S_{11} magnitude below -10 dB which correlates to less than 1 % power being reflected back to the source. This will be an indication that the impedance of the transmission line is well-matched throughout the volume of the cell ($R_{opt} = Z_c$).

We now understand the design parameters to consider, and this concludes our discussion on the theoretical guidelines for the design of the conical terminated TEM cell as presented by Giri and Baum, 1996. The discussion in the following chapter will cover the design, manufacture, and testing of the conical terminated TEM cell with a working volume of 10 × 10 × 10 cm.

CHAPTER 4: DESIGN AND MANUFACTURE OF THE CONICAL TERMINATED TEM CELL

4.1 Introduction

The CubeSat was originally designed by the California Polytechnic State University and Stanford University in 1999. The invention of the CubeSat allows private and educational institutions to actively participate in the space industry by conducting research in the field of space and satellite systems engineering; an opportunity previously only given to those able to afford such exposure and involvement (Brewer, 2012). A CubeSat is fundamentally a picosatellite with dimensions 10 × 10 × 10 cm, weighing 1.33 kg. It contains scientific, government and private payloads. One of these satellites is referred to as a 1U (one unit), being the standard configuration (Foley, 2012). CubeSats are required to undergo EMC testing to ensure reliability as they face harsh conditions in space. CPUT requires a pre-compliance EMC testing facility for a typical 1U CubeSat, this research aims to fulfil that need in the form of a conical terminated TEM cell.

We shift our focus to the design of a conical terminated TEM cell capable of housing a 1U CubeSat within its working volume. The working volume of the terminated TEM cell should thus be a minimum of 10 cm along each cross-section. We also consider the frequency range across which the conical terminated TEM cell exhibits sufficient impedance-matching and minimized reflections.

4.2 Cell geometry

To design a versatile, conical terminated TEM cell that sits on a test bench and is able to house a DUT of 10 × 10 × 10 cm the aspects of the cell geometry we focus on are:

- Staying within geometric limits that allows the cell to be usable as a desk-top setup.
- Maintaining a characteristic impedance, Z_c, of 50 Ω across the dimensions of the cell
- Designing within the boundaries of the cell that renders a working volume capable of testing DUT smaller than 10 cm × 10 cm × 10 cm.

Giri and Baum, 1996 states that to reduce spurious emissions and wave scattering between the DUT and the cell the maximum height of the test object must be < 60 % of the height of the top-plate in each cross-section.

Consider Figure 4.1 below, illustrating a side-view of a terminated TEM cell accommodating a DUT of 10 cm × 10cm × 10 cm with an evenly matched source and load where $Z_c = 50$ Ω.
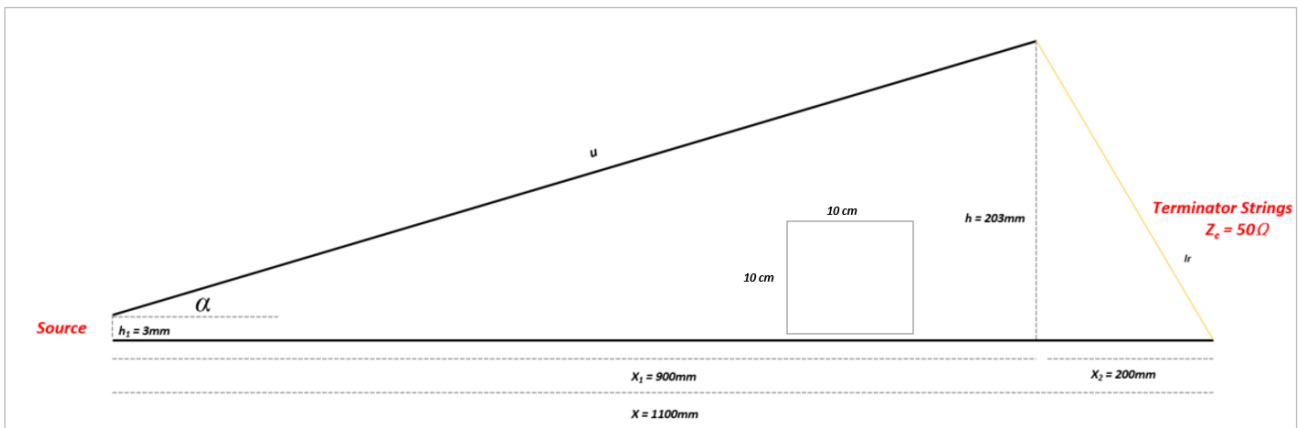
Figure 4.8: Side-view schematic of conical terminated TEM Cell

We select the longitudinal dimension of the ground-plane, x, to be 1100 mm and h = 203 mm.

Using trigonomerty we calculate $u = 921.95\ mm$ and $\alpha = 12.5°$.

To calculate the width of the top-plate at the source consider a micro strip with a dielectric thickness (h) of 3 mm as seen in Figure 4.2, The height of 3 mm is selected considering the width and height of the feeding SMA connector:
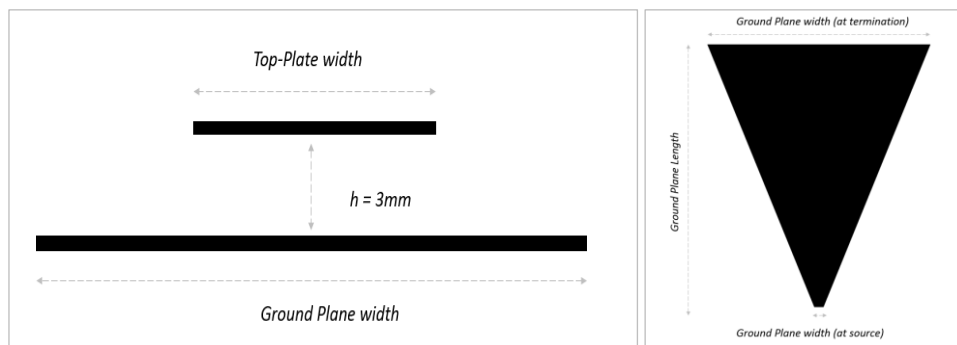
Figure 4.2: Side-view of micro strip, top-plate at source(left). Top-view of ground plane, source to termination (right)

Using Equation 4.1, the formula for calculating the width of a microstrip (www.everythingrf.com, n.d), we calculate the width of the top-plate at the source at a height of 3 mm (h) from the ground-plane (w). Then we calculate the width of the top-plate at a height of 203 mm (h_1) where the top-plate meets the terminator strings (w_1). The variables and values calculated are listed below in Table 2.

Table 2: Variables for determining plate width

Variable	Value
h	3 mm
h_1	203 mm
ε_r	1
z_o	50 Ω
t	0.1 mm
w	9.07 mm

33

w_1	625.98 mm

$$w = \frac{7.48h}{e^{\left(z_o\frac{\sqrt{\varepsilon_r+1.41}}{87}\right)}} - 1.25.t \qquad \text{Equation (4.1)}$$

As mentioned, the maximum height of the test object must be < 60 % of the height of the top-plate in each cross-section. The height of the top-plate was therefore selected to be 203 mm.

The TEM characteristic impedance, Z_0, is affected by the width of the ground plane where it exceeds the width of the top-plate (2*a*) by 2*b* as illustrated in Figure 3.4. For field uniformity it is recommended that d ≥ b (Carlisle, 1969).

$$Width_{GP} = 2a + 2 \times b, \qquad where\ 2a = w \qquad \text{Equation (4.2)}$$

Calculating the GP width at the source:

Table 3: Variables in determining ground plate width at the source

Variable	Value
2a	9.07 mm
b	3 mm
$Width_{GP\_source}$	15.07 mm

Calculating the GP width at the termination:

Table 4: Variables in determining ground plate width at the termination

Variable	Value
2a	625.98 mm
b	203 mm
$Width_{GP\_termination}$	1031.98 mm

Tapers are added, as discussed in Section 4.3, to avoid an abrupt connection between the distributed termination and the top-plate.

To have symmetry along the longitudinal dimension an equal number of termination strings is required. For an equal number of terminator strings, $n_{strings}$, we require an odd number of tapers; n_{tapers}.

It is decided to increase the number of tapers required, thereby minimising reflections in the cell.

Taper variables are illustrated in Figure 4.3 and defined in Table 5 below:
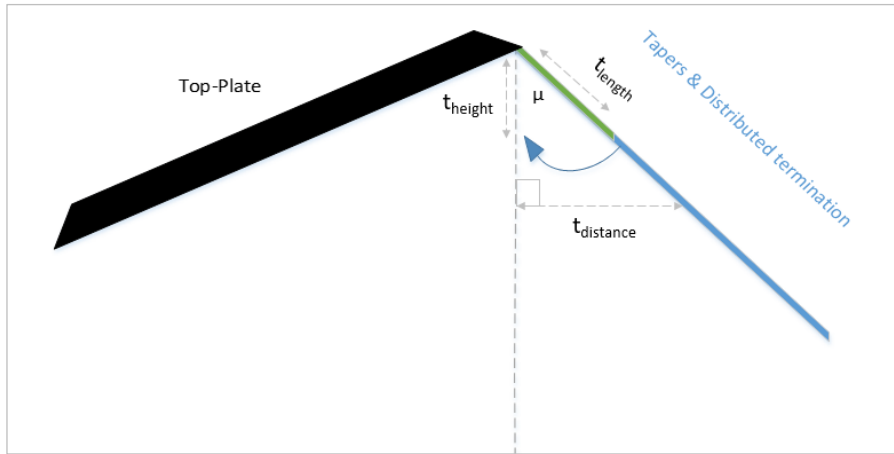
Figure 4.39: Diagram of taper geometry relative to top plate

Table 5: Dimensions of tapers

Variable	Value
$n_{strings}$	10
n_{tapers}	19
t_{height}	38 mm
t_{length}	54 mm
$t_{distance}$	t_{height}
μ	45°

Calculating taper width:

$$taper_{width} = \frac{Top\ Plate\ width}{n_{tapers}} \qquad \text{Equation (4.3)}$$
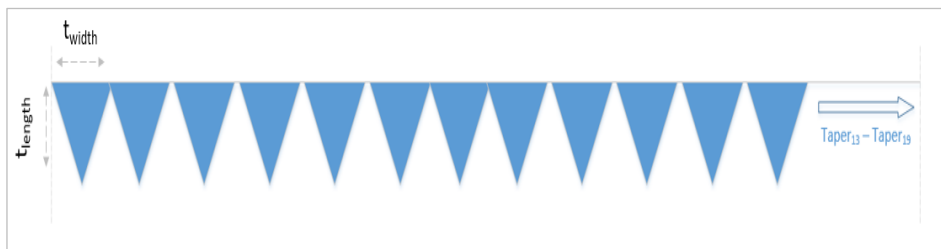
Figure 4.4: Front-view of taper geometry

Now that we have geometry of the top-plate, ground-plate and tapers we move to following section in which modelling, and simulation of the cell will be covered.

4.3   Design and Modelling

With the basic geometry of the top-plate, ground plane and their separating distance at source and termination covered we construct, model, and simulate the design in Altair Feko. The main objective was to determine which design would yield the lowest S_{11} metric, below -10 dB. This metric would determine how well the 50 Ω input and 50 Ω output impedance are matched and thereby determining how much power is reflected to the source between DC and 1 GHz

(Caspers *et al.*, 2010). Various designs were investigated during the simulation stage. These included varying the number of terminator strings and tapers and varying the configuration of terminator strings connected between the top-plate and ground plane.

The model is constructed utilizing two polygons for the top plate and ground plane. The ground plane and top plate are separated by 3 mm at the source (refer to Figure 4.6 to see the 3 mm separating distance at the source), and 203 mm at the termination. The ground plane length sits at 1100 mm and is coupled to the distributed termination at this point. At the source there is a wire simulating a connector with a 5 V input with each distributed terminating string connected in parallel with respect to the ground plane and top plate-taper configuration. For a 50 Ω impedance match between input and load we couple 10 × 500 Ω resistors in parallel.

A perspective view of the model of the conical terminated TEM cell in Altair Feko is shown below in Figure 4.5.
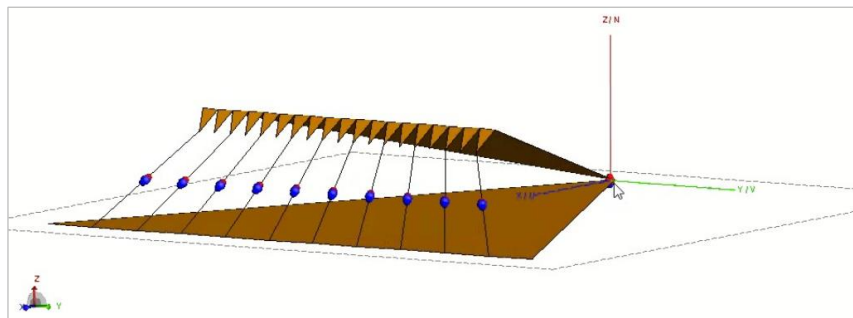
Figure 4.5 :3D view of Conical Terminated TEM Cell as modelled in Altair Feko

Due to the requirement of using the cell as a test setup within a lab environment the dimensions as previously calculated were altered, with less than 0.5 % deviation for the ground plate width (calculated at 1032 mm) and the top plate width (calculated at 626 mm) respectively.

Table 6: Initial dimensions for terminated TEM cell model

Parameter	Value (mm)
Ground plate length	1100
Ground plate width (at source)	15.1
Ground plate width (at termination)	622
Top plate length	922
Top plate width (at source)	9.1
Top plate width (at termination)	1028
Taper base	38
Taper sides	38
Spacing at source	3
Spacing between taper flange and ground plane	203
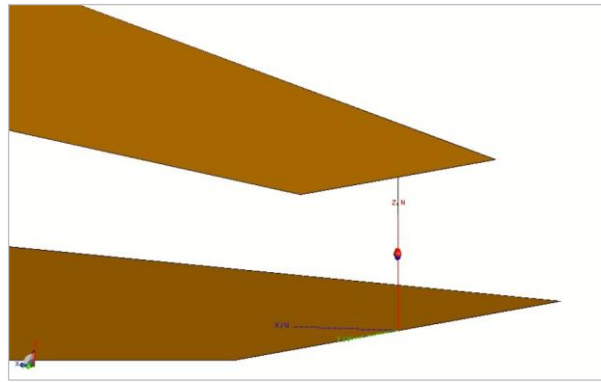
Figure 4.6: Zoomed image of 3mm spacing between top plate and ground plane at the source

With the manufacturing in mind, it was however decided to extend the top-plate and ground plate into a triangular shape at the source, seen in Figure 4.7, to better the integrity of the connector pin at the source.

The distance of the ground plate was thus extended along the x-axis as below, the difference removed from the top plate and ground plane.
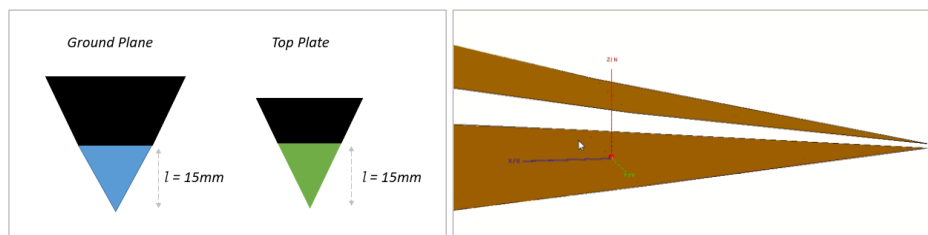
Figure 4.7: Diagram showing triangular extension to ground plane and top plate (left) and zoomed view of the triangular extension in Altair Feko

In Figure 4.8 we see 19 tapers and 10 resistor strings connected between the ground plane and top-plate and the conical terminated TEM cell is successfully modelled in Altair Feko
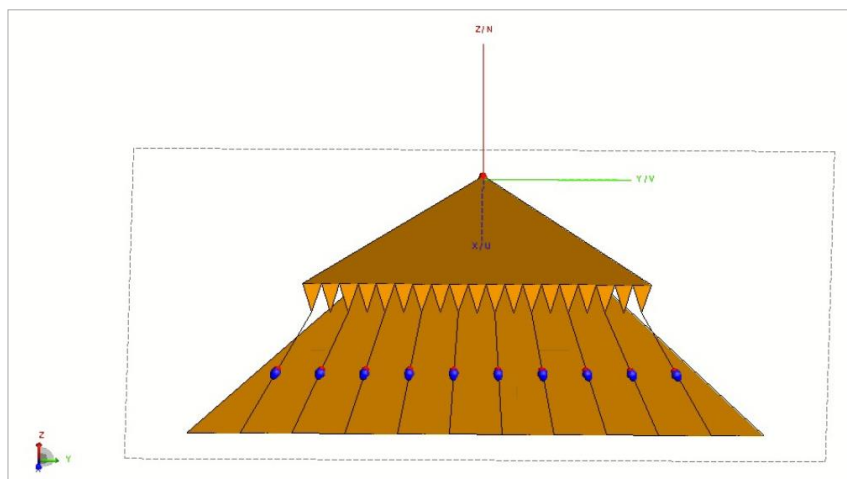
Figure 4.8: Front view of model showing tapers and termination connected to ground plane

During investigation, techniques such as shifting the termination strings in several configurations and increasing/decreasing the number of tapers to support 10 termination strings; variation of geometry at the source were employed; this was done to determine their effect on the working volume and S_{11} coefficient.

Having described the design and modelling of the conical terminated TEM cell the following section details the manufacturing of the cell. The measurement and simulation results are discussed in Chapter 5. The following section coves alternate designs which we investigated in obtaining an S_{11} below -10 dB across the frequency range from 0.1 to 1 GHz.

4.4 Alternative Designs

In the design of the conical terminated TEM cell alternate configurations with varying tapers, terminator strings and top-plate and ground plate were modelled and the S_{11} simulated in Altair Feko. These investigations were performed to determine if the adjustment of any of the design aspects would result in less reflections back to the source.

4.4.1 Adjustment of top-plate and ground plane length

We first looked at the effect the extension of the top-plate or ground plane would have on the S_{11}. We also investigated the possibility of less reflections back to the source from a circular top-plate and ground plane.
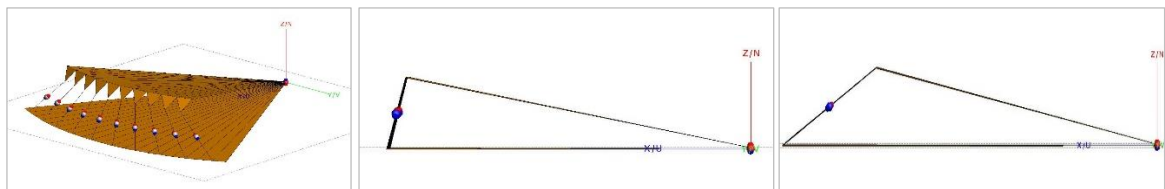
Figure 4.9: Circular top-plate and ground plane (left). Extended top-plate (centre). Extended ground plane (right).

For a circular top-plate and ground plane, See Figure 4.9 (left) the radius of the planes was selected to be equal to the original calculated dimensions (922 mm and 1100 mm respectively). Each plate was also simulated in equal width to the original triangular plates (622 mm and 1028 mm respectively. In this instance there were 10 tapers as opposed to 19 tapers in the original design, with 10 terminator strings. This resulted in reflections of a magnitude higher than anticipated, well above -10 dB across the frequency range, see Figure 4.10.

For Figure 4.9 (centre and right) the triangular shape of the top-plate and ground plane are adopted again. Figure 4.9 (centre) shows a side-view illustrating the extended top-plate length. The length of the top-plate was extended to the same length of the ground plane (1100 mm). In Figure 4.10 we see a satisfactory S_{11} below from 0.1 GHz to 0.5 GHz. We do, however, see that above 0.5 GHz the S_{11} increases to above -10 dB.

Figure 4.9 (right) shows a side-view of a conical terminated TEM cell with the ground plane extended to 1100 mm, the top-plate remains at 922 mm. In Figure 4.10 we see this model exhibites reduced reflections below 0.5 GHz compared to the other two designs. Similarly, from 0.45 GHz upwards we see the simulation follows similar peaks and troughs as when the top-plate is extended. In this scenario, however, S_{11} between 0.5 GHz and 0.7 GHz were too high to be accepted for manufacture.
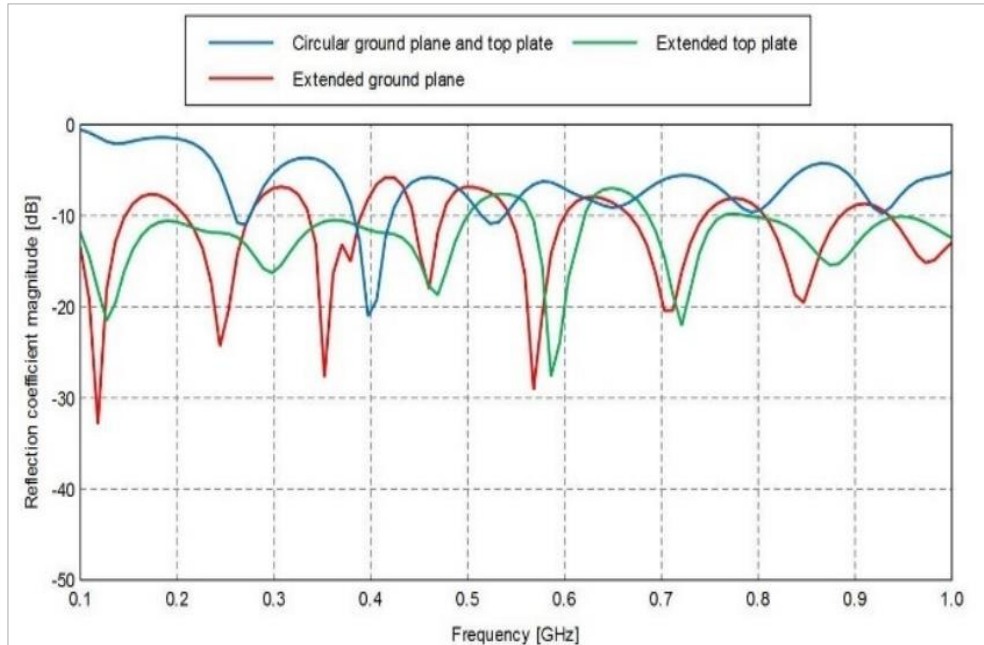
Figure 4.10: Investigation of top-plate and ground plane dimensions' effect on S_{11}.

We investigated the effect an alternate shape with dimensions equivalent to the calculated dimensions as well as the extension of those dimensions with reference to the top-plate and ground plane. Neither of these designs when simulated delivered an S_{11} output below -10 dB throughout the full frequency range.

4.4.2 Adjustment of tapers

Another design element investigated in determining its effect on the S_{11} was the tapers. We looked at varying the number of tapers, the size of the tapers, and the position of the tapers.
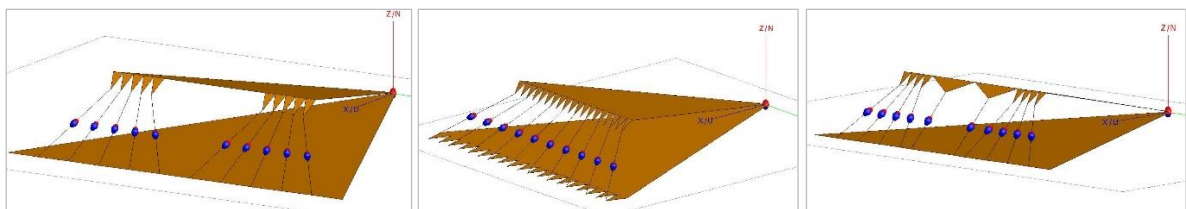
Figure 4.11: Tapers bundled outside edges (left). Tapers on top plate and ground plane (centre). Broad tapers added to outside bundles (right).

We investigated the reduction in the number of tapers with an equal number of terminator strings to minimise reflections back to the source, see Figure 4.11 (left). As illustrated in Figure 4.12, this resulted in an adequate S_{11} response. We do, however, see that at certain frequencies (+/- 0.17 GHz, 0.3 GHz, 0.45 GHz, 0.75 GHz) reflections above -10 dB are evident. As losses due to manufacturing were expected this design was not selected for manufacturing.

We then added two broad tapers in the centre with corresponding terminator strings, Figure 4.11 (right). This response followed a similar pattern to the previously discussed design with a slightly lower S_{11} below 0.5 GHz, see Figure 4.12. Above 0.5 GHz the S_{11} again increases, with noticeable variations in peaks and troughs between 0.6 GHz and 0.8 GHz. In this scenario with added tapers the S_{11} only increases above the -10dB threshold at approximately 0.65 GHz and 0.75 GHz by approximately 5 dB.

Giri and Baum, 1996, describe the necessity of including tapers to minimise reflections due to the abrupt connection between top-plate and terminator strings. As the terminator strings are also connected to the ground plane, we investigate the inclusion of tapers here as well, see Figure 4.11 (centre). This design exhibited the poorest S_{11} response across the frequency range, see Figure 4.12. The reflection coefficient magnitude increased above -10 dB at several points across the range compared to the other two designs. The addition of tapers on the ground plane resulted in more reflections with the S_{11} exceeding -10 dB by approximately 5 dB. Although this is not a major variation S_{11} exceeded the -10 dB threshold more frequently than the other simulated designs.
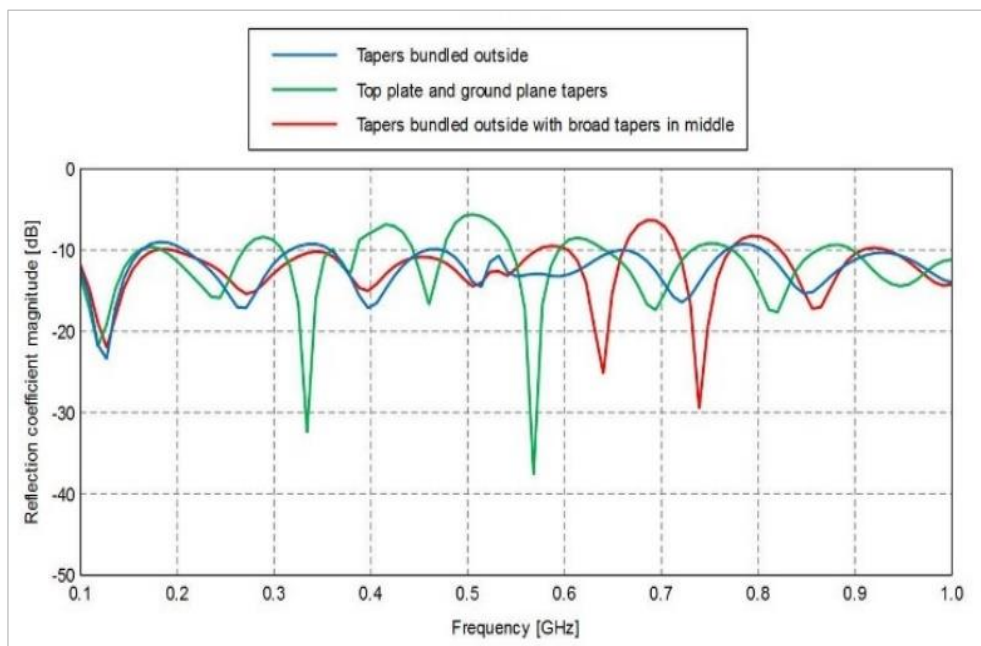
Figure 4.12: Investigation of the effect on S_{11} by varying tapers.

Looking at the effect on the S_{11} by making the taper adjustments it can be said that none of these designs are viable. These designs when simulated did not deliver an S_{11} output below -10 dB throughout the full frequency range.

4.4.3 Adjustment of terminator strings

The final design element investigated in determining its effect on the S_{11} was the configuration of the terminator strings, see Figure 4.13. As discussed in Section 4.2 and Section 4.3, 19 tapers and 10 terminator strings remained constant in both simulations with the grouping of the terminator strings being varied.
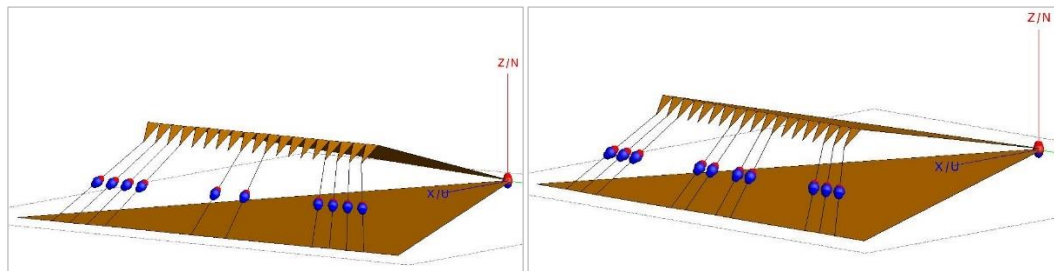
Figure 4.13: Terminator strings bundled on outside (left). Terminator strings bundled inside (right).

The simulated S_{11} result for these two string configurations follows each other very closely, see Figure 4.14. Peaks and troughs are similarly replicated throughout the range of simulated frequencies. The S_{11} remains below -10 dB up to approximately 0.55 GHz. After this the S_{11} continues to exceed -10 dB up to 1 GHz. Between 0.65 GHz and 0.7 GHz the S_{11} exceeds -10 dB by a maximum of 5 dB.
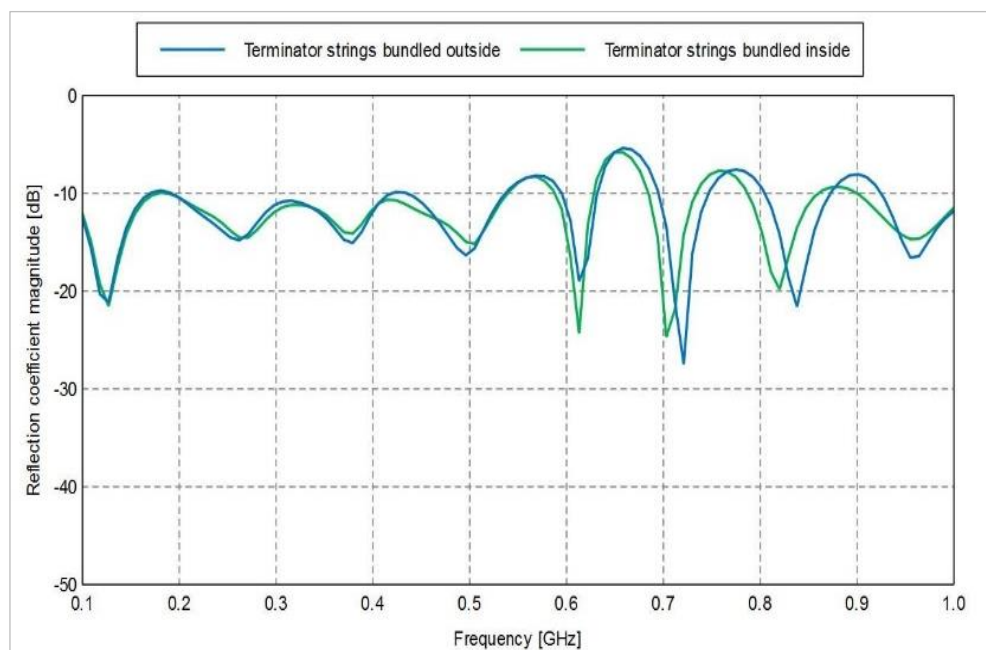
Figure 4.14: Investigation of the effect on S_{11} by varying terminator string configuration.

For the varied terminator string configurations (bundled inside and outside) the S_{11} output across 0.1 GHz to 1 GHz, did not exhibit an output below -10 dB across the full range of frequencies.

We investigated design adjustments in tapers, ground plane and top-plate, and the terminator strings. The most favourable S_{11} result exhibited originated from Figure 4.11 (left). To recall, that design considered moving the tapers and terminator strings outwards on the top-plate. As the simulated S_{11} response was near to the -10 dB threshold this design was not selected. As mentioned, losses due to manufacturing must be considered. As such, the original calculated dimensions as described in Chapter 3 are manufactured and the S_{11} measured and compared to simulation.
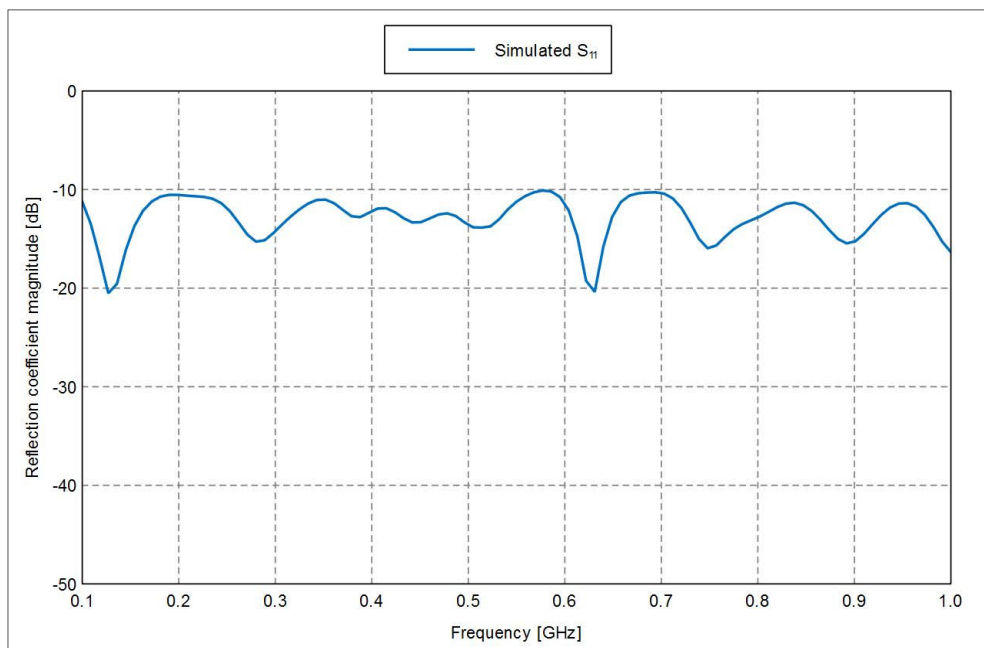
Figure 4.15: Simulated S_{11} of selected model

The simulated S_{11} result of the selected model is seen above in Figure 4.15.

4.5   Manufacturing

After a rigorous study of the design in Altair Feko a satisfactory S_{11}, below -10 dB across the frequency range of 100 Hz to 1 GHz was obtained.

A low-cost artefact was then manufactured. By manufacturing the artefact, it would allow us to determine the complexity in manufacturing the conical terminated TEM cell. It would also allow us to determine the accuracy of the cell compared to simulated results.

Figure 4.16 illustrates a 3D perspective view and side-view of the conical terminated TEM cell.

The top plate and ground plane are connected by a 4-hole SMA panel mount connector at the source (part number: 132354, by Amphenol Corporation). The connector had a thick dielectric material surrounding the centre conductor, this proved very useful due to the limited spacing between the top plate and ground plane. The distributed termination was constructed using 10 × 500 Ω ¼ W Resistors in a parallel configuration.
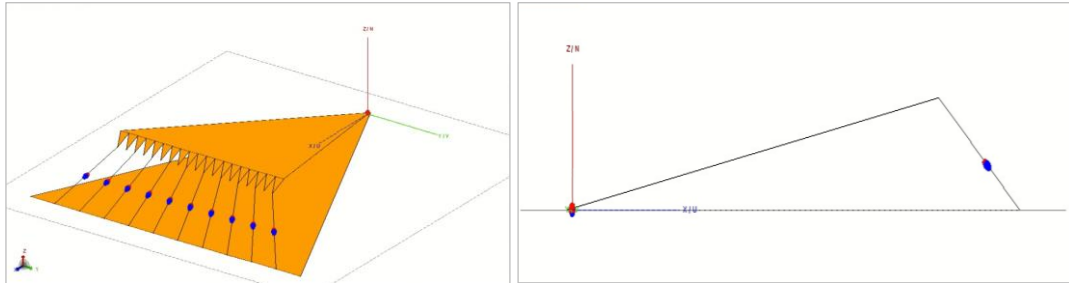
Figure 4.16: 3D perspective of the conical terminated TEM cell with dimensions of 1100 mm × 1028 mm × 203 mm (left) and Side view of conical terminated TEM cell in Altair Feko (right)

There were 3 major design steps in the fabrication of the cell, the first being the manufacturing of the top plate and the ground plane. The top plate and ground plane were manufactured from 0.7 mm thick laser-cut aluminium.

Manufactured dimensions and images for ground plane are indicated in Figure 4.17 and in Figure 4.18 we see the manufactured dimensions and an image of the top plate.
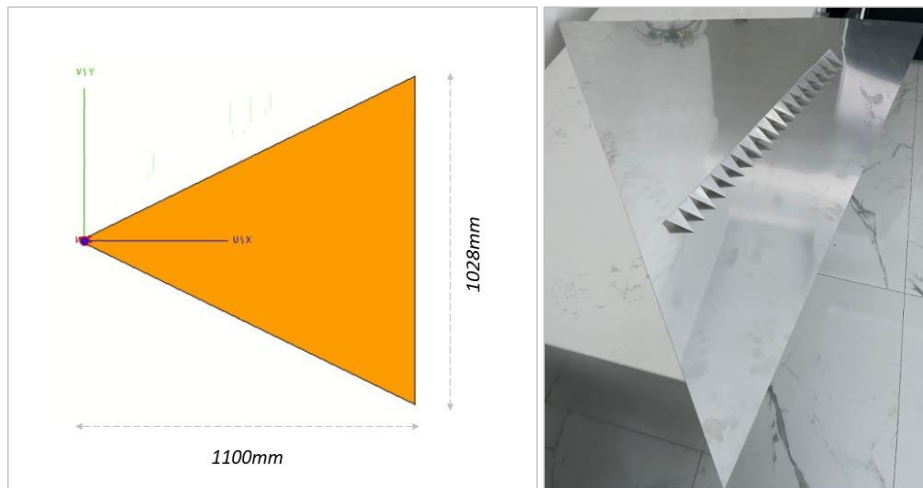
Figure 4.17: Manufactured dimensions and image of ground plane
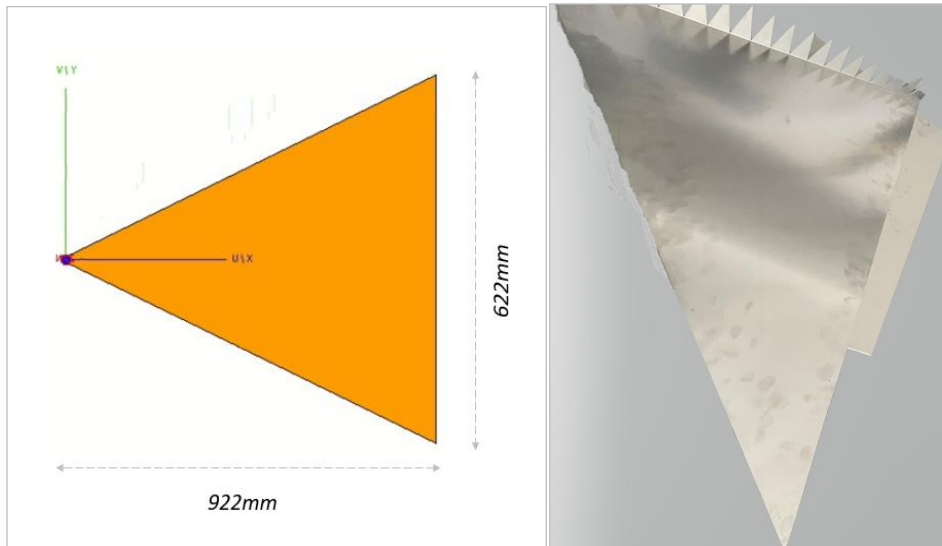
Figure 4.18: Manufactured dimensions and image of top plate

PVC pipes were cut into smaller pieces at an angle and glued on the top and on the bottom to provide vertical separation between the top plate and ground plane, see Figure 4.19 below.

Figure 4.19: Cut PVC pipe plate (left). Photograph illustrating cut PVC pipe used to support top plate (right)

The second step in manufacturing was the fabrication of the distributed termination. Individual sections of veroboard were cut and soldered to the 500 Ω ¼ W resistors with a grounded termination point. As the resistors could not make electrical contact with the ground plane the Vero board was attached to individual sections of polystyrene sheet. Figure 4.20 illustrates the use of polystyrene to insulate the veroboard from the ground plane. The challenge of soldering onto aluminium necessitated 2 mm holes being drilled into the ground plane and the ground termination being bolted to the aluminium sheet via insulated ring terminals.
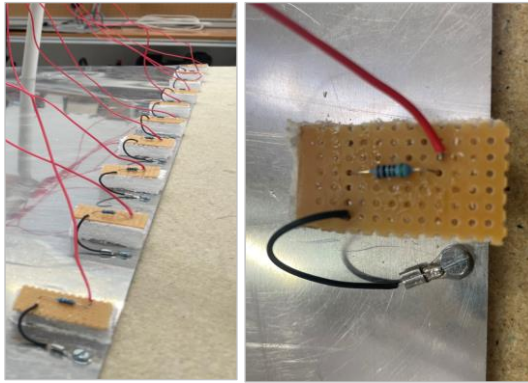
Figure 4.20: Resistors mounted on polystyrene sheet and ground termination connected via insulated ring terminals

Soldering onto the aluminium and ensuring effective electrical conductivity between the distributed termination and tapers proved to be challenging and so the 0.2 mm gauge wire connecting the veroboard and tapers was soldered onto 22 mm croc clips. Figure 4.21 illustrates the connection of the resistive termination between ground plane and tapers using croc clips. Although this introduced a manufacturing constraint it did however allow ease of removal and change of configuration of the load.
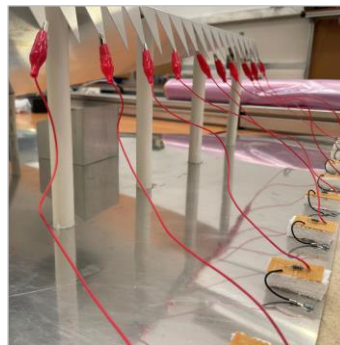
Figure 4.21: Manufactured distributed termination connected to tapers using 22 mm croc clips

The next and most challenging aspect of the manufacturing process proved to be the mounting of the beryllium copper 4-hole flange 50 Ω SMA panel connector at the apex of the structure due to the small vertical separation of 3 mm. Figure 4.22 (left) shows the 50 Ω SMA panel connector from Amphenol Corporation used in manufacturing.

The connector's dielectric length originally measured at 15.01 mm was shaved down to approximately 3.7mm ensuring accommodation for the 3 mm vertical spacing and the thickness of the aluminium sheet. A 1.5 mm hole was drilled into the top plate and ground plane through which the connector was threaded from below the ground plate. Again, ensuring electrical conductivity from the connector pin to the top plate was integral and merely soldering on to the top plate would be ineffective. 2 holes are drilled into the bottom plate, to bolt the connector onto the ground plate. Copper tape was then attached to the top and bottom plate

so that upon insertion of the connector pin additional solder could be applied. The process is detailed below.
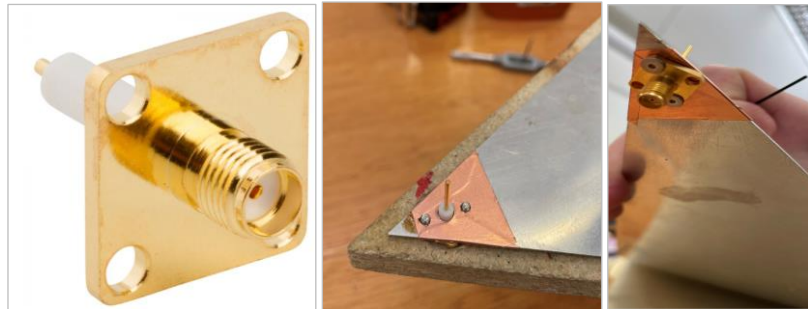
Figure 4.22: Amphenol SMA connector (part number: 132354) (left). Top view of ground plane with holes drilled, wound in copper tape and connector inserted (centre). Bottom of ground plane showing bolted connector with copper tape (right)

Figure 4.22 (centre) shows the top-view of the SMA panel-mount connector when inserted in the ground plane after shaving of the dielectric to $\simeq 3.7$ mm. Figure 4.22 (right) illustrates the bottom-view of the SMA panel-mount connector bolted to the ground plane and copper tape.

To ensure electrical conductivity the bolted SMA connector was soldered onto copper tape and then onto the ground plane, this is illustrated in the photograph in Figure 4.23 (left).
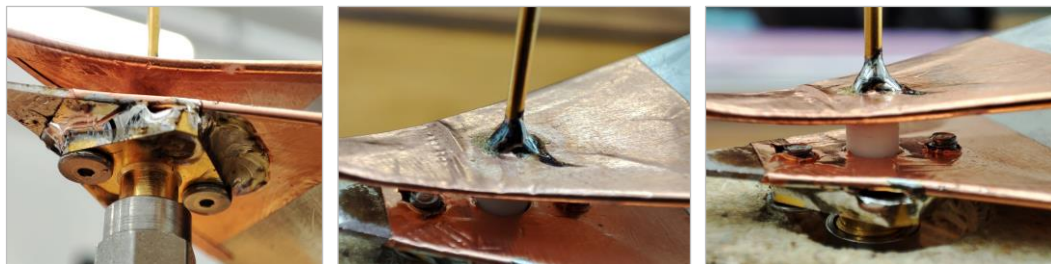
Figure 4.23: Connector bolted and soldered onto ground plane (left). Top view showing connector soldered onto top plate using copper tape and aluminium solder (centre). Side view of soldered SMA panel mount connector with 3 mm vertical spacing connecting top plate and ground plane (right).

In Figure 4.23 (centre) we see a photograph of conductor pin of the SMA panel connector protruding the top-plate, this was also soldered onto the copper tape to ensure electrical conductivity. Figure 4.23 (right) shows the vertical separation of approximately 3 mm between the top-plate and ground plane with SMA panel connector centre conductor bolted and soldered to achieve electrical conductivity.

The final manufactured artefact is illustrated in Figure 4.24 and Figure 4.25. A triangular base of chip board was used to support the model as it provided stability when transporting. The wooden base was also drilled at the termination and at the connector so that the model would sit flush on the base.
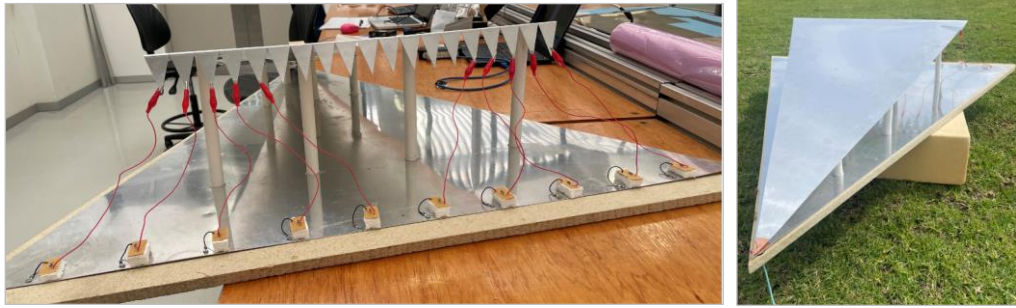
Figure 4.24: Front view of final manufactured product (left). View of manufactured model from the top (right).

A view of the model, from the top, is shown in Figure 4.24 (right) where one can also see the comparable size of the top-plate in respect to the ground plane.
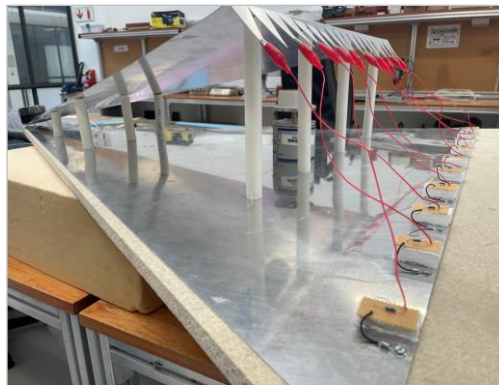
Figure 4.25: Perspective view of final manufactured product.

A perspective of the final manufactured artefact is shown in Figure 4.25 with PVC support, resistive termination, tapers, ground plane and top-plate within view.

4.6   Conclusion

The model was fairly simple to manufacture and was completed over a period of two weeks. The most challenging aspect of this model was working with aluminium sheet – in this instance, aluminium was used due to its lightweight and cost-effectiveness for application. It did however prove to be troublesome at times where if copper had been used it would have been easier to solder directly onto it as opposed to drilling. The manufactured artefact weighs less than 6 kg and can be carried through doors when turned on its horizontal axis. The biggest contributor to the overall weight is the wooden stand used to support the artefact. Although the unit is not excessively heavy it does require two individuals to carry it due to its size.

In the following chapter we will discuss the working volume of the cell.

CHAPTER 5: WORKING VOLUME OF THE CONICAL TERMINATED TEM CELL

5.1 Introduction

To determine the working volume of the conical terminated TEM cell simulations were compared to results. The working volume was investigated considering S_{11} changes in the measurement as well as E-field changes in simulations in relation to the IEC 61000-4-3 standard for testing and measurement techniques concerning radiated, radio-frequency, electromagnetic field immunity tests.

5.2 S_{11} simulation and measurements

All simulations presented are executed in Altair Feko. Designs were built and simulated in CADFeko and results were then manipulated in PostFeko into a structured, readable format. The material below informs the simulated vs measured results of the conical terminated TEM cell from 0.1 GHz to 1 GHz with 201 plotting points and further between 100 Hz to 2.5 GHz. We observe the S_{11} for three scenarios:

- Conical terminated TEM cell without a DUT
- Conical terminated TEM cell with a DUT flat on the ground plane (635 mm from the feeding SMA connector)
- Conical terminated TEM cell with a DUT raised 40 mm along the vertical axis (635 mm from the feeding SMA connector)

All the scenarios above are measured from 0.1 to 1 GHZ as this is the original research requirement. We extend the measured frequency range up to 2.5 GHz to determine what effects this may have on the S_{11} magnitude and working volume, with and without a DUT. The insertion loss was measured to at 0.2 dB loss on the lower end of the spectrum with a maximum S_{21} of 3.2 dB loss at 2.5 GHz.

These three scenarios were chosen as we want to measure the S_{11} of the conical terminated TEM without the interference of a DUT and compare those results to those when a DUT is placed within the bounds of the cell. Research Question 1 aimed to establish the maximum achievable working volume inside the conical terminated TEM cell with dimensions practical enough for benchtop use. For practical considerations we must consider the effect the introduction of a DUT has on the S_{11}, thereby determining the viability of the conical terminated TEM cell for benchtop pre-compliance testing. The DUT introduces source/DUT interactions that result in higher-order modes being generated (see Section 3.5), as such we measure the effect the DUT has on the S_{11} of the conical terminated TEM cell, if at all. Giri and Baum, 1996 also note the practical working volume of the cell being that when the DUT is raised, thus eliminating any galvanic interactions the DUT may exhibit on the ground plane. For practical

setups it may not always be possible to raise the DUT from the ground plane and so we measure the effect the DUT has on the S_{11} when laid flat on the ground plane.

A field is considered uniform if at least 12 of 16 points across a defined area are measured within - 0 dB to + 6 dB. This specification applies to a field uniformity across an area of 1.5m × 1.5m. It is thus translated to consider the smaller geometry of a TEM cell, meaning that to determine the useful working volume within a TEM cell 75% of the measured points needs to be within – 0 dB to + 6 dB of each other.

The S_{11} was measured using a NanoVNA V2 (S-A-A-2) vector network analyzer, the diagram below in Figure 5.1 shows the test setup with the conical terminated TEM cell as DUT. In practice the NanoVNA was connected to the feeding SMA connector which joins the top-plate and ground plane. Measurements obtained using the NanoVNA were downloaded as Touchstone (.s1p) files. These files were then imported to PostFeko and data manipulated to produce the graphs below.
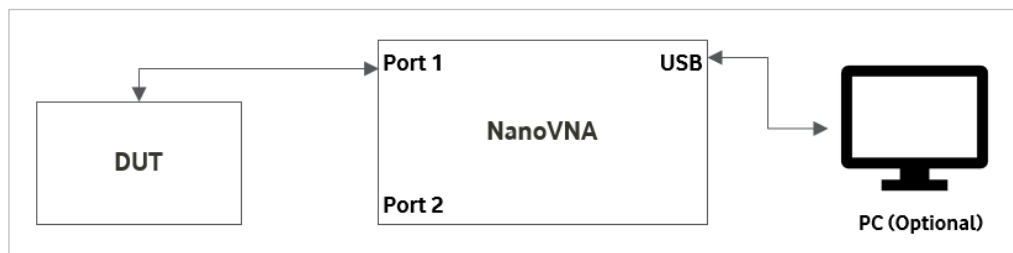
Figure 5.1: Diagram of setup for measuring the S_{11} reflection coefficient of the conical terminated TEM cell using the NanoVNA v2 (S-A-A-2)

Measurements were conducted inside a conventional postgraduate laboratory. The laboratory does not provide any shielding to against ambient interference; however, the levels of ambient interference were measured to ensure it does not negatively affect the reflection coefficient measurements. Measurements were repeated on different days and on different times of the day thereby verifying the repeatability of the setup. Confidence in the measured results depends upon the repeatability and reproducibility of the measurements. The repeatability of the measurements being the alignment between successive measurements under the same conditions. S_{11} measurements of the conical terminated TEM cell were conducted three times in the CPUT lab and twice in the reverberation chamber at SARAO. Reproducibility of the conical terminated TEM cell is thus verified by conducting S_{11} testing under different laboratory environments. Accuracy of the conical terminated TEM cell is verified by comparing the S_{11} measured versus the simulated, expected output.
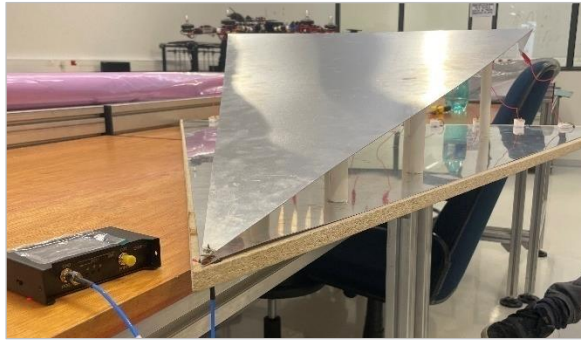
Figure 5.2: Picture of test setup measuring S_{11} with NanoVNA connected to conical terminated TEM cell via feeding SMA connector

A picture of the test setup is shown in Figure 5.2 with the NanoVNA connected to the conical terminated TEM cell.

5.2.1 Measured results vs simulated results without DUT

We compare the measured and simulated results of the conical terminated TEM cell without a DUT.

Comparing the first null we see a variation of 150 MHz. This variation can be attributed to two factors: the coaxial cable to top-plate transition manufacture and slight mismatch between simulated top plate length and manufactured top-plate length.

The first challenge faced was the coaxial to top-plate transition. The dielectric enveloping the centre pin conductor of the SMA connector was cut down to size with a hand saw. Due to the slight inaccuracy, there was a difference, in the order of mm, between simulated and measured centre conductor length.

The second challenge faced was the difference between the actual top-plate length and the simulated length. The number of PVC supports used in manufacturing resulted in slack. When the top-plate was placed on the structure, it exhibited a slight concave shape at certain points. This resulted in a reduced width and height.
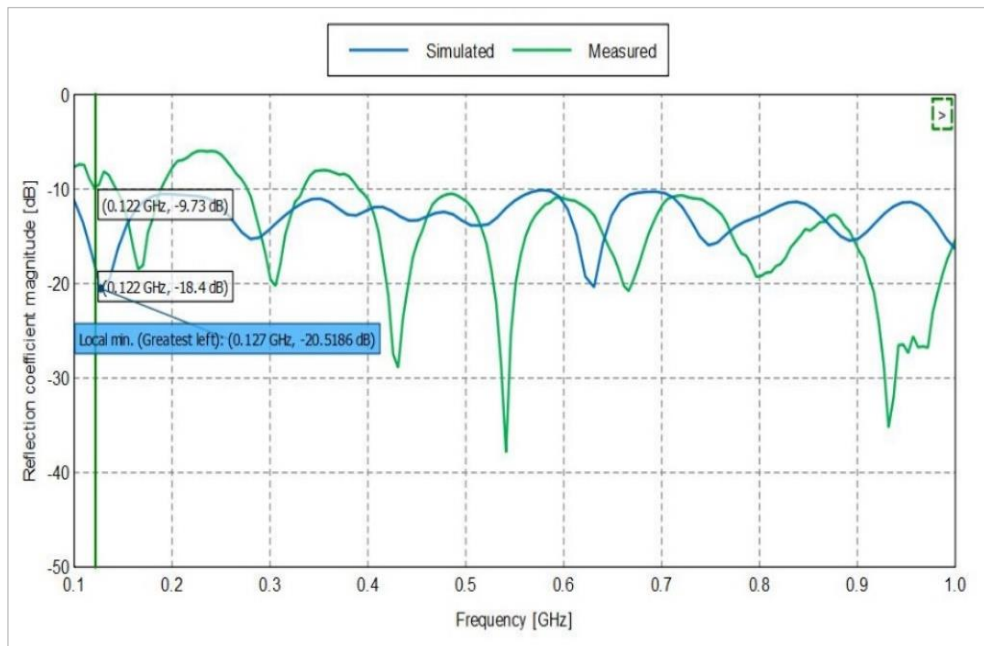
Figure 5.3: Simulated S_{11} vs measured S_{11}, no DUT

Looking at Figure 5.3, where no DUT is inside the TEM cell, the simulated reflection coefficient magnitude results are better than the measured, as expected. Although there is some misalignment in specific resonant frequencies due to the difference in practical dimensions, e.g. termination wire length, general trends can be seen to agree. Above 400 MHz, the measured results show good matching of the manufactured TEM cell with S_{11} below -10 dB up to 1 GHz. The primary resonant frequency simulated: 0.127 GHz and measured: 0.122 GHz closely agree and thus illustrate that the impedance of the conical terminated TEM cell is well matched throughout the length of the cell with specific frequencies in close agreement.

Some of the discrepancies may also be attributed to ambient reflections resulting from the unshielded environment as well as manufacturing considerations. We focus on some of the manufacturing variances. Simulated measurements do not consider any imperfections in manufacturing. A noticeable variance are the concave bends in the top-plate resulting from a limited support structure. In manufacturing the terminator strings, they were not taut, and each string differed in length from taper to ground plane by a few mm. The length of terminator strings was, also, further increased using croc clips in connecting the terminator strings to the tapers on the top-plate. A last manufacturing consideration is that compared to the measured result, the simulated results do not account for inductive elements of the resistive wire which further influences the measurements, most notably at higher frequencies.

5.2.2 Measured results vs simulated results with DUT flat on the ground plane

To maintain a working volume within the cell, the maximum height of the test object must be < 60 % of the height of the top-plate in each cross-section.

With the DUT at a height of 90 mm, and the height of the top-plate at that corresponding coordinate at ≃ 150 mm it meets the requirement as set out by Giri and Baum for a working volume where the height is > 1.6 × height of DUT. The dimensions of the DUT can be seen in Figure 5.4 (left and centre). It was preferred to position the DUT as close to the limit of this recommendation to test the boundaries of the working volume. A photograph of the aluminium cavity used as DUT to test the working volume conditions is shown below in Figure 5.4 (right).
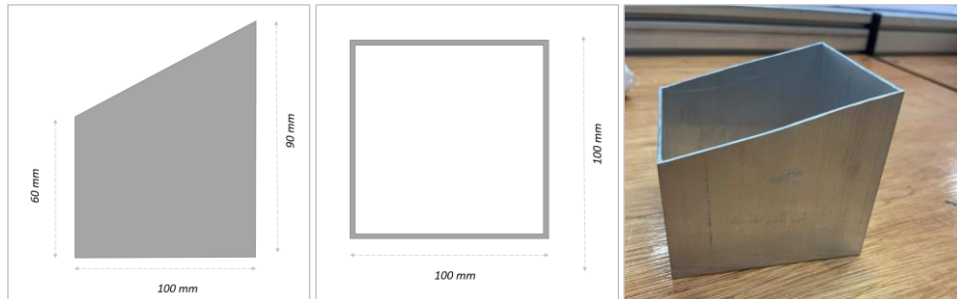
Figure 5.4: Dimensions of aluminium DUT (Side and top view). Picture of aluminium DUT

Figure 5.5 shows a photograph of the aluminium DUT placed within the boundaries of the conical terminated TEM cell at 635 mm from the feeding SMA (subMiniature Version A) connector.

Figure 5.5: Picture of DUT inside cell with centre at 635 mm from feeding SMA connector
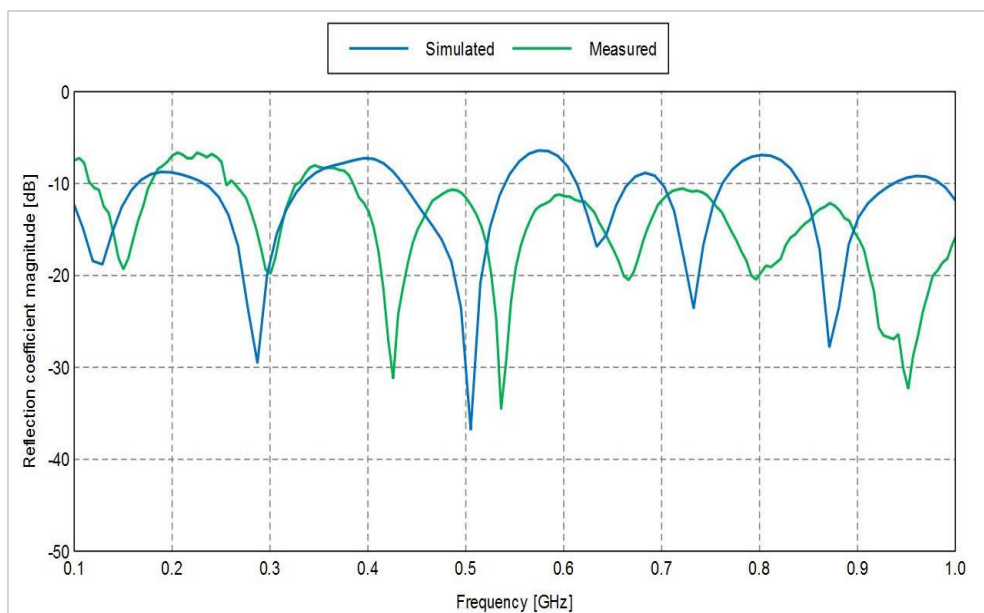
Figure 5.6: Simulated S_{11} vs measured S_{11}, DUT flat on Ground plane

In Figure 5.6 a higher number of reflections, especially in the simulation, are observed due to the insertion of the DUT. The measured results exhibited a better result above 0.4 GHz compared to simulation, well below -10 dB compared to the simulated results. With the insertion of the DUT we observe improved alignment of the resonant frequency points at lower frequencies. In the measured results we also notice less reflections above 0.4 GHz, compared to the simulated result, showing a better than anticipated result.

5.2.3 Measured results vs simulated results with DUT raised

The DUT was then placed on a polystyrene stand to test the effect on the working volume when the DUT is raised on a polystyrene base of 40 mm.

Figure 5.7 illustrates the raised DUT within the boundaries of the conical terminated TEM cell at 635 mm from the feeding SMA connector.
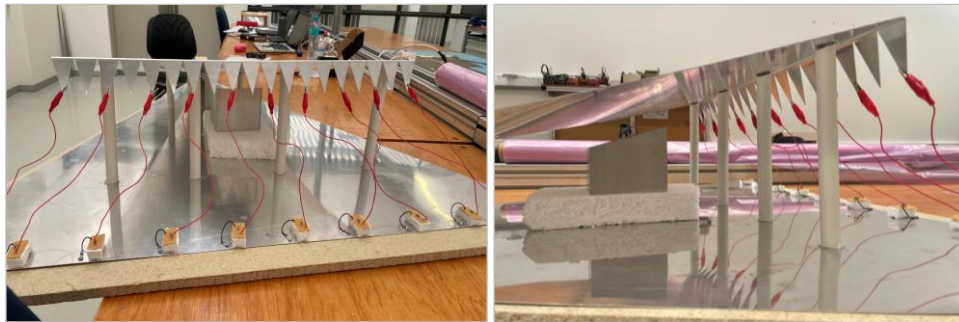
Figure 5.7: Front and side view of DUT on stand in cell to test S_{11} and working volume
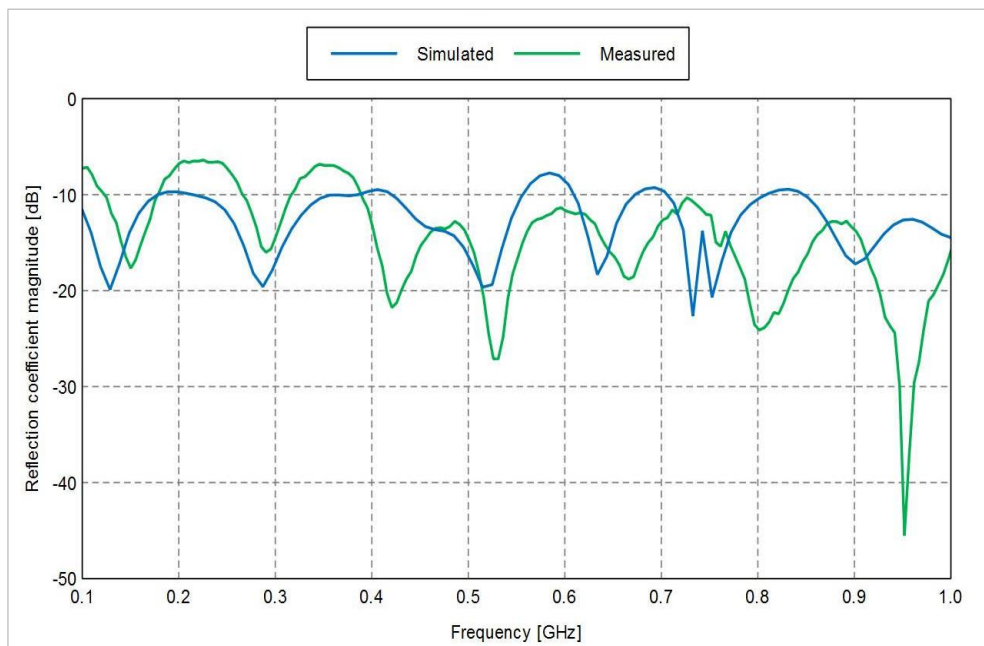
Figure 5.8: Simulated S_{11} vs measured S_{11}, DUT raised by 40 mm

Compared to the two previous scenarios, without DUT and DUT flat on ground plane. In this instance, see Figure 5.8, with the raised DUT we observe a favourable measured outcome compared to the S_{11} of the simulated artefact, above 0.4 GHZ. Similarly, as when comparing the measured and simulated S_{11} with the DUT flat on the ground plane in this scenario we observe even better alignment of the resonant frequency points at lower frequencies, below 0.4 GHz. With a DUT raised we again see that above 0.4 GHz there are fewer reflections than the simulated result. It is evident that the measured result surpasses the anticipated result.

5.2.4 Measured results vs simulated results comparing no DUT, DUT flat and DUT raised

We extend the frequency range to test the effect on the working volume and S_{11} when there is no DUT, when the DUT is raised and when the DUT flat on the ground plane. From Giri and Baum we understand that the conical terminated TEM cell is theoretically designed in such a manner that at higher frequencies the propagating wave should effectively radiate forward out through the distributed termination. We thus extend the frequency range up to 2.5 GHz to determine what effects, if any, this will have on the S_{11} magnitude and working volume.
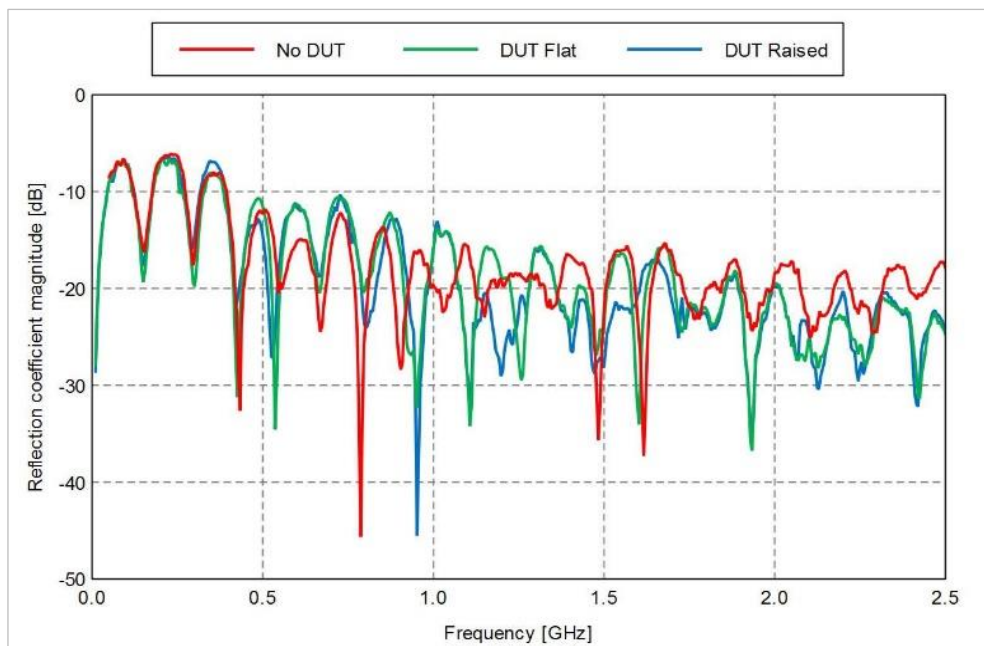
Figure 5.9: Measured S_{11}, no DUT vs DUT flat vs DUT raised (0.1 to 2.5GHz)

Comparing the DUT when it is raised from the ground plane and when it is flat, we expect the scenarios where the DUT is touching the ground plane, to yield a higher S_{11} magnitude. However, in Figure 5.9, we note that between 0.28 GHz and 0.4 GHz this is not the case. This indicates that the DUT and its placement has minimal effect at the lower frequency range. When increasing the frequency range along which the artefact is tested to 2.5 GHz, we also

observe little effect on the response comparing the two DUT scenarios. In addition, the frequency range over which the cell is tested even further may provide further insight into the exact upper useful frequency, it was however not extended beyond 2.5 GHz as the initial requirement was to test up to 1 GHz. For this research we found that the conical terminated TEM cell renders favourable S_{11} magnitude, below -10 dB, between 0.4 GHz and 2.5 GHz. Although the S11 magnitude below 0.4 GHz is not ideal, it is still less than -8 dB and would be usable.

5.3   Electromagnetic Simulations and Studies

To support the investigation of the working volume of the conical terminated TEM cell, studies of the near-field were conducted in CADFeko in relation to the IEC 61000-4-3 standard considers an electric uniform if 75 % of measured points across a defined area within - 0 dB to + 6 dB. This section focuses on how the simulations are used to verify and or prove the compliance to the standard for uniformity.

Three near-field slices were considered, see Figure 5.10. A slice running parallel to the ground plane, to measure the E-field closest to the ground plane and the effect a DUT would have when galvanically connected to the ground plane. The second slice considered is a slice running parallel to the top-plate and positioned midway between the top-plate and ground plane. This slice was selected to observe the magnitude of the effect a DUT would have on the E-field. The last slice selected runs closest and parallel to the top-plate. This slice was considered as it is the furthest position, in height. To effectively test the size of the working volume we compare the E-field along the length of these 3 slices/planes with and without a DUT. Additionally, the E-fields are measured at 0.5 GHz and 1 GHz. Along the frequency range of 0.1 GHz to 1 GHz the S_{11} measured above 0.4 GHz was above -10 dB. Along the rest of the frequency range the S_{11} measured proved satisfactorily below -10 dB, as per the design. We thus observe the E-field consistency of the working volume at 0.5 GHz and 1 GHz.
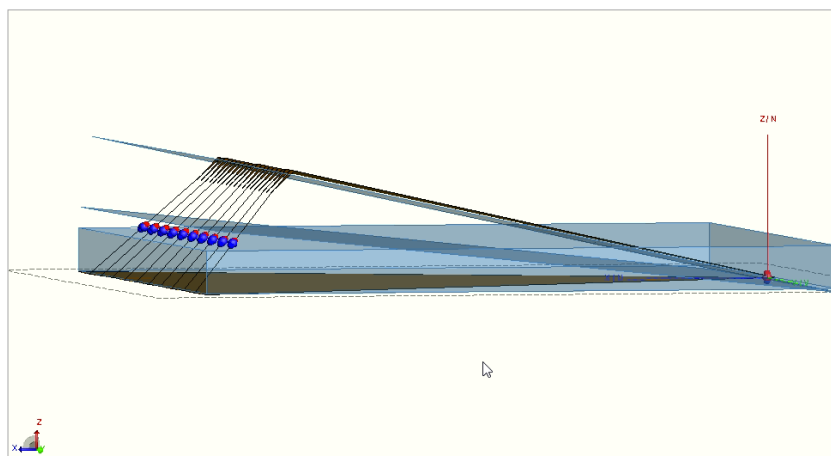
Figure 5.10: Perspective view of conical terminated TEM cell showing near E-field slice along ground plane, middle and top-plate in Altair Feko.

We look at the magnitude of the E-field observed along the x-axis along the ground plane, a slice running through the DUT and a slice along the top-plate, Figure 5.10. The working volume is further compared at 0.505 GHz and 1.0 GHz. Further to this, the response of the E-field running through the DUT at *y = 5 mm* and along the side of the DUT where *y = 85 mm*, is compared.
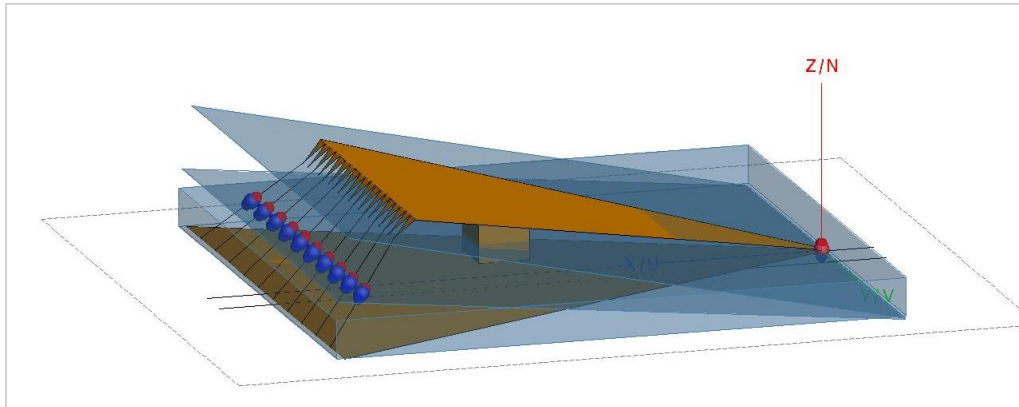
Figure 5.11: Side-view of conical terminated TEM cell showing near E-field slice along ground plane, middle and top-plate in Altair Feko and two lines illustrating y = 85 mm and y = 5 mm.

5.3.1 Electric near-field with raised DUT at 0.505 GHz and 1.0 GHz

In Figure 5.11 we explore the E-field magnitude when the DUT is raised 40 mm off the ground plane at 0.505 GHz. We explore the E-field behavior when the DUT is raised to determine the size of the working volume, as mentioned the height of the DUT when raised is close to the maximum working volume of the conical terminated TEM cell. The figures that follow include a y-axis specification, that value eg. y = 5 mm, indicating the distance from y = 0, through the DUT.
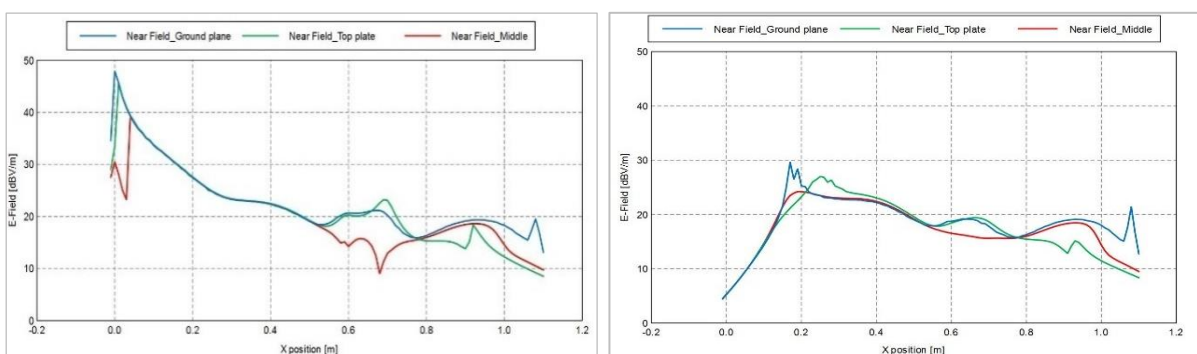
Figure 5.12: E-field at 0.505 GHz when the DUT is raised, the points are measured where y = 5 mm (left) and y = 85 mm (right)

In Figure 5.12 we observe the E-field running through the DUT at y = 5 mm and y = 85 mm. What is evident at 0.505 GHz is that the near-field slice directly through the DUT (Near-Field_Middle) follows the response of the other 2 slices (closest to ground plane and top-plate)

closely where it deviates between 0.55 m and 0.8 m. This x-coordinate matches the position of the DUT along the x-axis. The deviation of less than 10 dBV/m is due to the metallic DUT shielding effect on its inside. Further observations include the E-field decreasing steadily for all 3 near-field slices after 0.9 m. Recall the dimensions of the conical terminated TEM cell where the terminating resistive wires are connected to the top-plate at 0.9 m along the x-axis and terminate at 1.1 m on the ground plane.
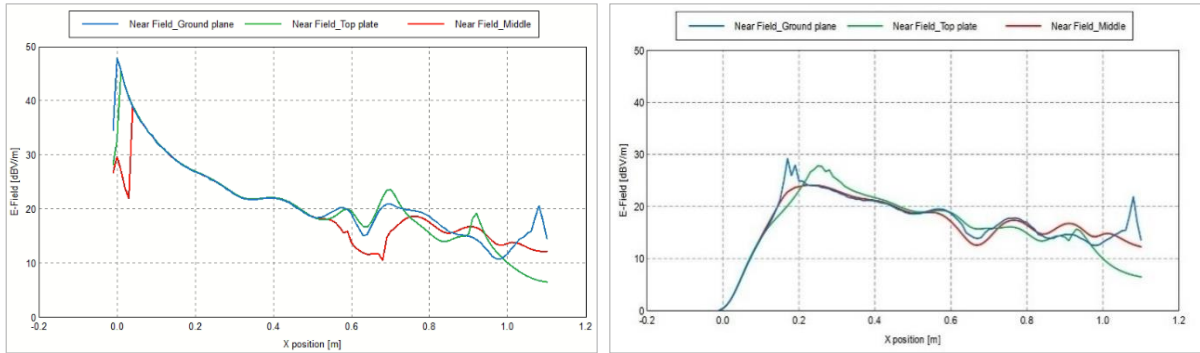
Figure 5.13: E-field at 1.0 GHz with DUT raised at y = 5 mm (left) and y = 85 mm (right)

In Figure 5.13, the analysed frequency is 1.0 GHz. We see similar E-field behaviour as to 0.505 GHz. Observations include the greatest deviation being the scenario where the slice runs directly through the DUT (Near Field_Middle), although deviation is approximately < 10 dBV/m compared to the slices along the ground plane and the top-plate. The other observation is that the E-field beyond the bounds of the conical terminated TEM cell (> 0.9 m) is not defined. Additionally, the greatest deviation we see is when the E-field is measured at 5 mm along the y-axis, compared to 85 mm along the y-axis.

5.3.2 Electric near-field along ground plane with and without DUT 1.0 GHz

We now observe the E-field behaviour along the ground plane with no DUT, when the DUT is flat on the ground plane and when the DUT is raised 40 mm from the ground plane.
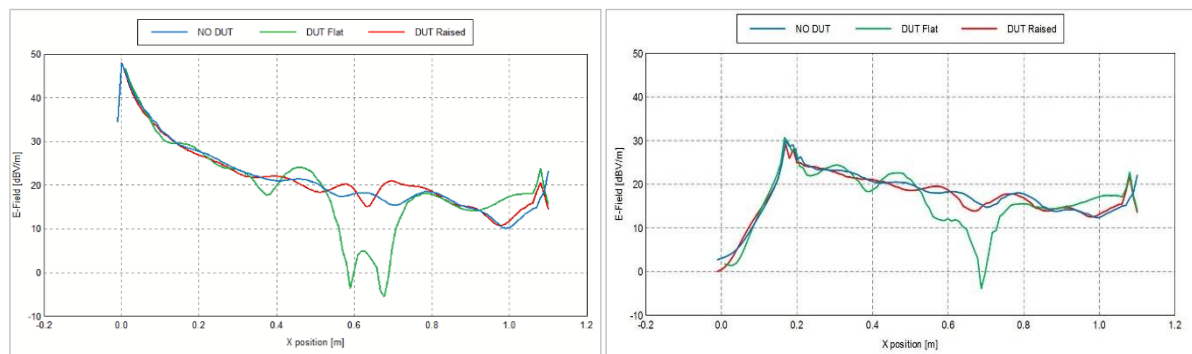
Figure 5.14: E-field at 1.0 GHz with and without DUT, y = 5mm (left), y = 85 mm(right)

From Figure 5.14 we observe a difference in the measured E-field around x = 0.55 m to x = 0.85 m, with the DUT is positioned flat on the ground plane. This is expected as the DUT and ground plane are galvanically connected and allow the interaction of fields, compared to galvanically isolated materials. Along the rest of the longitudinal axis (at y = 5 mm and y = 85 mm) we see that the E-field measured in all 3 scenarios is closely replicated. Thus, further informing the viability of the working volume of the conical terminated TEM cell. Bentz, 1996 advises that for immunity testing in TEM cell a tolerance of 0 dB to 6 dB should be maintained in at least 75 % of the measurement points across the defined area. In our case, this is across the area from 0.4 m to 0.9 m. We see conducive results with the near electric-field when no DUT is present and when the DUT is raised.

5.4   Conclusion

To conclude, when analyzing the measured and simulated results we observe a positive indication that the difference between them are minimal, with some shift in resonant frequencies as expected. The S_{11} remains below -10 dB up to 2.5 GHz. The conical terminated TEM cell thus shows good matching well above the designed frequency range and exceeds expected outcomes. Additionally, when observing the EM simulations performed in Altair Feko we note that the E-field along all three E slices is negligibly affected with and without a DUT. The greatest difference is evident when the DUT is flat on the ground-plane.

The following chapter explores the S_{11} performance of the conical terminated TEM cell versus other EMC testing facilities.

CHAPTER 6: COMPARISON TO OTHER EMC TESTING FACILITIES

6.1   Introduction

Research questions 3 and 4 are focused on comparing performance of the conical terminated TEM cell to other EMC testing facilities. This chapter will cover this comparison, specifically with regards to a conventional TEM cell and a reverberation chamber.

6.2   Comparison to conventional TEM cell

In the absence of a conventional TEM cell, we do a theoretical comparison based on commercially available TEM cells of similar size with a 50 Ω termination. We compare the size of the working volume and S_{11} reflection coefficient over a representative frequency range.

6.2.1 Comparison to TEM cell of similar size

We first look at an open TEM cell by TekBox®, the below image in Figure 6.1 shows a TBTC1 model, we are however interested in the TBTC3 model as it is comparatively sized compared to the manufactured conical terminated TEM cell, provided in the technical data in Table 7.
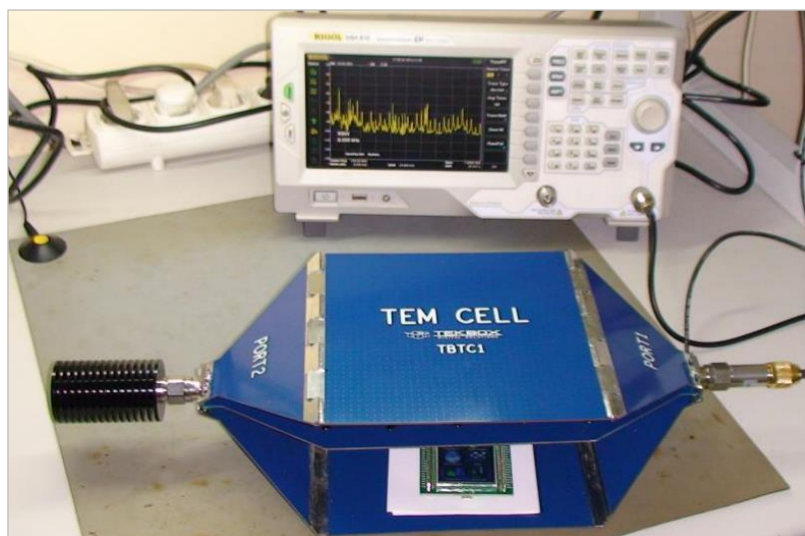
Figure 6.1: "Radiated emission measurement of a controller board using the TBTC1 TEM cell and a Rigol DSA815 spectrum analyser" (Tekbox, 2019).

Dimensions			
Length: 1038mm	Width: 501mm	Height: 305mm	Septum Height: 150mm

Rectangular area under septum	36cm × 48cm × 15cm
TEM Cell connectors	N- Female
Nominal cell impedance	50Ω
Wave impedance	377Ω
Maximum RF input power	25W (limited by supplied 50Ω termination)

As seen in Figure 6.1, for the TBTC3 TEM cell the S_{11} is below -15dB between 0.3MHz and 700 MHz, and from 700 MHz to 1 GHz increases to between -10dB and - 15dB.
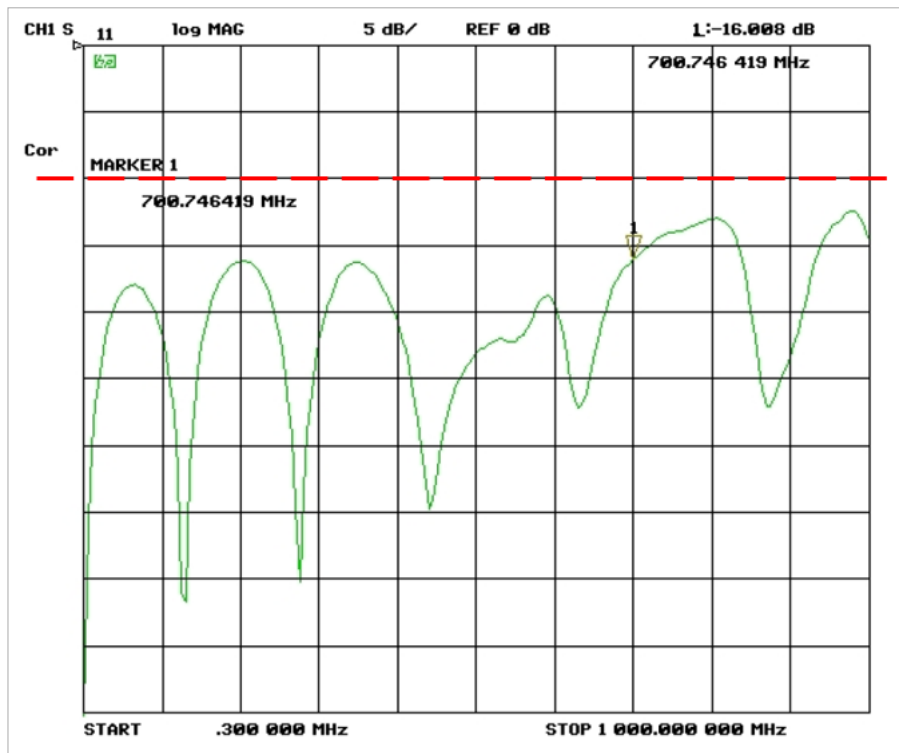
Figure 6.2: S_{11} of TBTC3 TEM cell (Tekbox, 2019).

Tekbox does note that their TEM cells render enhanced frequency performance compared to TEM cells of similar size because of a unique design feature that employs the use of resistance perpendicular to the desired direction of wave propagation.

The Tekbox TEM open TEM cell thus exhibits superior behaviour. For the Tekbox TBTC3 the S_{11} < -10 dB from DC to 1 GHz when compared to the manufactured conical terminated TEM that < -10 dB at > 0.4 GHz.

6.2.2 Comparison to TEM cell designed to operate at higher frequencies

As a reminder, the frequency range of a conventional TEM cell is inversely related to the size of the cell. The larger the size, the lower the upper usable frequency and vice versa.

We analyse the S_{11} of a smaller TEM cell, designed to operate > 2 GHz.

Deng *et al*, 2007 designs a modified closed TEM cell used to analyse RE of integrated circuits with an operating frequency of up to 2.5 GHz, the dimensions are given below. The TEM cell, with dimensions given below in Figure 6.3, shows an addition of an aluminium box that was part of the optimization of the cell, for the S_{11} output given below this should be ignored.
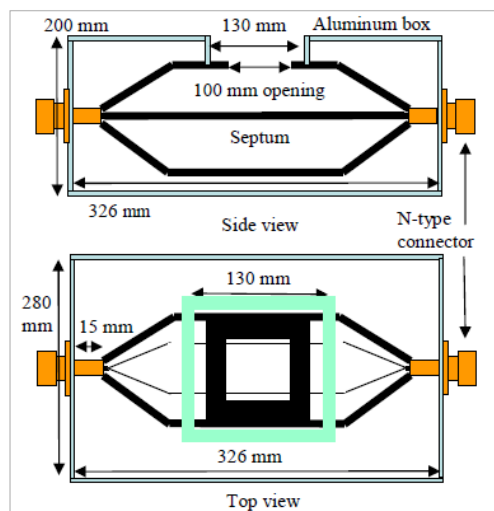
Figure 6.3: Side view and top view of closed TEM cell (Deng et al, 2007)

The dimensions of this TEM cell are significantly smaller than the manufactured conical terminated TEM cell, by approximately a 1/3 along the length and less than half of the width although it is similar is height.

The simulated S_{11} for this cell is given in the Figure 6.4, with an S_{11} output below -10 dB from DC to approximately 1.7 GHz. Above that, 3 major resonant frequencies are observed at 1.87 GHz, 2.23 GHz and 2.63 GHz, according to Deng *et al*, 2007. The simulation was conducted over a frequency range from DC to 3 GHz.
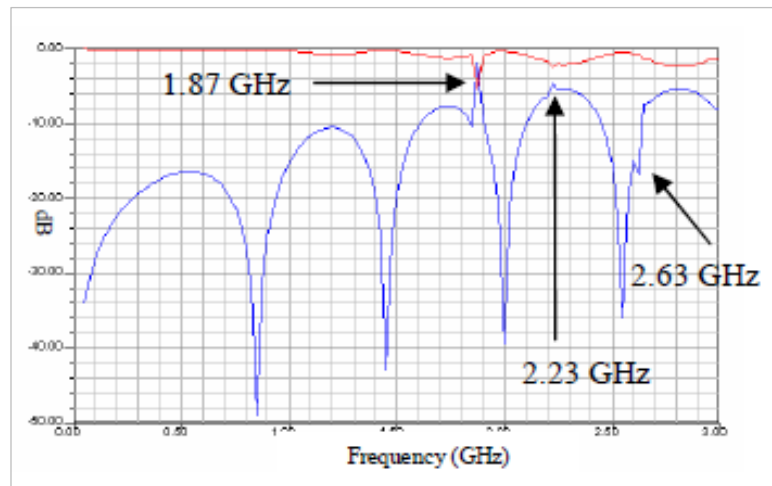
Figure 6.4: S_{11} and S_{21} magnitude of standard closed TEM cell simulated in CST Microwave Studio (Deng et al, 2007).

For the conical terminated TEM cell we also measured and simulated the S_{11} magnitude from 0.1 GHz to 2.5 GHz, the result is given in Figure 6.5.
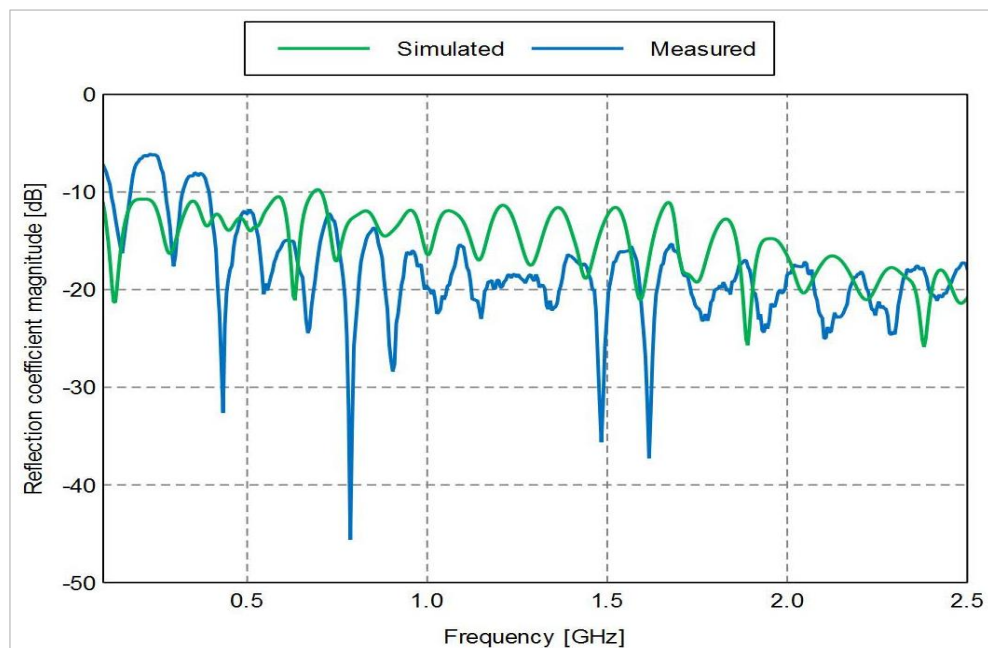
Figure 6.5: S_{11} of conical terminated TEM cell (Simulated vs Measured) 0.1 GHz to 2.5 GHz

The conical terminated TEM cell exhibits favourable S_{11} magnitude across the range 0.4 GHz to 2.5 GHz (< -10 dB) with the measured result below -15 dB from approximately 0.8 GHz. Deng *et al*, had tested for a working volume of 10 cm × 10 cm, similarly to this research. The difference being that the closed TEM cell in this case was smaller but however unable to achieve S_{11} < -10 dB above ≈ 2.1 GHz.

An RF analyzer with a vector network analyzer capability was then used to determine the conical terminated TEM cell's S_{11} to an even higher frequency range. This measurement was performed across a bandwidth of 0.1 GHz to 4.0 GHz.
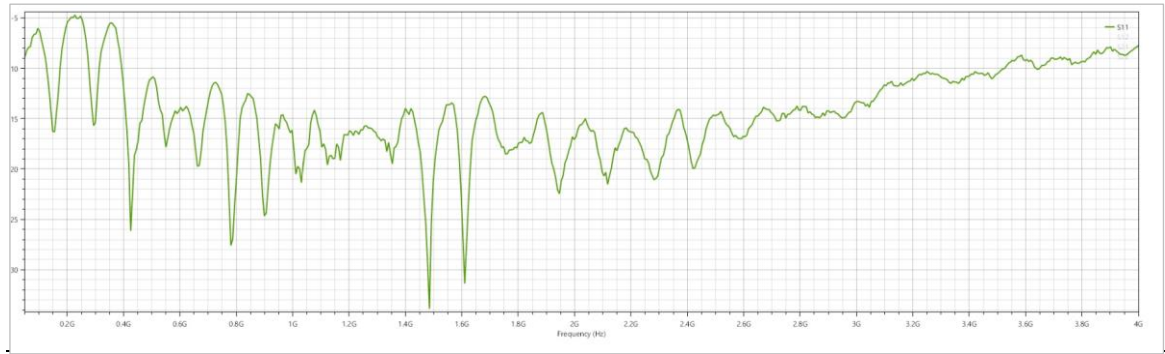
Figure 6.6: Measured conical terminated TEM cell S_{11}, from 0.1 GHz to 4 GHz, using RF analyzer

From this measurement we see a similar response in Figure 6.6, as with the VNA, S11 above -10 dB below 0.4 GHz. With this insight we note that the S_{11} remains below -10 dB between 0.4 GHz up to 3.5 GHz.

6.3   Comparison to reverberation chamber

We were able to compare the calibration results of a comb generator emitter (CGE), provided by the South African Radio Astronomy Observatory (SARAO) and MESA solutions that was calibrated in a reverberation chamber. The IEC 61000-4-20 standard for emissions and immunity testing in TEM waveguides prescribes a 0 to 6 dB variation across the calibrated area for each frequency, for an empty TEM waveguide. Furthermore, an emissions correlation is accepted if the standard deviation is within 4 dB across 10 or more frequencies, and the average remains within 0 to 3 dB (Harrington & Bronaugh, 2001).
This lends validation to the results obtained using the conical terminated TEM cell.

6.3.1 Comb generator emission results obtained at CPUT lab

Measurements were performed using an Anritsu MS2090A Fieldmaster Pro Spectrum Analyzer capable of analysis across a bandwidth of 9 kHz to 14 GHz.

As seen in Figure 6.7, the CGE was placed 630 mm from the feeding SMA connector, the same distance from the centre conductor as the aluminium cut-out used as a DUT.

Figure 6.7: York EMC CGE01 - 50 MHz to 18 GHz (Eurofins York LTD, 2022)

The aim of this measurement was to compare a reverberation chamber measurement to the conical terminated TEM cell measurement using a calibrated, known emitter. The radiated coupling between CGE and cell, and the CGE's power emitted with 2001 points measured across a bandwidth of 0 GHz to 4 GHz. Results are modelled using MATLAB.

Measurements were performed in a noisy lab environment and in the enclosed and shielded reverb chamber. We also consider the loading effect that the setup has on the comb generator. This is done by comparing the reverberation chamber measurement of the CGE without the conical terminated TEM cell and with the CGE in the cell.
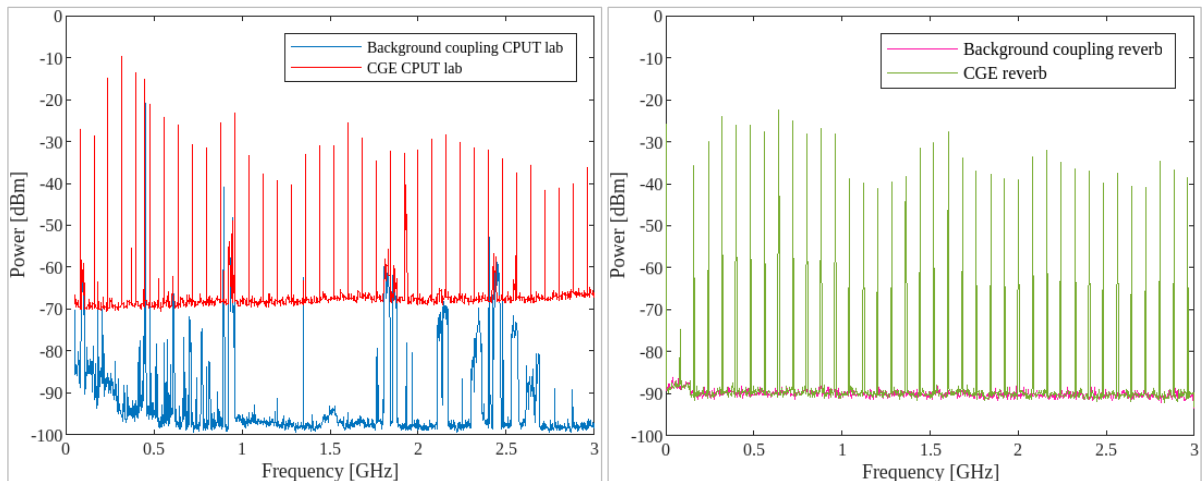
Figure 6.8: Background coupling and CG emissions measured by the conical terminated TEM cell in CPUT lab (left). Background coupling and CG emissions measured by the conical terminated TEM cell in SARAO reverberation chamber (right).

From Figure 6.8 (left) we observe peaks around 0.4 GHz, 0.8 GHz and 1.7 GHz, 2.2 GHz and 2.5 GHz, this is attributed to the ambient RF environment. Looking at the CG emissions measured by the conical terminated TEM cell we note that the CGE emission levels are all higher, except at 0.4 GHz.

To understand the accuracy of the conical terminated TEM cell we compare the CGE emissions results measured by the conical terminated TEM cell to CGE emission results obtained in a reverberation chamber.

These tests were conducted at SARAO facilities in Observatory, Cape Town, South Africa.

To compare the background coupling obtained in a lab to those obtained in a reverberation chamber, the reverberation chamber is calibrated to measure 801 points across a frequency range of 1 kHz to 3 GHz with the reference level set to -10 dBm, see Figure 6.8 (right).

The noise level is favourable, as we do not see any spikes indicating ambient RF interference at the three intervals described when testing was conducted in the student lab at CPUT.

6.3.2 Comb generator emission results obtained in reverberation chamber

Comb generator emissions in the reverberation chamber, without the TEM cell were then tested. The spectrum analyzer settings were as follows:

- Continuous-mode with stirrers rotating at 15 °/ second
- Resolution BW = 100 kHz
- Max-hold function
- Positive Peak detection

Figure 6.9: Picture of Comb Generator in reverberation chamber at SARAO facilities.

In Figure 6.10 we compare the peaks of the CGE power across a frequency range of 100 kHz to 3 GHz when the comb generator is placed within the bounds of the conical terminated TEM in the CPUT lab versus the comb generator results obtained in the reverberation chamber.
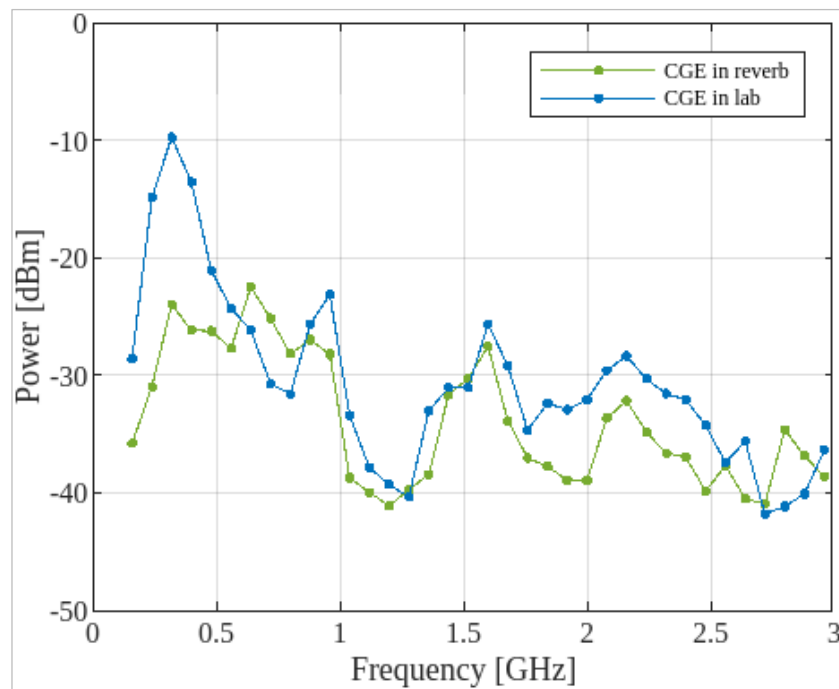
Figure 6.10: CGE measured in conical terminated TEM cell at CPUT plotted against CGE measured in SARAO reverberation chamber

From this comparison we note that the comb generator emissions measured in the conical terminated TEM cell in the student lab at CPUT are largely the same compared to that obtained in the reverberation chamber at SARAO. As in Hamann *et al*, 2014, TEM waveguide measurements may be used without correlation. We can therefore say these measurements are in close agreement. That is, except for the three spikes observed in the student lab at approximately 0.3 GHz 0.43 GHz and 0.8 GHz. The spikes at 0.3 GHz an 0.8 GHz are expected and are present due to environmental noise. The spike at 0.43 GHz is present due to the comb generator.

In Figure 6.11 below we note the dBm difference between the measurements, where the CGE measured in SARAO reverberation chamber is deducted from the CGE measured in the conical terminated TEM cell in the student lab at CPUT. The larger difference below 300 MHz is expected as the reverberation chamber does not effectively measure below this frequency. Beyond 300 MHz, the difference in measured power does not exceed an upper or lower limit of 5 dB. The larger E-field variation below 400 MHz is due to the lowest usable frequency of the reverberation chamber.
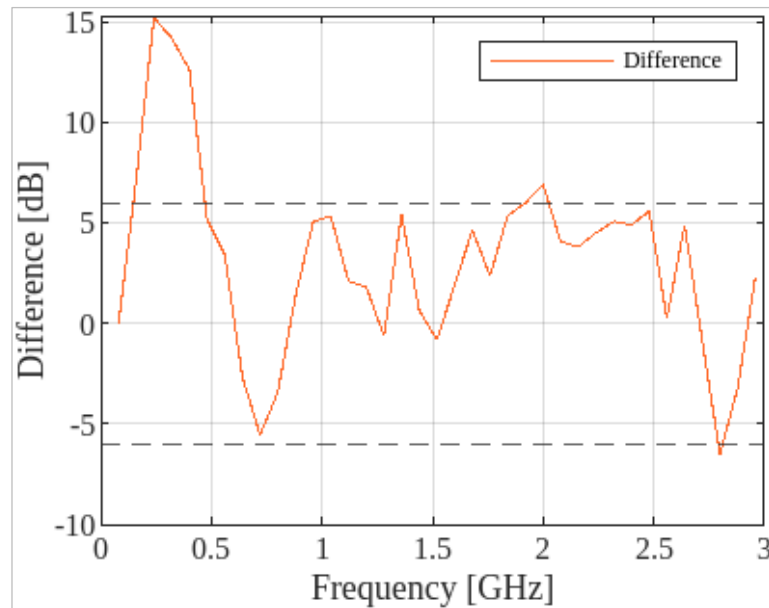
Figure 6.11: Plot showing the difference between CGE measured in conical terminated TEM cell at CPUT minus the CGE measured in SARAO reverberation chamber

We turn our focus to the comb generator emission measurements obtained when it is hosted inside the bounds of the conical terminated TEM cell and placed inside the reverberation chamber. In Figure 6.13 below, we note the highest power output observed around 0.3 GHz.

Figure 6.12: Comb generator housed inside conical terminated TEM cell and inside reverberation chamber at SARAO.

As the objective here is to show the loading effect that the TEM cell has on the total radiated power from the CGE, we display the comparison between the CGE emission results obtained when:

- The comb generator is placed in the bounds of the conical terminated TEM cell inside the reverberation chamber.
- When the CGE is placed inside the reverberation chamber on its own.
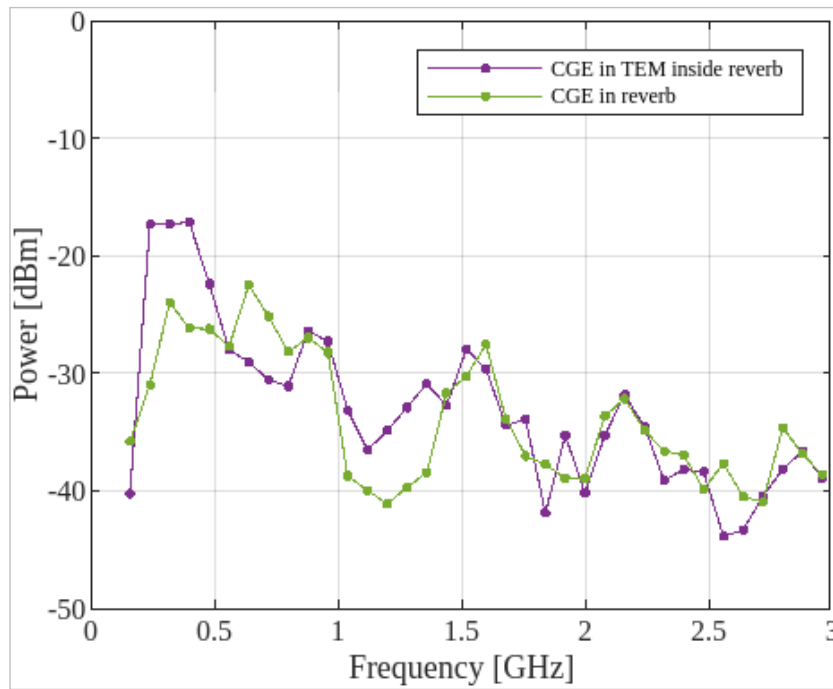
Figure 6.13 Comparison of comb generator emissions in reverberation chamber and conical terminated TEM cell.

Figure 6.13 above shows the peaks of the comb generator emission measurements obtained when the CGE was placed inside the bounds of the reverberation chamber on its own and when placed inside the conical terminated TEM cell inside the reverberation chamber. We can say that these two measurements are in very close agreement.

The measurements in the reverberation chamber are calibrated to include reverberation chamber losses and the standard deviation prescribes to the IEC limit of - 3 dB. The difference in power between the two measurements in Figure 6.14 is seen below.
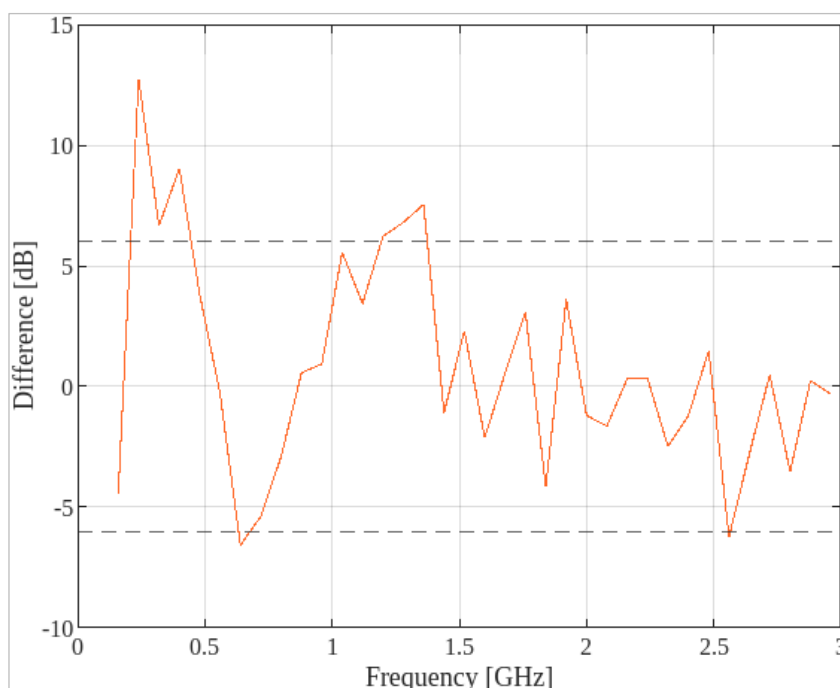
Figure 6.14: Plot showing difference between CGE inside TEM in reverb minus CGE in reverb

A factor identified in the offset of the CGE measurements is that although testing was conducted between 0.1 GHz and 3 GHz the operational bandwidth of the reverberation chamber is 0.3 GHz to 8 GHz and so below the lower usable frequency (LUF) the variation in measured data values can increase significantly.

6.4 S_{11} measurement validation

We discuss the S_{11} measurements and results below, by comparing the measured results obtained in the student lab at CPUT and results obtained inside a shielded chamber at SARAO, without stirring. The same testing instrument, a NanoVNA V2 (S-A-A-2) VNA was used to perform S_{11} magnitude tests on both days. 'CPUT Open Lab' refers to measurements taken on one day in the student lab at CPUT and 'Inside Shielded Chamber' refers to measurements taken on a different day at SARAO facilities.

We observe three test cases:

- Conical terminated TEM cell, no DUT (DC – 2.5 GHz)
- Conical terminated TEM cell, DUT flat (DC – 2.5 GHZ)
- Conical terminated TEM cell, DUT raised (DC – 2.5 GHz)
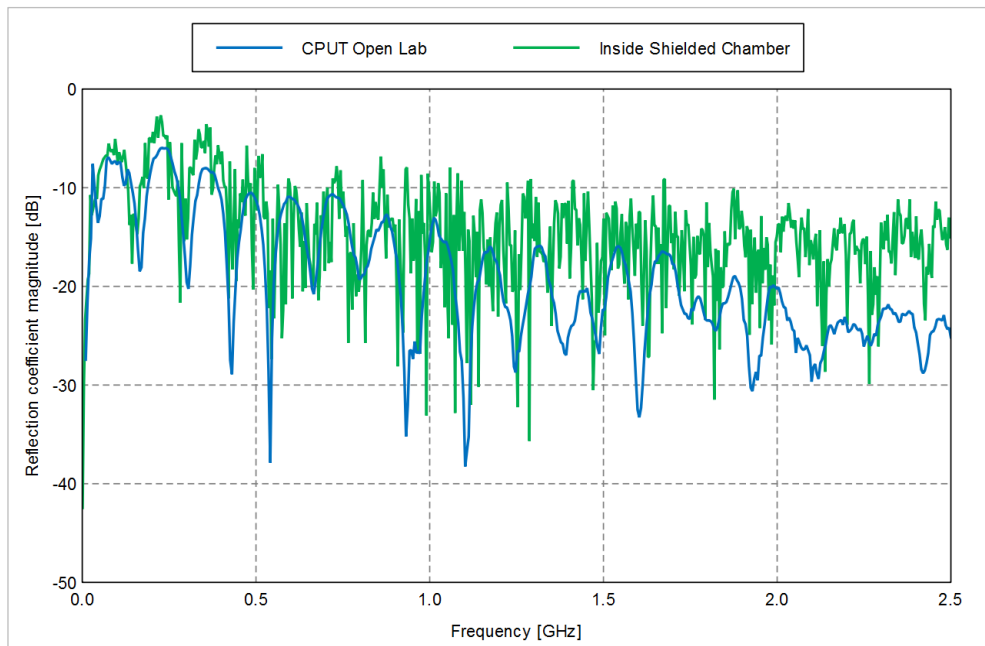
Figure 6.15: S_{11} magnitude comparison with no DUT

Looking at the S_{11} magnitude in Figure 6.15, across the DC to 2.5 GHz frequency range we observe that the shielded chamber measurement exhibits a higher S_{11} magnitude than that initially conducted in the CPUT lab. As measurements were conducted inside a reverberation chamber, although the stirrer was not moving, the metallic nature of the environment would contribute to a higher number of reflections and thus increase the S_{11} magnitude component of the conical terminated TEM cell. As noted in Section 4.9 both measured results do not yield an S_{11} reflection coefficient below -10 dB between DC and 0.4 GHz, this is consistent throughout both measurements. The variation in the measurements conducted on the two separate occasions is less than 5 dB between DC and 1.5 GHz. However, the reflection coefficient remains below -10 dB across most of the frequency range above 0.4 GHz inside the shielded environment.

Figure 6.16: Photograph of DUT flat on ground plane of the conical terminated TEM cell, SARAO facilities
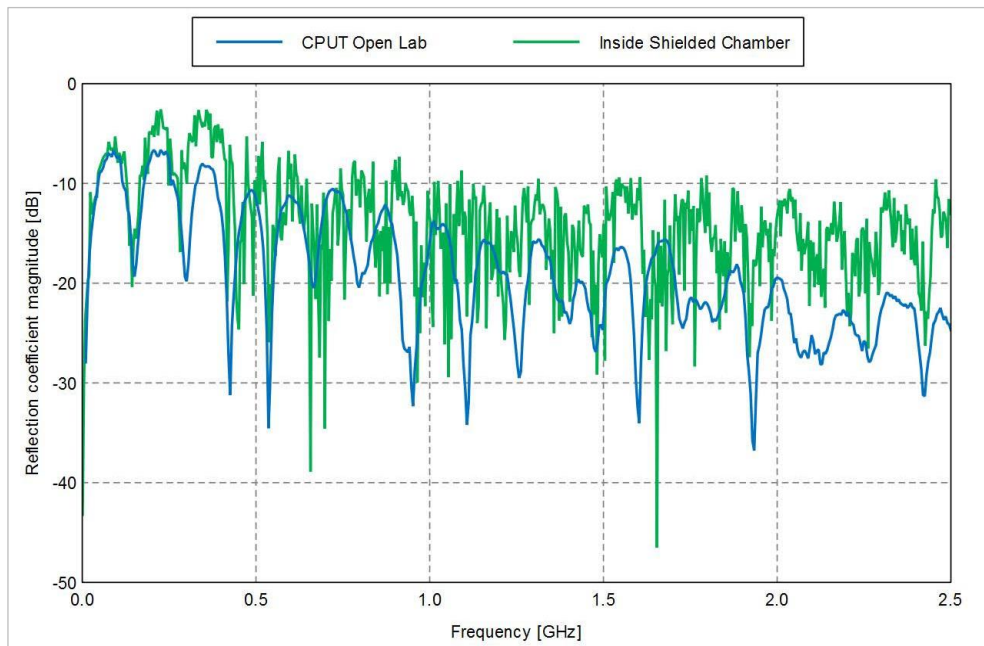
Figure 6.17: S_{11} magnitude comparison with DUT flat on ground plane

For this test case where the DUT is laid flush with the ground plane 635 mm from the centre conductor, the results are displayed in Figure 6.17. Below 0.4 GHz the S_{11} reflection magnitude is above -10 dB in both measurements. Above 0.6 GHz, the S_{11} magnitude of this scenario remains consistent and well below the prescribed threshold of -10 dB in for both measurements. Looking at the measurement inside the shielded chamber, we do, however, see increases in the comparative magnitude between 0.6 GHz and 0.9 GHz. Below approximately 1.7 GHz the variation between the measurements is lower than 5 dB, above 1.7 GHz the difference increases to about 10 dB along the frequency range. Considering this result together with the field uniformity result of Section 5.3, it is clear that the DUT should not be placed flush to the ground plane for accurate measurements.
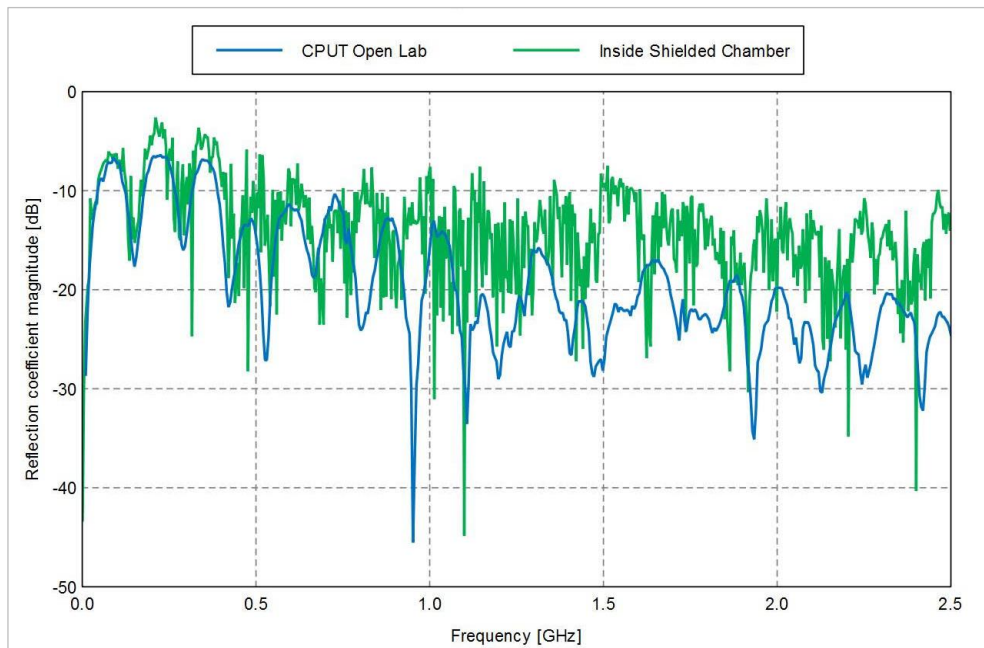
Figure 6.18: S_{11} magnitude comparison with DUT raised 40mm from ground plane

The last test case presented in Figure 6.18, is that where the DUT is raised 40 mm above the ground plate, 635mm from the centre conductor along the length of the cell. We see close comparability between the two measurements from DC to 0.4 GHz. The measurements compare very closely up to 1.5 GHz, from this point they diverge by up to 10 dB toward the limit of 2.5 GHz. Although we see a few spikes above -10 dB where measurement inside the shielded chamber intersects the -10 dB limit, at a few frequencies these are negligible and for the most part remains below -10 dB. This is a good result considering the vertical component of 40 mm was chosen for the DUT as it nears the extremities of the working volume as calculated in Section 4.5.

6.5 Conclusion

In this section we have answered Research Question 3 and Research Question 4 concerning the performance of the conical terminated TEM cell, with respect to a conventional TEM cell and other EMC testing facilities. By performing tests, measuring outputs, analysis and presenting the findings comparing to the conventional TEM cell and found that the conical terminated TEM cell exhibits favourable S_{11} magnitude across the range between 0.4 GHz to 2.5 GHz compared to the closed, conventional TEM cell (Deng *et al).*

Looking at the comparisons between the CGE in the reverberation chamber and at the CPUT student lab it is noted that there is a difference of approximately 5 dB along the frequency range with the conical terminated TEM cell producing the higher measurement. We can say with conviction that the terminated conical TEM cell operates as designed and can be used as a EMC pre-compliance testing setup in the absence of a shielded chamber.

CHAPTER 7: CONCLUSION

A conical terminated TEM cell for benchtop-use at CPUT was successfully designed, simulated, manufactured, and tested. The frequency range for which the cell was initially designed (DC to 1 GHz) was achieved and beyond that the cell showed an S_{11} magnitude below – 10 dB up to 2.5 GHz. This was achieved without a DUT, when a DUT was galvanically connected to the ground plane and when it was raised by 40 mm from the ground plane. In investigating the maximum achievable working volume, we note consistency in electric near-field responses with the no DUT and raised DUT scenarios along the longitudinal component of the conical terminated TEM call. We observe the greatest variance in the electric-near field occurs when the DUT is flat on the ground plane. This indicates that any DUT should not be placed directly on the ground plane for testing, but raised from the ground plane. From the study, it has been proven that the conical terminated TEM cell is suitable for EMC pre-compliance testing of a 1U CubeSat and CubeSat subsystems.

We reflect on the research questions and research objectives and summarise our findings below. Refer to Section 1.6 as a reminder of the research questions and objectives.

- **Response to RQ 1**: The maximum achievable working volume is the full-longitudinal component of the conical terminated TEM cell, without a DUT. When a DUT is inserted, it must maintain a cross-sectional size of less than 60% of the cell's height (roughly 121 mm), at that point, for the working volume to remain stable. The working volume is large enough to house a 1U CubeSat within its bounds.

- **Response to RQ 2:** The measured S_{11} results indicate that the cell reflects less than 1% of the signal power back to the source (-10 dB) between 0.4 GHz and up to 3.5 GHz. This is verified by measurements using the NanoVNA vector network analyzer (up to 2.5 GHz), see Figure 6.5. For this measurement we tested with and without a DUT and the result is consistent. However, it is noted that the DUT should not be placed directly on the ground plane, but raised and not touching it. The measurement conducted using a RF analyzer (up to 4.0 GHz), the S_{11} measurement remained below -10 dB up to 3.5 GHz. This measurement was conducted without a DUT, see Figure 6.6.

- **Response to RQ 3:** The open TEM cell from TekBox, of similar size to the conical terminated TEM cell, is designed to operate up to 1 GHz (see Figure 6.2). It maintains an S_{11} below -10 dB throughout the full frequency range. This specific cell employs resistance perpendicular to the desired direction of wave propagation. The S_{11} of the TekBox cell outperforms the conical terminated TEM cell up to 1 GHz. It is however not suitable for use above 1 GHz as the conventional TEM cell cut-off frequency is inversely related to its dimensions. Looking at the closed TEM cell in Figure 6.4, it is about 1/3 of

the size of the conical terminated TEM cell and is designed to operate above 2.0 GHz. This cell only maintains a S_{11} below -10 dB below 1.7 GHz. In this regard, the conical terminated TEM cell is observed to exceed performance of this closed TEM cell. Additionally, due to the limitation this closed TEM cell introduces, it would not be able to accommodate a 1U CubeSat.

- **Response to RQ 4:** Above 300 MHz the conical terminated TEM cell performed well against the reverberation chamber. If we look at the S_{11} obtained in the shielded chamber we see slightly higher output, due to the reflections introduced in the chamber. With more reflections in the chamber we still note that the output remained below -10 dB, for the most part. When comparing the conical terminated TEM cell measured results to the calibrated reverberation chamber total radiated power results, we see we see a maximum difference of 5 dB. This is within the bounds of reverberation chamber and TEM cell uncertainty levels as specified by CISPR 16-4-1 and confirms the suitability of the cell for EMC testing.

Some recommendations are included below for future improvements of a conical terminated TEM cell.

We identified a variation in first resonant frequency between simulated and measured results. This was largely attributed to the actual length from source to edge of top plate as well as the length of the terminating wires. This can be resolved by using a frame in manufacturing, ensuring that length of the actual top plate and simulated top plate would be aligned. This will eliminate the concave bends found in the artefact. Similarly, the conical terminated TEM cell was designed with a 3 mm centre conductor length. The measured separation of the centre conductor, after manufacture, between the top plate and ground plate was slightly larger ($\approx$ 1 mm).

With time-constraints, minimised accessibility to resources, and a lightweight material requirement aluminium was used for manufacture of ground plate and top plate. Although it proved easy to handle it proved to be challenging when soldering components onto the aluminium. This was solved by adhering copper tape to the aluminium and soldering onto the tape.

During testing the cell was exposed to interference, especially at low frequencies, where commonly used devices such as such as remotes and two-way radios operate. It is recommended to perform testing in a shielded environment like an EMC anechoic chamber, or even an unstirred reverberation chamber.

REFERENCES

Adams, AT. 2014. 'Principles of Electromagnetics Five: Wave Applications', Momentum Press, New York. Available from: ProQuest Ebook Central. [02 July 2021].

Altair Feko. (n.d.). Electromagnetic Simulation for Connectivity, Compatibility, and Radar | Altair Feko. [online] Available at: https://altair.com/feko [Accessed 9 Jul. 2023].

Baum, C.E. 1966. 'Impedances and field distributions for parallel plate transmission line simulators'. *Sensor Simulation Note 21*.

Bentz, S. 1996. 'Use of the TEM cell for compliance testing of emissions and immunity, an IEC perspective'. *In Proceedings of Symposium on Electromagnetic Compatibility*, pp. 43-47. IEEE.

Brewer, M. 2012. *CubeSat Attitude Determination and Helmholtz Cage Design*. Unpublished Masters Thesis, Air Force Institute of Technology, Ohio.

Carlisle, G. 1969. 'Impedance and fields of two parallel plates of unequal breadths'. *Sensor Simulation Notes*, *90*.

Caspers, F., McIntosh, P. and Kroyer, T. 2010. 'RF Engineering Basic Concepts. S-Parameters', CAS, [Online] Available at: https://cas. web. cern. ch/cas/UK-2007/Afternoon, 20 [accessed 12 October 2022]

Chhaya, L. 2013. 'World's Quietest Room: Anechoic Chambers For EMC Testing', *i-Manager's Journal on Electronics Engineering,* vol. 3, no. 4, pp. 1-3. https://doi.org/10.26634/jele.3.4.2391

Clark, T.L., McCollum, M. B., Trout, D. H., Javor, K. 1995. 'Marshall Space Flight Center Electromagnetic Compatibility Design and Interference Control (MEDIC) Handbook'. NASA, Reference Publication, 1368

Crawford, M.L.1974. 'Generation of Standard EM Fields Using TEM Transmission Cells'. *IEEE transactions on electromagnetic compatibility*. [Online] EMC-16 (4), 189–195.

Dawson, L. & Marvin, A. 1999. 'Procedure for new draft of Defence Standard 59-41-calibrating screened room antenna combinations against OATS'. *IEEE transactions on electromagnetic compatibility*. [Online] 41 (4), 368–374.

Deng, S., Pommerenke, D., Hubing, T., Drewniak, J., Beetner, D., Shin, D., Kim, S. and Kwak, H., 2007, July. Mode suppressed TEM cell design for high frequency IC measurements. In *2007 IEEE International Symposium on Electromagnetic Compatibility* (pp. 1-6). IEEE.

emcsupplies.com. (n.d.). *TBTC2 - Open TEM Cell for EMC Pre-Compliance Testing, 100mm Septum.* [online] Available at: https://emcsupplies.com/collections/tem-cells/products/tekbox-tbtc2-open-tem-cell-for-emc-pre-compliance-testing-100mm-septum [Accessed 6 Aug. 2023].

Eurofins York Ltd. 2022. 'Comb Generator Emitter CGE01 – 50 MHz to 18 GHz'. [Online] Available at: <https://www.yorkemc.com/products/cge-comb-generator-emitters/cge01/> (Accessed 28 October 2022)

www.everythingrf.com. (n.d.). *Microstrip Width Calculator*. [online] Available at: https://www.everythingrf.com/rf-calculators/microstrip-width-calculator.

Foley, J. 2012. Calibration and Characterization of CubeSat Magnetic Sensors using a Helmholtz Cage. Unpublished Masters Thesis. California Polytechnic State University, San Luis Obispo.

Frey, D., 2003. 'Epistemology in Engineering Systems'. Massachusetts Institute of Technology Engineering Systems Division.

Ghosh, S., Singhley, M.R., Shastry, S.V.K., Chakrabarty, A. 1999. 'Design and characterisation of GTEM cell', in *Proceedings of the International Conference on Electromagnetic Interference and Compatibility*. [Online]. 1999 IEEE. pp. 274–279.

Giri, D.V. & Baum, C.E. 1996. 'Design guidelines for flat-plate conical guided-wave EMP simulators with distributed terminators'. *Sensor Simulation Note 402*.

Giri, D.V., Liu, T.K., Tesche, F.M., King, R.W.P. 1980. 'Parallel plate transmission line type of EMP simulators: A systematic review and recommendations. *Sensor Simulation Note 261*.

Giri, D.V., Baum, C.E., Schilling, H. 1978. 'Electromagnetic considerations of a spatial modal filter for suppression of non-TEM modes in the transmission-line type of EMP simulators'. *Sensor Simulation Note 247*.

GTEM 250 F – GTEM250 F SAE – GTEM FV. Absolute EMC. https://absolute-emc.com/product/gtem-250-f-gtem250-f-sae-gtem-fv [Online]
Hewlett-Packard Company, 1998. 'Making radiated and conducted compliance measurements with EMI receivers', *Application Note 1302.*

Hamann, D., Peikert, T., Ostowar, A.S. and Garbe, H., 2014, August. On the equivalent use of TEM waveguides for EMC measurements and calibrations. In *2014 XXXIth URSI General Assembly and Scientific Symposium (URSI GASS)* (pp. 1-4). IEEE.

Harrington, T. E. & Bronaugh, E. L. (2001) 'EUT directivity and other uncertainty considerations for GHz-range use of TEM waveguides', in *2001 IEEE EMC International Symposium. Symposium Record. International Symposium on Electromagnetic Compatibility (Cat. No.01CH37161)*. [Online]. 2001 IEEE. pp. 117–122 vol.1.

Hariyawan, M Y, R S Darwis, and B A Habibi. "Low-Cost Transverse Electromagnetic (TEM) Cell Design for Radiated Emission Measurement." *IOP conference series. Materials Science and Engineering* 1073.1 (2021): 12040–. Web.

Icheln, C. 1995. 'The construction and application of a GTEM cell'. (Masters thesis, Technical University of Hamburg-Harburg & Helsinki University of Technology).

IEC 61000-4-3 ed4.0: Electromagnetic Compatibility (EMC) Part 4-3: Testing and measurement techniques - Radiated, radio-frequency, electromagnetic field immunity test. IEC, 2020.

IEC 61000-4-20 ed2.0: Electromagnetic Compatibility (EMC) Part 4-20: Testing and measurement techniques, Emission and immunity Testing in Transverse Electromagnetic (TEM) Waveguides. IEC, 2010.

IEC 61000-4-21 ed2.0: Electromagnetic Compatibility (EMC) – Part 4-21: Testing and measurement techniques – Reverberation chamber test methods. IEC, 2011.

IEC 61000-4-22 ed1.0: Electromagnetic compatibility (EMC) – Part 4-22: Testing and measurement techniques – Radiated emissions and immunity measurements in fully anechoic rooms (FARs). IEC, 2010.

IEC CISPR, 16-1-1 ed5.0: Specification for radio disturbance and immunity measuring apparatus and methods - Part 1-1: Radio disturbance and immunity measuring apparatus - Measuring apparatus. IEC, 2019.

IEC CISPR, 16-2 ed2.0: Specification for radio disturbance and immunity measurement apparatus and methods - Part 2: Methods of measurement of disturbances and immunity. IEC, 2003.

IEC CISPR 16-3 ed4.0: Specification for radio disturbance and immunity measurement apparatus and methods - Part 3: Reports and recommendations of CISPR. IEC, 2020.

IEC CISPR 16-4 ed2.2: Specification for radio disturbance and immunity measurement apparatus and methods - Part 2: Uncertainties, statistics and limit modelling — Uncertainties in standardized EMC tests. IEC, 2018.

Intel Platform Testing Services. https://designintools.intel.com/platformtestingservices. [Online].

Khan, M. 2018. 'Damage Evolution of High Chromium Steels Utilised for High Temperature Components' (Master's thesis, Technische Universität).

Leferink, F. B. 1998. 'High field strength in a large volume: the balanced stripline TEM antenna', in *1998 IEEE EMC Symposium. International Symposium on Electromagnetic Compatibility. Symposium Record (Cat. No.98CH36253)*. [Online]. 1998 IEEE. pp. 350–354 vol.1.

Mathur, P & Raman, S. 2020. 'Electromagnetic Interference (EMI): Measurement and Reduction Techniques'. *Journal of electronic materials*. [Online] 49 (5), 2975–2998.

Mazzola, S. 2009. 'MIL-STD-461: The basic military EMC specification and it's evolution over the years', in *2009 IEEE Long Island Systems, Applications and Technology Conference*. [Online]. 2009 IEEE. pp. 1–5.

MIL-STD-461, MILITARY STANDARD: Electromagnetic Interference Characteristics Requirements For Equipment (31 July 1967).

Morgan, D. 1994. 'Chapter 9 - EMC Test Regimes and Facilities'. *A Handbook For EMC Testing and Measurement*. IET. © 1994. Books24x7. *<http://library.books24x7.com.libproxy.cput.ac.za/toc.aspx?bookid=8668>* (accessed June 23, 2021)

NanoRFE, *User Manual - NanoVNA V2*, *<https://nanorfe.com/nanovna-v2-user-manual.html>* (accessed October 17, 2022)

Nothofer, A., Alexander, M.J., Bozec, D., Welsh, D., Dawson, L., McCormack, L., Marvin, A.C. 2003. A GTEM best practice guide–applying IEC 61000-4-20 to the use of GTEM cells. In *15th International Zurich Symposium on Electromagnetic Compatibility.*

Omollo, N.A. 2019. 'Shielding effectiveness investigations using a reverberation chamber'. (Doctoral dissertation, Stellenbosch University)

Pozar, D. M. 2012. 'Microwave Engineering'. 4th ed. Hoboken, NJ: Wiley.

Pywell, M. & Midgley-Davies, M. 2017. 'Aircraft-sized anechoic chambers for electronic warfare, radar and other electromagnetic engineering evaluation'. *Aeronautical journal*. [Online] 121 (1244), 1393–1443

Rajamani, V., Bunting, C., Freyer, G. 2008. 'Why consider EMC testing in a reverberation chamber', in *2008 10th International Conference on Electromagnetic Interference & Compatibility*. 2008 IEEE. pp. 303–308.

RF Design. 2019. 'RF Test Equipment Series: RF Anechoic Chambers', https://rf-design.co.za/2019/11/22/rf-test-equipment-series-rf-anechoic-chambers/. [Online]

Satav, S.M. and Agarwal, V. 2008. 'Do-it-yourself fabrication of an open TEM cell for EMC pre-compliance'. *IEEE EMC Society Newsletter*, *218*, pp.66-71.

Saunders, M., Lewis, P. and Thornhill, A., 2019. Research methods for business students. 8[Th] Ed. Pearson education

Sim, D., Kwak, S., Kwon, J.H., Park, S. 2019. 'Design of new reverberation chamber for electromagnetic compatibility and wireless device measurement applications and its reproducibility performance validation'. *Microwave and optical technology letters*. [Online] 61 (3), 801–804.

Stander, T. and Sinha, S. 2013. 'Development, simulation and construction of cost-effective GTEM cell'. In *2013 23rd International Conference Radioelektronika (RADIOELEKTRONIKA)* (pp. 39-44). IEEE.

Tengli, M. 2020. 'Blog 132-Research Onion: A systematic approach to designing research methodology'. [Online] Available at: https://www.researchgate.net/publication/357284560/ [Accessed 10 April 2022].

Tekbox Digital Solutions, 2019. 'Open TEM Cells for Pre-Compliance Testing'. *<https://www.tekbox.com/product/open-tem-cells-emc-compliance-testing>* (Accessed 22 October 2022)

Yıldız, C., Demirel G., Caliskan, F. 2016. 'Numerical and experimental analysis of transverse electromagnetic cell'. *International journal of RF and microwave computer-aided engineering.* [Online] 26 (4), 373–378.

Yousaf, J., Nah, W., Hussein, M.I., Yang, J.G., Altaf, A., Elahi, E. 2020. 'Characterization of Reverberation Chamber - A Comprehensive Review.' *IEEE access.* [Online] 81–1.

York EMC Services. ND. 'CGE 01 Comb Generator Emitter'. https://www.yorkemc.com/wp-content/uploads/CGE01_Product_Flyer.pdf (Access 28 November 2022)

APPENDICES

Appendix A

Aluminium Specification Sheet

Ref.: SK 2345   <mark>MILL TEST CERTIFICATE</mark>

Product Standard: GB/T 3880/2012 – Aluminium flat rolled conforming to EN 10204-3:1

Mechanical Properties - AA 1050 H14 sheet & treadplates

Customer : Eurosteel [CAPE TOWN] Ref.: PO 33662 – 21 packages [39532 Kg Net]

B-BBEE STATUS – LEVEL 1
B-BBEE PROCUREMENT – 135%
Cert. No.: XY2022050701

Descriptions of Goods	Alloy-Temper	Sizes (mm)	N.W.(kg)	Tensile Strength (Mpa)	Elongation (%)	Yield Strength (Mpa)	Chemical Composition(%)							
							Al	Si	Fe	Cu	Mn	Mg	Zn	Cr
Aluminium Sheet	1050 H14	0.9*1250*2500	1594	126	10	100	99.653	0.055	0.236	0.005	0.009	<0.003	<0.003	<0.008
Aluminium Sheet	1050 H14	0.9*1250*2500	1356	126	10	106	99.653	0.055	0.236	0.005	0.009	<0.003	<0.003	<0.003
Aluminium Sheet	1050 H14	1.5*1250*2500	1756	125	11	105	99.643	0.061	0.241	0.006	0.008	<0.003	<0.003	<0.003
Aluminium Sheet	1050 H14	1.5*1250*2500	1756	125	11	105	99.643	0.061	0.241	0.006	0.008	<0.003	<0.003	<0.003
Aluminium Sheet	1050 H14	1.5*1250*2500	1756	125	11	105	99.643	0.061	0.241	0.006	0.008	<0.003	<0.003	<0.003
Aluminium Sheet	1050 H14	1.2*1500*3000	1732	125	12	106	99.642	0.049	0.251	0.006	0.008	<0.003	<0.003	<0.003
Aluminium Sheet	1050 H14	2.0*1500*3000	2044	123	12	104	99.659	0.057	0.229	0.005	0.009	<0.003	<0.003	<0.003
Aluminium Sheet	1050 H14	2.0*1500*3000	1970	123	12	104	99.659	0.057	0.229	0.005	0.009	<0.003	<0.003	<0.003
Aluminium Sheet	1050 H14	2.0*1500*3000	1982	123	12	104	99.659	0.057	0.229	0.005	0.009	<0.003	<0.003	<0.003
Aluminium Sheet	1050 H14	2.0*1500*3000	1966	123	12	104	99.659	0.057	0.229	0.005	0.009	<0.003	<0.003	<0.003
Aluminium Sheet	1050 H14	2.0*1500*3000	1985	123	12	104	99.659	0.057	0.229	0.005	0.009	<0.003	<0.003	<0.003
Aluminium Sheet	1050 H14	2.0*1500*3000	1965	123	12	104	99.659	0.057	0.229	0.005	0.009	<0.003	<0.003	<0.003
Aluminium Sheet	1050 H14	2.0*1500*3000	1961	123	12	104	99.659	0.057	0.229	0.005	0.009	<0.003	<0.003	<0.003
Aluminium Sheet	1050 H14	2.0*1500*3000	1965	123	12	104	99.659	0.057	0.229	0.005	0.009	<0.003	<0.003	<0.003
Aluminium Sheet	1050 H14	2.0*1500*3000	1996	123	12	104	99.659	0.057	0.229	0.005	0.009	<0.003	<0.003	<0.003
Aluminium Sheet	1050 H14	3.0*1500*3000	1986	121	13	103	99.659	0.048	0.236	0.006	0.008	<0.003	<0.003	<0.003
Aluminium Sheet	1050 H14	3.0*1500*3000	1990	121	13	103	99.659	0.048	0.236	0.006	0.008	<0.003	<0.003	<0.003
Aluminium Sheet	1050 H14	3.0*1500*3000	1992	121	13	103	99.659	0.048	0.236	0.006	0.008	<0.003	<0.002	<0.003
Aluminium Sheet	1050 H14	3.0*1500*3000	1814	121	13	103	99.659	0.048	0.236	0.006	0.008	<0.003	<0.003	<0.003
ALUMINIUM TREADPLATE	1050 H14	2.0*1250*2500	2008	125	12	106	99.636	0.055	0.253	0.005	0.009	<0.003	<0.003	<0.003
ALUMINIUM TREADPLATE	1050 H14	3.0*1250*2500	1968	124	13	105	99.641	0.054	0.249	0.006	0.007	<0.003	<0.003	<0.003

Appendix B

RF Connector Technical Drawing
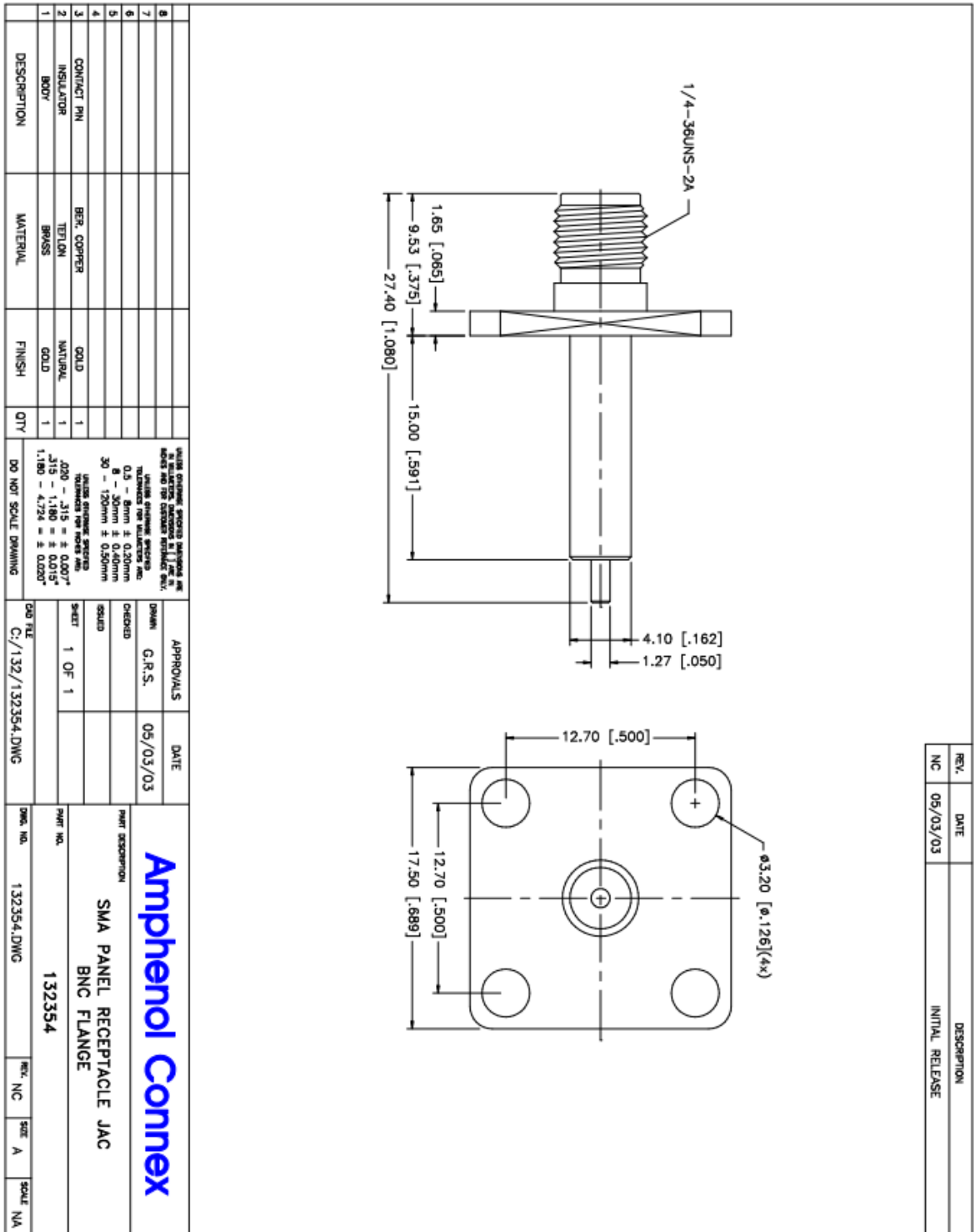
Product Technical Information
Comb Generator Emitter: CGE01

The Comb Generator Emitter 01 (CGE01) is a compact, battery powered, reference signal source that generates a broadband radiated and/or conducted output up to 18 GHz. When used as a verification reference source, the known output allows unknowns within systems or components to be measured or calculated. The compact size allows small enclosures to be evaluated when used as a reference source for shielding effectiveness measurements.

The CGE01 can be supplied with a 50 Ω SMA output connector (CGE01C) for direct connection to conducted test systems, or to an external antenna in order to generate test fields for evaluating radiated emission test systems. Alternatively, to achieve the best repeatability and compactness for purely radiated applications, the CGE01 can be supplied with an integrated antenna (CGE01R).

The CGE01 harmonic steps can be switched between 80 MHz and 100 MHz as standard, allowing more frequency points to be measured than is possible with a fixed-frequency source. A 50 MHz/80 MHz step option is available by special request, allowing measurements compliant with chamber validations above 1 GHz according to CISPR 16.

CGE01C with MCN02 and BP01 battery pack

Features

- Stable output
  - Repeatable measurements
- Conducted and radiated options
  - Evaluation of both conducted and radiated systems
- 50 MHz to 18 GHz output
  - Applications across a broad frequency spectrum
- 50 MHz step size
  - Complies with CISPR 16 validation methods
- Compact and portable
  - Comparisons between sites and environments
  - Shielding effectiveness measurements even of small enclosures
- Battery powered
  - No power or interconnecting cables affecting measurements

Applications

- CISPR 16 verifications
- Shielding effectiveness of small enclosures e.g. PCs, servers, wireless communications equipment
- Radiated measurement systems validation and verification
- Reference source for:
  - Daily pre-test verification checks if required by the accreditation authorities
  - Long term performance monitoring
  - Spectrum analyser / receiver pre-checks
- Investigation of reverberation (mode stirred) chamber behaviour
- Characterisation of filter performance
- Cable loss measurements
- Inter-laboratory test programs
- Proficiency test programs

Manufacturer's calibrations

CAL13   Conducted output power, 0 GHz to 18 GHz, measured using a spectrum analyser (CGE01C only)

CAL09   Radiated field strength, 1 GHz to 18 GHz, measured at 3 m in a FAR using a spectrum analyser (CGE01R or CGE01C with monocone antenna only)

Specifications

Frequency range	50 MHz to 18 GHz direct connection into a 50 Ω system 1 GHz to 18 GHz radiated using the integral antenna (CGE01R) or additional monocone antenna (CGE01C)
Step Size	80 MHz or 100 MHz switchable (50 MHz or 80 MHz switchable version available to special order)
Output connector	50 Ω SMA socket (CGE01C only)
Temperature stability	1 GHz to 16 GHz: <0.5 dB or 100 MHz to 18 GHz: <2 dB, at an ambient temperature of 15 °C to 35 °C
Time stability	Typically <1 dB over a 12 month period
Dimensions	CGE01C with battery pack – 76 mm diameter × 64 mm (74 mm incl. connector) CGE01C without battery pack – 76 mm diameter × 18 mm (28 mm incl. connector) CGE01R with battery pack – 76 mm diameter × 92 mm CGE01R without battery pack – 76 mm diameter × 46 mm
Weight	Approx 550 g (including battery)
Power supply	5 V 2 AHr battery pack External input 4.75 V to 7.5 V, 300 mA
Operating time	6.5 hours typical with a fully charged battery pack
Indicators	Mode 1; 80 MHz steps. Mode 2; 50 MHz or 100 MHz steps

Accessories

MCN02   Detachable monocone antenna (1 GHz to 18 GHz optimum when used with CGE01C)

BP01   5 V 2 AHr detachable battery pack